AD-A114 889 ORLANDO TECHNOLOGY INC SHALIMAR FL F/G 11/6
THE EFFECT OF MATERIAL PROPERTIES ON THE DEFORMATION OF RODS ST--ETC(U)
SEP 81 J J OSBORN F08635-81-C-0131
UNCLASSIFIED AFATL-TR-81-81 NL

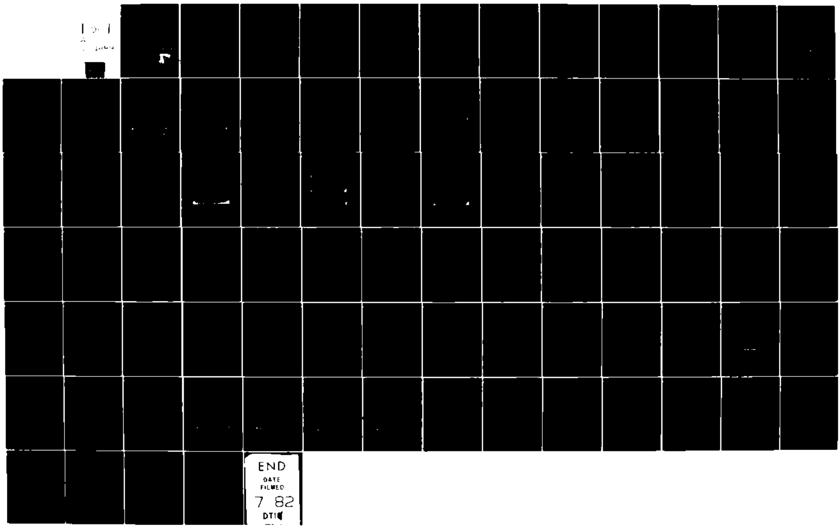

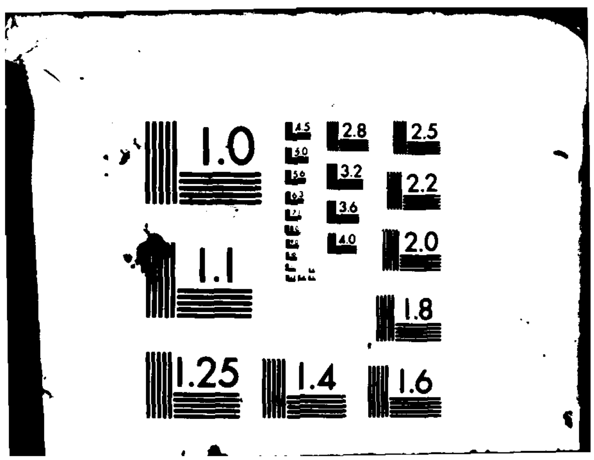
1.0
1.1
1.25
1.4
1.6
1.8
2.0
2.2
2.5
2.8
3.2
3.6
4.0

2

AFATL-TR-81-81

The Effect Of Material Properties On The Deformation Of Rods Stretching Under Large Velocity Gradients

John J Osborn

ORLANDO TECHNOLOGY, INCORPORATED
POST OFFICE BOX 855
SHALIMAR, FLORIDA 32579

AD A114889

SEPTEMBER 1981

FINAL REPORT FOR PERIOD MAY-AUGUST 1981

Approved for public release; distribution unlimited

Air Force Armament Laboratory
AIR FORCE SYSTEMS COMMAND ★ UNITED STATES AIR FORCE ★ EGLIN AIR FORCE BASE, FLORIDA

NOTICE

Please do not request copies of this report from the Air Force Armament Laboratory. Additional copies may be purchased from:

National Technical Information Service
5285 Port Royal Road
Springfield, Virginia 22161

Federal Government agencies and their contractors registered with Defense Technical Information Center should direct requests for copies of this report to:

Defense Technical Information Center
Cameron Station
Alexandria, Virginia 22314

UNCLASSIFIED

SECURITY CLASSIFICATION OF THIS PAGE (When Data Entered)

REPORT DOCUMENTATION PAGE

READ INSTRUCTIONS BEFORE COMPLETING FORM

1. REPORT NUMBER AFATL-TR-81-81	2. GOVT ACCESSION NO. AD-A114 889	3. RECIPIENT'S CATALOG NUMBER
4. TITLE (and Subtitle) THE EFFECT OF MATERIAL PROPERTIES ON THE DEFORMATION OF RODS STRETCHING UNDER LARGE VELOCITY GRADIENTS		5. TYPE OF REPORT & PERIOD COVERED Final Report May - August 1981
		6. PERFORMING ORG. REPORT NUMBER
7. AUTHOR(s) John J. Osborn		8. CONTRACT OR GRANT NUMBER(s) F08635-81-C-0131
9. PERFORMING ORGANIZATION NAME AND ADDRESS Orlando Technology, Incorporated P.O. Box 855 Shalimar, Florida 32579		10. PROGRAM ELEMENT, PROJECT, TASK AREA & WORK UNIT NUMBERS PE: 62602F JON: 2502-06-43
11. CONTROLLING OFFICE NAME AND ADDRESS Air Force Armament Laboratory Armament Division Eglin Air Force Base, Florida 32542		12. REPORT DATE September 1981
		13. NUMBER OF PAGES 87
14. MONITORING AGENCY NAME & ADDRESS (if different from Controlling Office)		15. SECURITY CLASS. (of this report) Unclassified
		15a. DECLASSIFICATION/DOWNGRADING SCHEDULE

16. DISTRIBUTION STATEMENT (of this Report)

Approved for public release: unlimited distribution

17. DISTRIBUTION STATEMENT (of the abstract entered in Block 20, if different from Report)

18. SUPPLEMENTARY NOTES

19. KEY WORDS (Continue on reverse side if necessary and identify by block number)

Stretching	Strength effects	Metals
Jets	Density effects	
Necking	Velocity gradients	
Deformation	Rods	

20. ABSTRACT (Continue on reverse side if necessary and identify by block number)

This report presents analytical solutions for the velocity and position of necks in a rod stretching under large velocity gradients. Solutions are based on assuming various forms for the yield strength of the rod. The model predicts many phenomena seen in stretching shaped charge jets without recourse to probalistic perturbations.

DD FORM 1 JAN 73 1473

UNCLASSIFIED

SECURITY CLASSIFICATION OF THIS PAGE (When Data Entered)

PREFACE

The research in this report was performed from May through August 1981 by Orlando Technology, Incorporated, Post Office Box 855, Shalimar, Florida 32579. The research was performed under Contract F08635-81-C-0131 for the Bombs and Warheads Branch, Munitions Division, Air Force Armament Laboratory, Armament Division, Eglin Air Force Base, Florida 32542. The program manager for this effort was Mr. William Cook (DLJW). The principal investigator for Orlando Technology, Incorporated was Mr. John Osborn.

This report describes theoretical research into the effects of material properties on the deformation of rods subject to large velocity gradients. The work provides insight into many phenomena seen in shaped charge jets.

The Public Affairs Office has reviewed this report, and it is releasable to the National Technical Information Service, where it will be available to the general public, including foreign nationals.

This technical report has been reviewed and is approved for publication.

FOR THE COMMANDER

CARL A. FORBRICH, JR., Lt Colonel, USAF
Chief, Munitions Division

(The reverse of this page is blank)

TABLE OF CONTENTS

LIST OF FIGURES

LIST OF FIGURES (CONTINUED)

LIST OF FIGURES (CONCLUDED)

LIST OF TABLES

(The reverse of this page is blank.)

SECTION I
INTRODUCTION

This report presents equations which describe the deformation and necking in a rod stretching under a large velocity gradient. The equations duplicate wave propagation computer program solutions for rods of varying densities, yield strengths, and other properties being stretched under uniform velocity gradients.

The equations provide insight into similar phenomena seen in stretching jets from shaped charge munitions and provide a purely mechanistic approach to understanding such phenomena. They suggest tailoring of jet gradients and material properties to achieve specific weapon objectives.

The basic equations are solved for right circular cylinders stretching under a linear velocity gradient. Nonlinear gradients and shapes other than constant-diameter rods are modelled by the basic differential equations. General solutions are not presented for these cases since the equations must be solved numerically.

SECTION II
ROD STRETCHING CALCULATIONS

The TOODY two-dimensional Lagrangian Wave Propagation computer program (Reference 1) was used to calculate deformation in stretching rods of initially constant diameters. Several calculations were undertaken with varying gradient, length, density, yield strength, and sound speeds. Several of these calculations will be discussed in this section to provide an introduction to the basic phenomenology.

Figure 1 shows the initial grid structure for a 10-cm-long, 1-cm-diameter rod. The top figure is drawn with the same scale on both axes. The z, or radial, direction is amplified in the bottom figure. The x axis is an axis of rotational symmetry.

In this calculation the rod is copper with a density of 8.9 gm/cc, an initial bulk sound speed of $4x10^5$ cm/sec, a shock velocity/particle velocity slope of 1.5, a Gruneisen ratio of 2.0, a Poisson's ratio of 0.35, and a Von Mises yield strength of 5 kilobars (Kb). The yield strength is not allowed to vary with strain or internal energy. At startup time a velocity gradient of $2x10^4$ sec^{-1} is imposed on the 10-cm-long rod. The velocity is set to 0 at the X=0 point and varies linearly with X to $2x10^5$ cm/sec at the X=10 cm point.

Figure 2 shows the rod in both the equal and amplified scale along with X-velocity, in cm/sec, versus X, in cm, at 20 microseconds. The plot clearly shows relief waves moving into the rod from both ends, stabilizing velocity in the relieved sections. The velocity in the relieved, or elastic, sections increases from initial values in the tail (low velocity end) of the rod and decreases from initial values in the tip (high velocity end) of the rod. Between these constant velocity segments the rod is continuing to stretch plastically at the same velocities initially given to the rod.

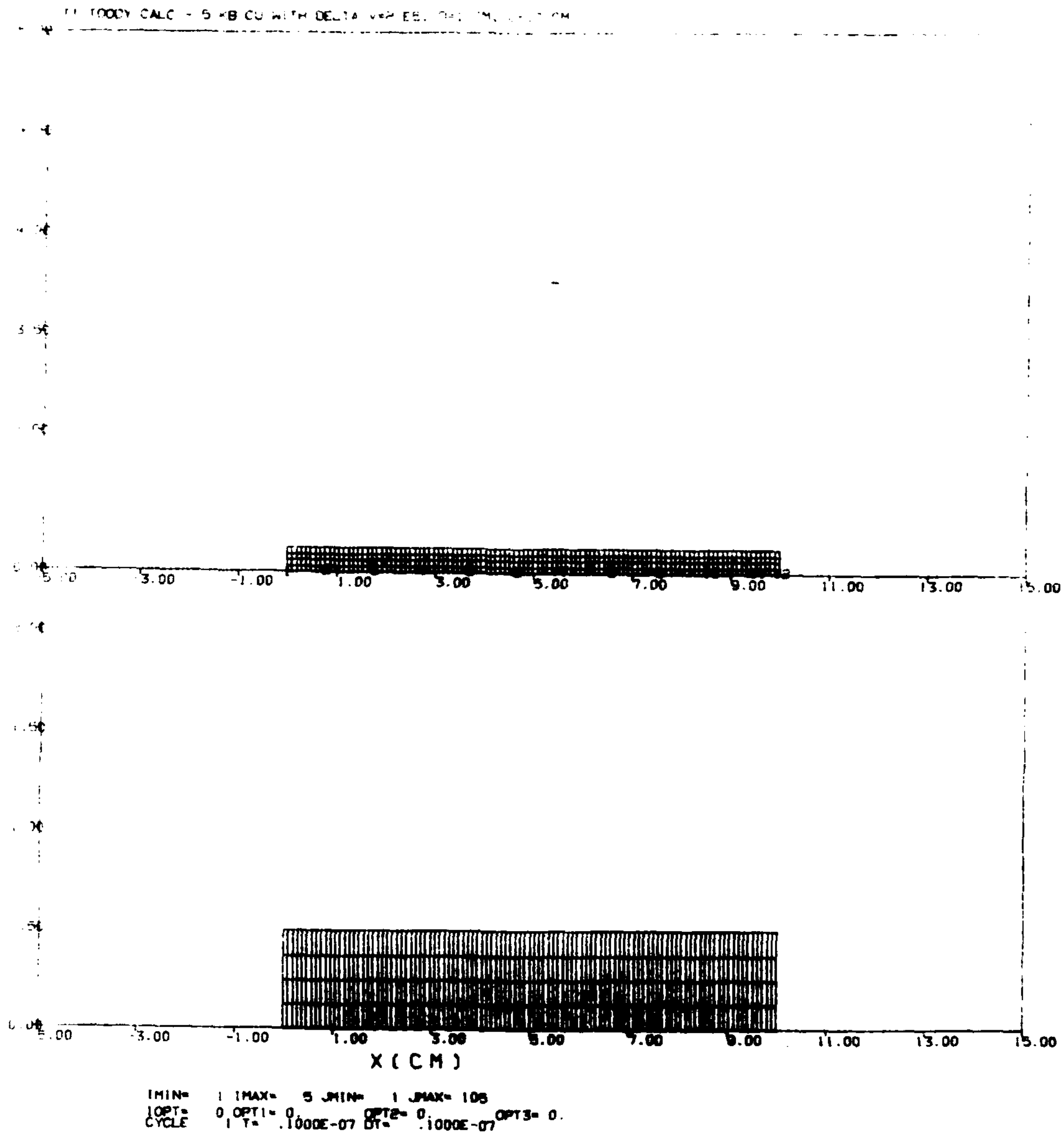

Figure 1. Initial 10-cm-Rod Geometry

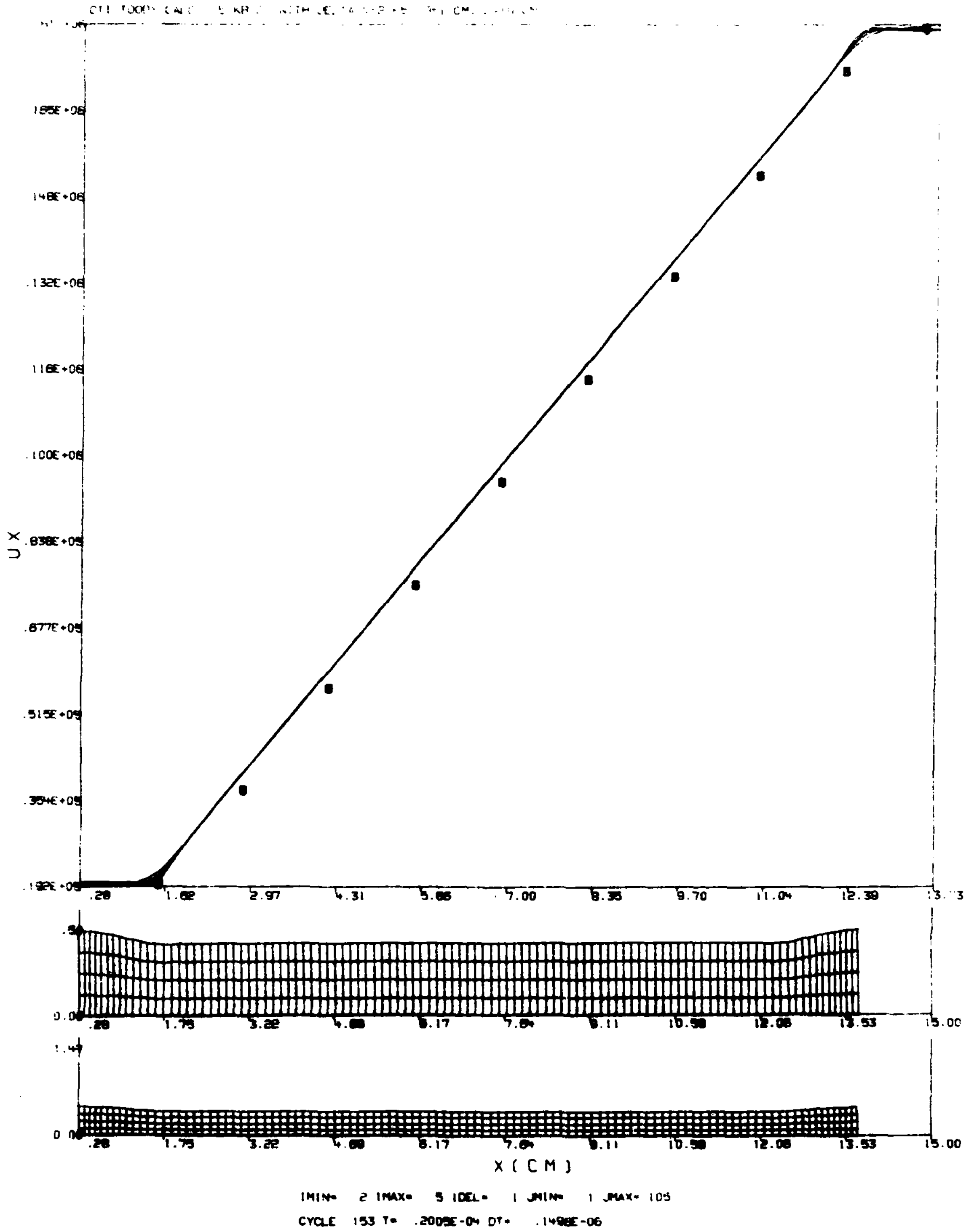

Figure 2. Grid and Velocity Plot at 20 Microseconds - 5-Kb Copper with 2×10^4 sec^{-1} Gradient

Figure 3 presents the same data for the rod at 60 microseconds. At this time the stabilized end sections have grown to approximately 2 cm, with a slight neck visible at the end of the relieved sections. The velocity and amplified grid plot show another set of necks forming approximately 2 cm ahead of the first necks.

By 100 microseconds (Figure 4), the second necks are well formed and two new necks are beginning to form. The stabilized elastic end sections are each approximately 2.5 cm in length and an elastic region also exists within the adjacent segment, as signified by the constant velocity region. Figure 5 plots axial stress in dynes/cm^2 versus axial position along the rod for the zones which exist in the radial direction across the rod.

In the central rod section stress is at the 5×10^9 dynes/cm^2 (5 Kb) level. It rises above this level within each neck region and decays below the level in each elastic region. The rise is caused by an increase in pressure (mean stress) due to the curvature at the neck. This rise in mean stress is similar to that measured in tensile tests and described by P. W. Bridgman in the early 1950's (Reference 2). As discussed in Section III, it is this rise in mean stress which causes more than the first necks to form. Figures 6 and 7 are plots of axial strain and internal energy per unit mass versus axial position at the 100-microsecond time. Strain along the completely plastic central section of the rod is predictable from the gradient and is 1.1 (110 percent). Axial strain rises at each neck location and decays in each elastic segment, as would be expected. The strain level at the very ends of the rods is virtually zero since these ends were relieved almost instantaneously. The internal energy density plot in Figure 7 shows similar phenomenology. The energy is a constant, predictable value along the unrelieved central rod section and rises as strain rises in each neck. In this calculation, the rod began at zero internal energy at the start of the problem.

Figure 8 plots three times the square root of the second stress invariant (i.e., the quantity which cannot exceed the Von Mises yield strength) in dynes/cm^2 versus axial position at 100 microseconds. It demonstrates that the

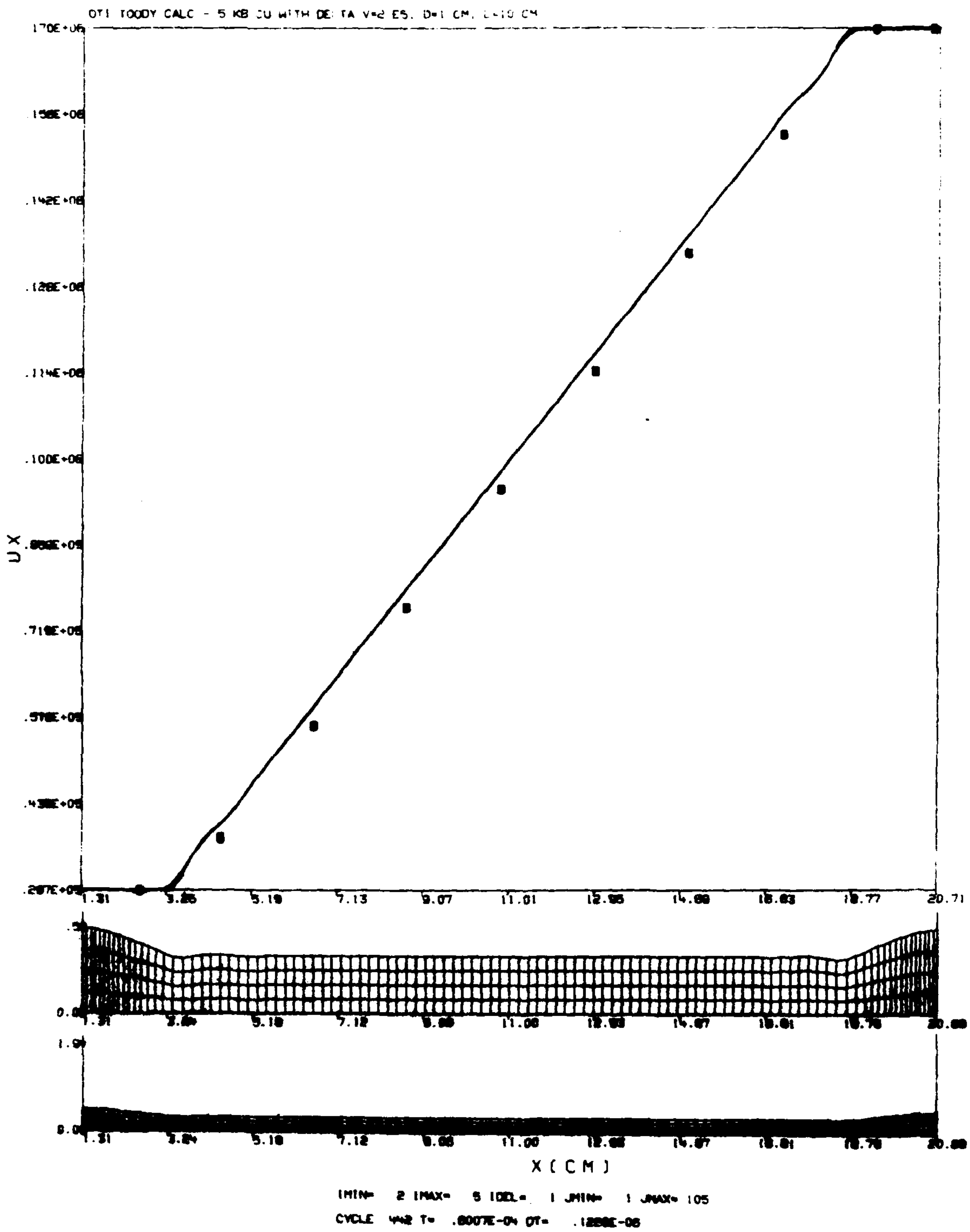

Figure 3. Grid and Velocity Plot at 60 Microseconds - 5-Kb Copper with $2x10^4$ sec^{-1} Gradient

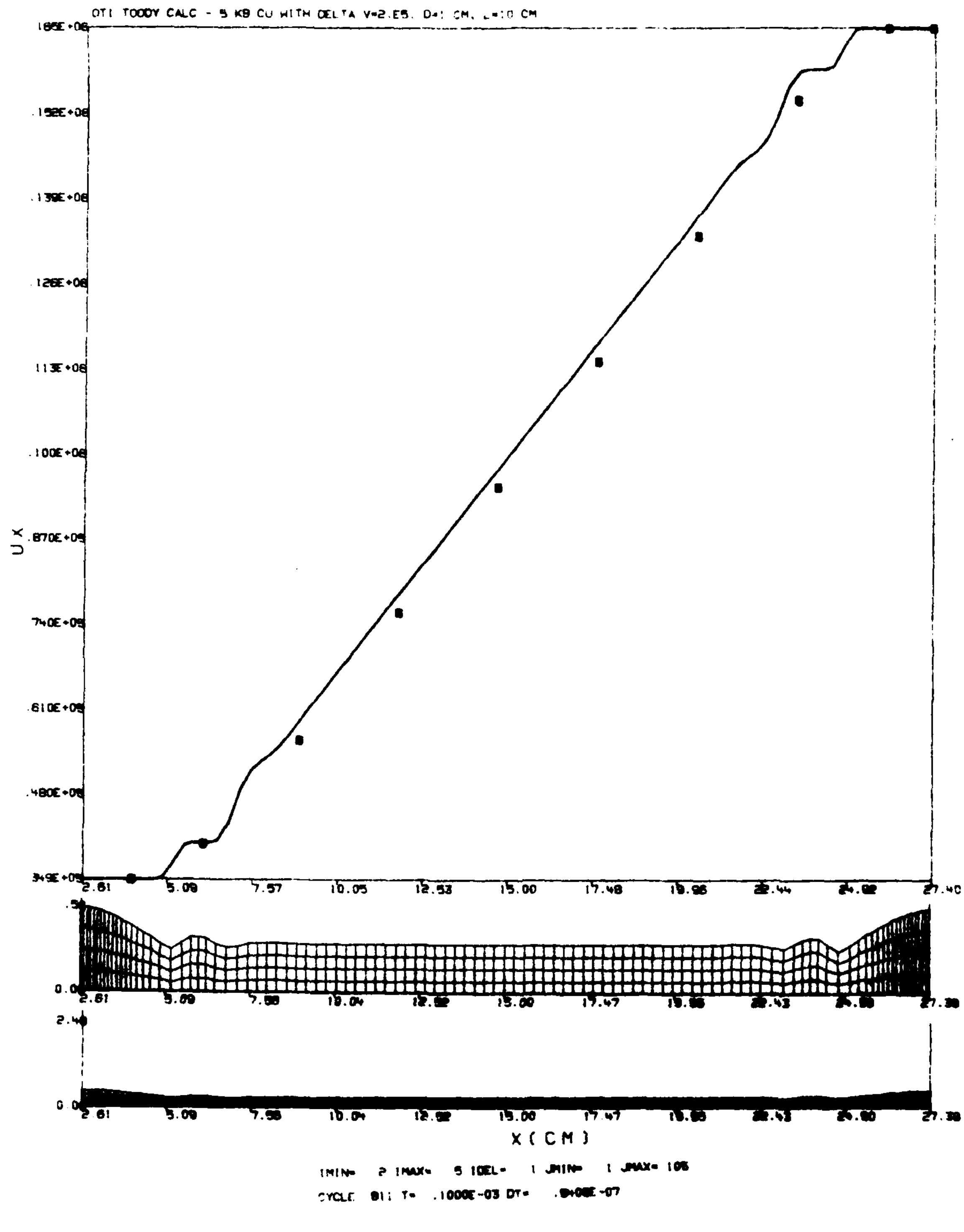

Figure 4. Grid and Velocity Plot at 100 Microseconds - 5-Kb Copper with 2×10^4 sec^{-1} Gradient

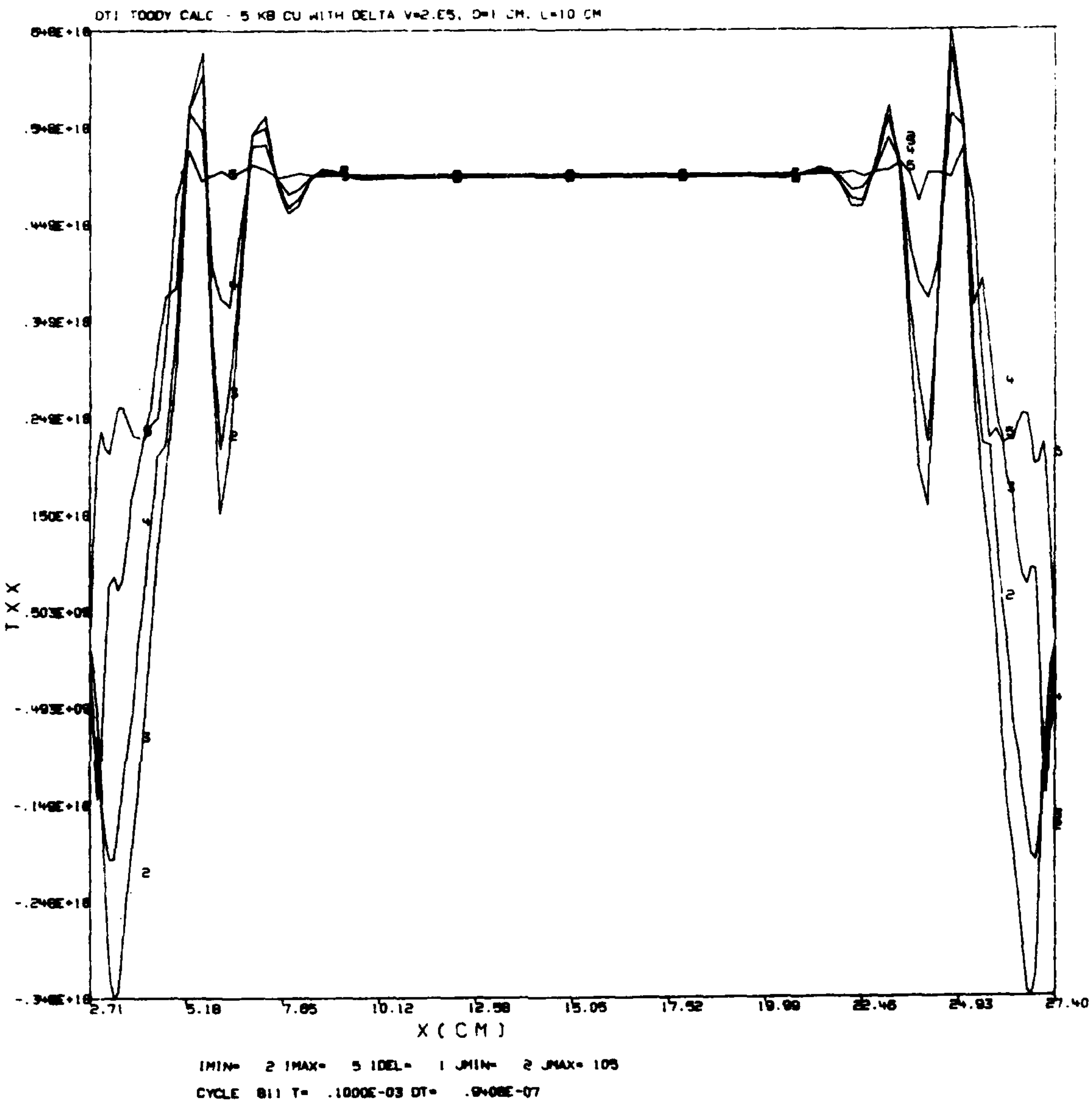

Figure 5. Axial Stress Versus Axial Position at 100 Microseconds
5-Kb Copper with $2x10^4$ sec^{-1} Gradient

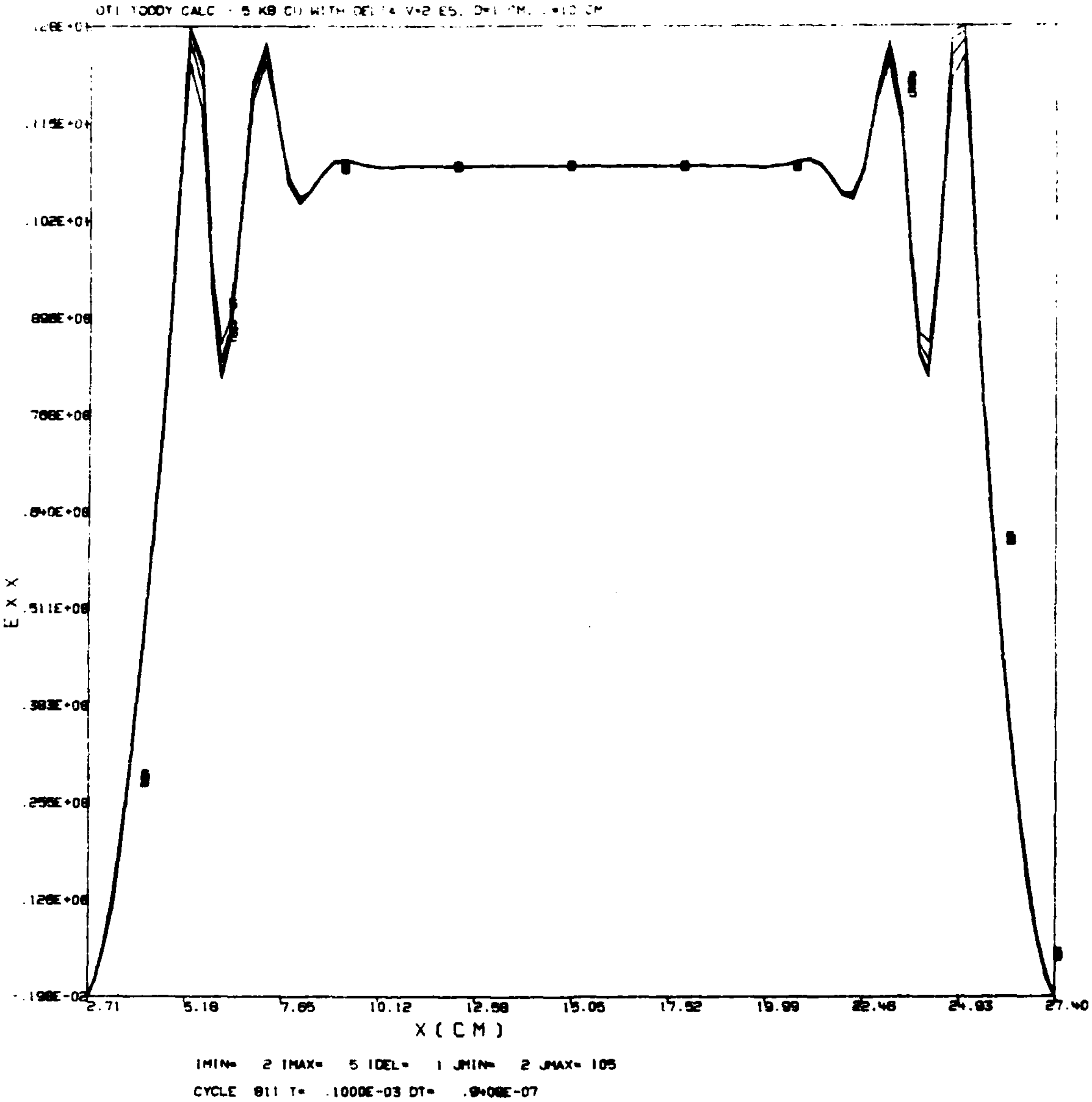

Figure 6. Axial Strain Versus Axial Position at 100 Micro-seconds - 5-Kb Copper with $2x10^4$ sec^{-1} Gradient

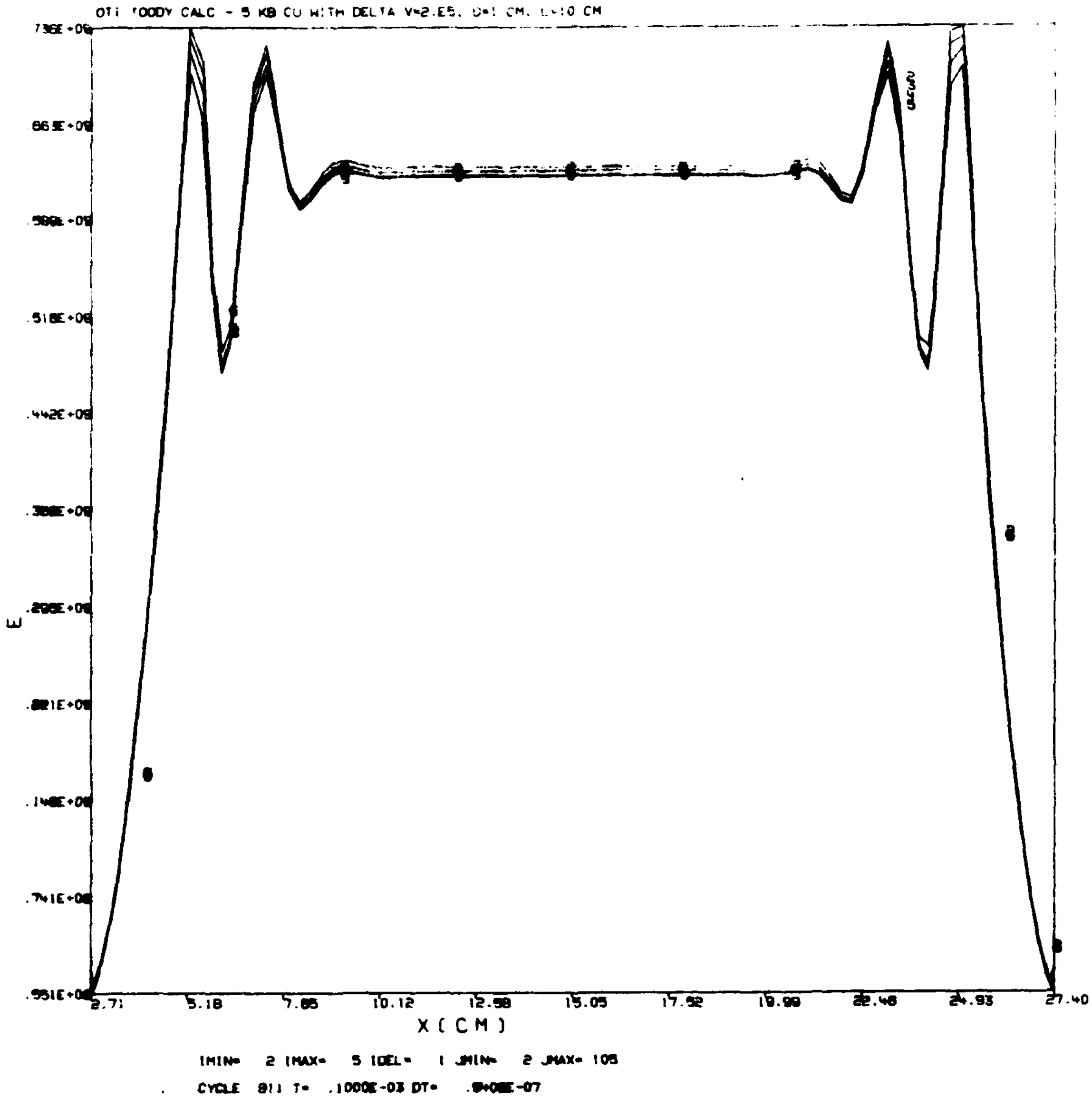

Figure 7. Internal Energy Density Versus Axial Position
5-Kb Copper with $2x10^4$ sec^{-1} Gradient

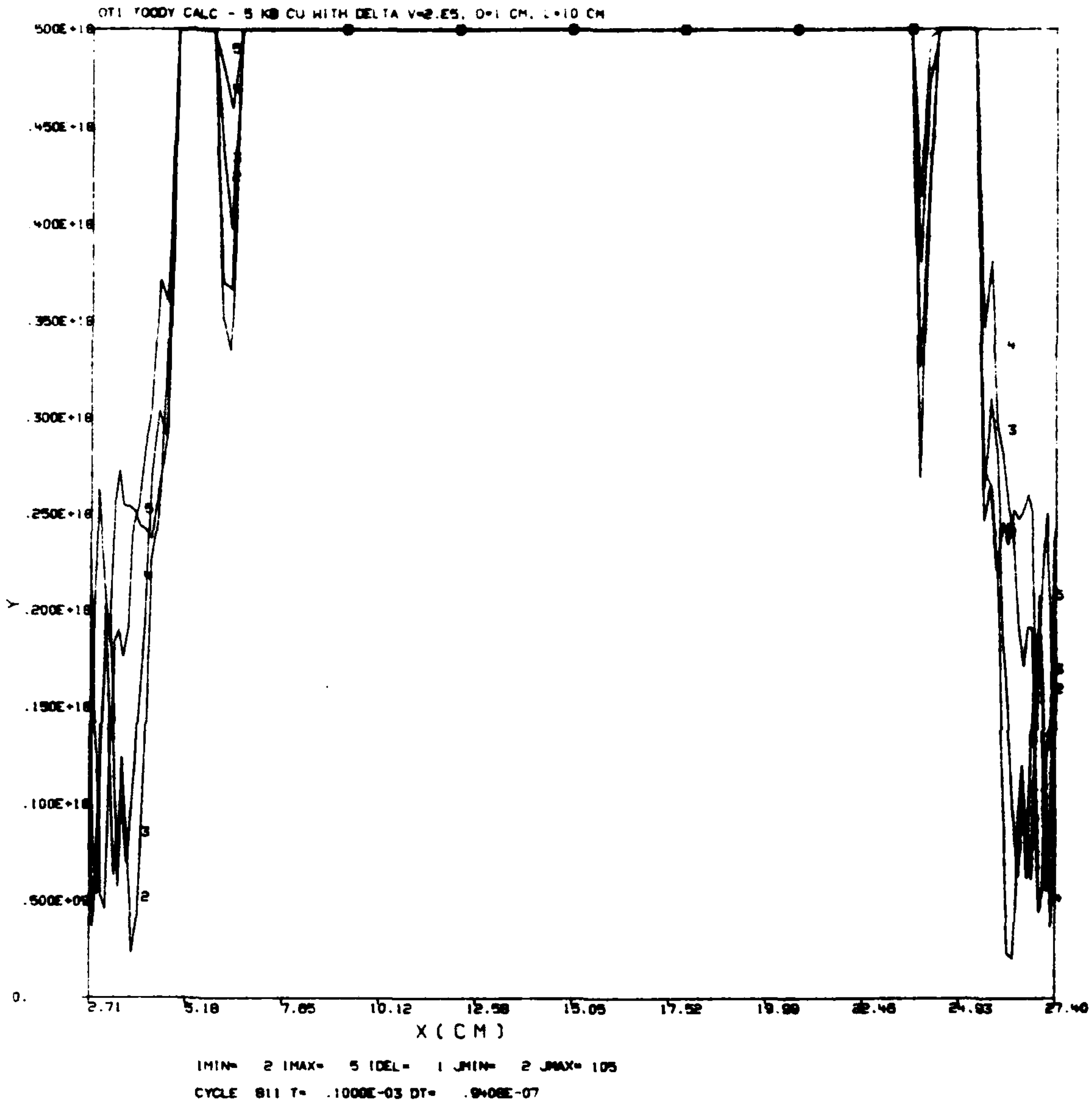

Figure 8. Second Stress Invariant Versus Axial Position 5-Kb Copper with $2x10^4$ sec^{-1} Gradient

rod is indeed elastic in the end sections, plastic at the necks and the still-stretching central rod section and elastic in the second set of stabilized segments from each end. Variations at the same axial position are variations within zones at different radii (Z position) at that axial position.

Figure 9 is a plot of kinetic energy density (kinetic energy per unit mass) versus axial position at 100 microseconds. It shows again the stabilized velocity sections and the curvature in the center section expected from a constant velocity gradient.

Necks continue to multiply, moving in from each end, until all of the rod has been subjected to the phenomenon.

Figures 10 through 15 show grid and axial velocity plots for the same rod with a smaller velocity gradient. In this case the gradient is 1×10^4 sec^{-1}, i.e., the tail velocity is zero and the tip velocity is 1×10^5 cm/sec. Necks and stabilized regions are seen to form in the same manner as previously but with different sizes and velocities. The last three figures--130, 140, and 150 microseconds—show in detail the formation, stabilization, and growth of the second set of elastic regions.

Changing the length of the rod has no effect other than to provide more rod within which necks can form. Figure 16 is a velocity versus axial position plot at 150 microseconds for a rod with the same 1×10^4 sec^{-1} velocity gradient but with length increased to 20 cm. The stabilized velocities and positions are identical to those in Figure 15. Whereas the 10-cm rod will form perhaps one more set of necks and a neck at the center as it continues to stretch, the 20-cm rod will form many more. Figure 17 shows the neck system for the 20-cm rod at 250 microseconds. Eight necks are clearly visible, and more necks will form as the rod continues to stretch.

The effect of varying yield strength from 2 to 5 kilobars in a staballoy rod is seen in Figures 18 and 19. These are grid plots (amplified in the radial direction) at various times for rods initially 10-cm long, 1 cm in diameter with a velocity gradient of 1×10^4 vm/sec. All are assumed to have

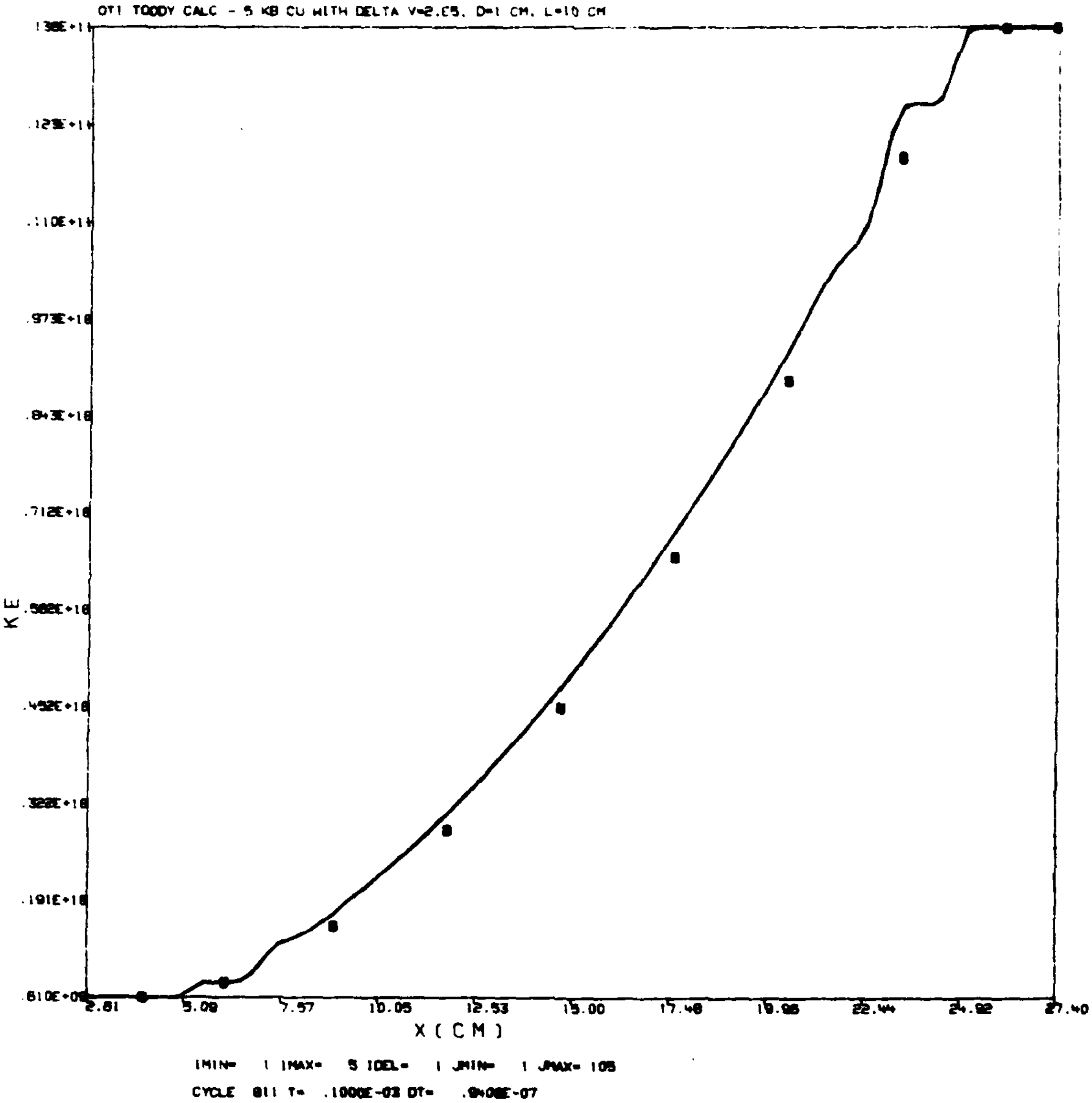

Figure 9. Kinetic Energy Versus Axial Position - 5-Kb Copper with 2×10^4 sec^{-1} Gradient

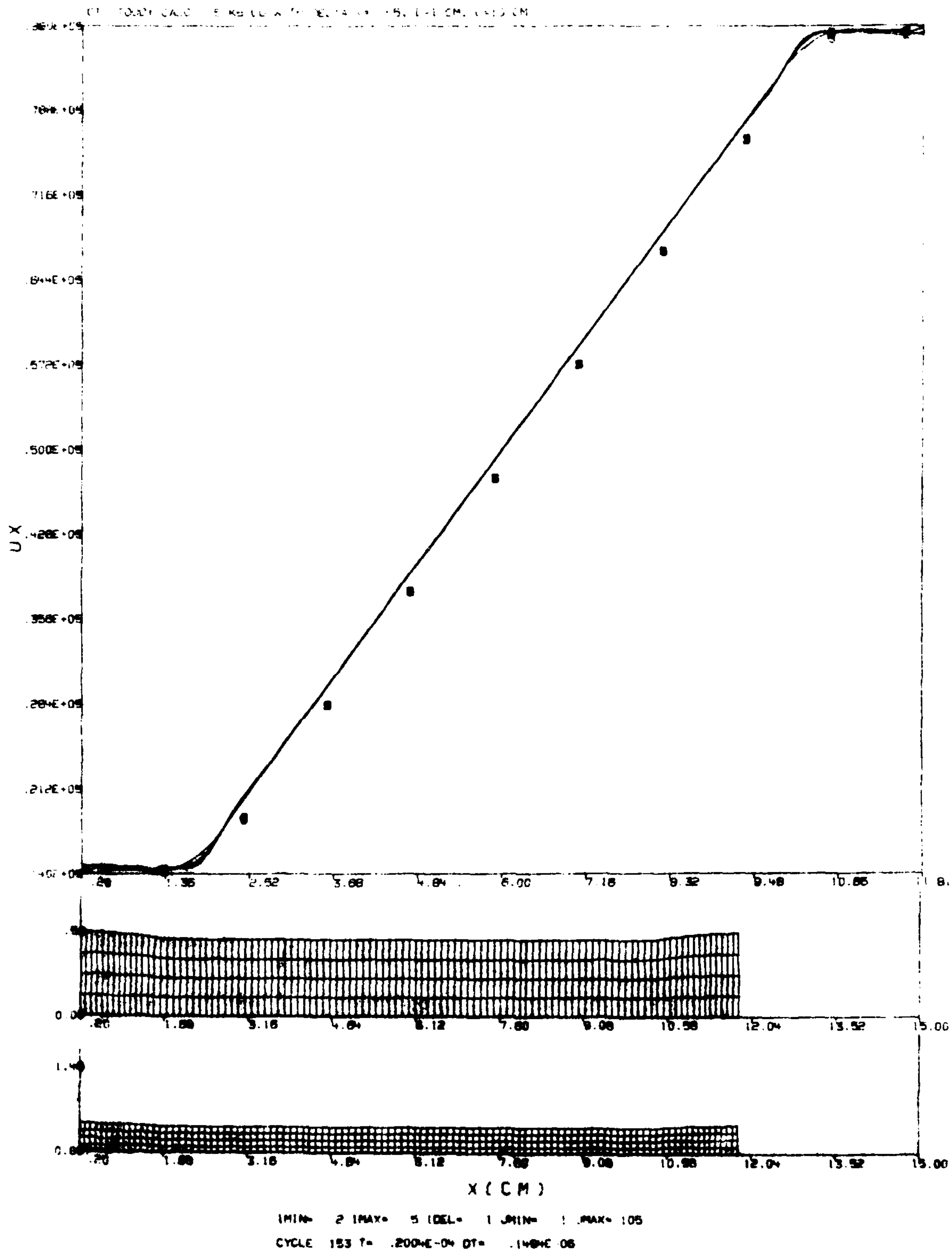

Figure 10. Grid and Velocity Plot at 20 Microseconds - 5-Kb Copper with 1x10^{4} sec^{-1} Gradient

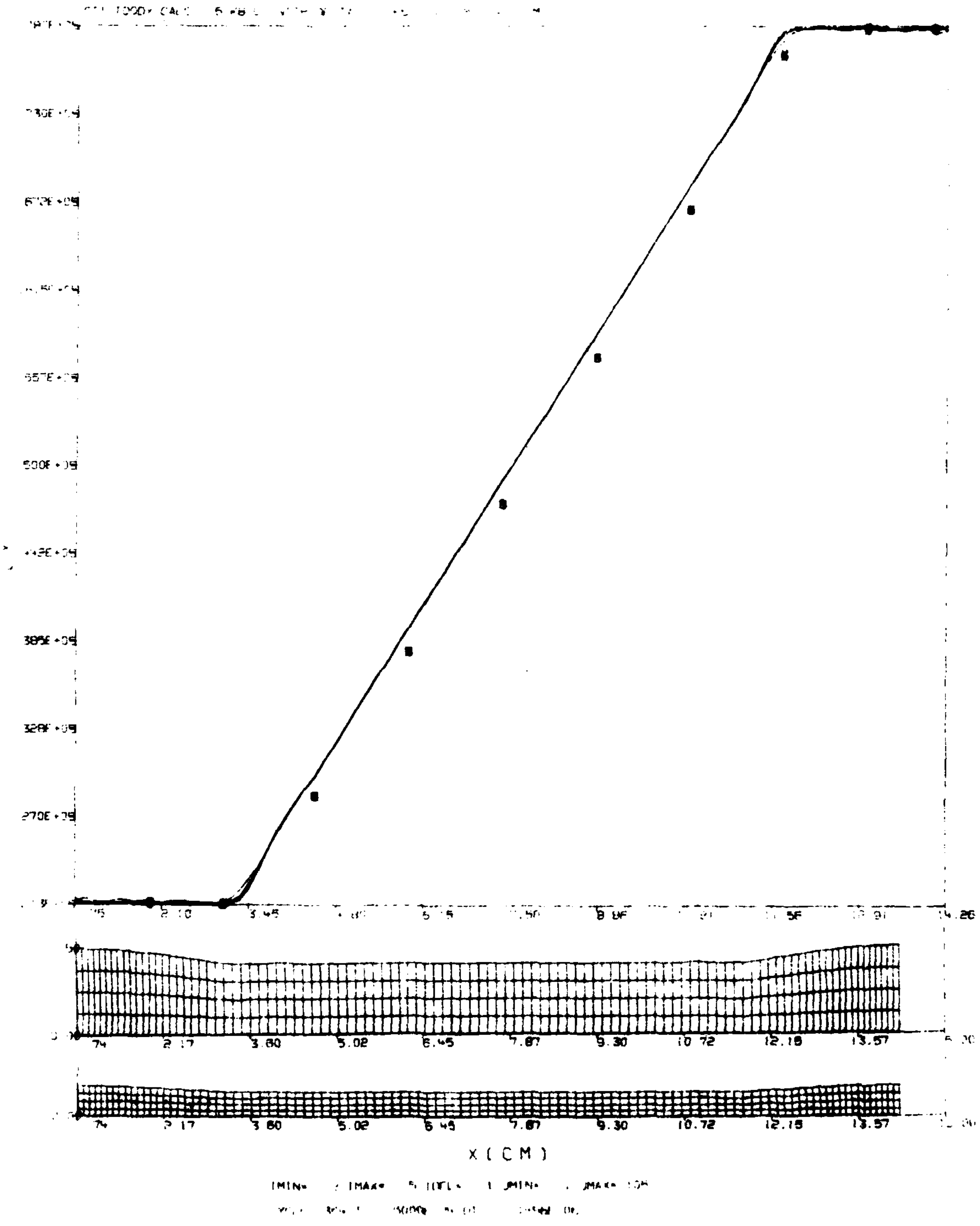

Figure 11. Grid and Velocity Plot at 50 Microseconds - 5-Kb Copper with $1x10^4$ sec^{-1} Gradient

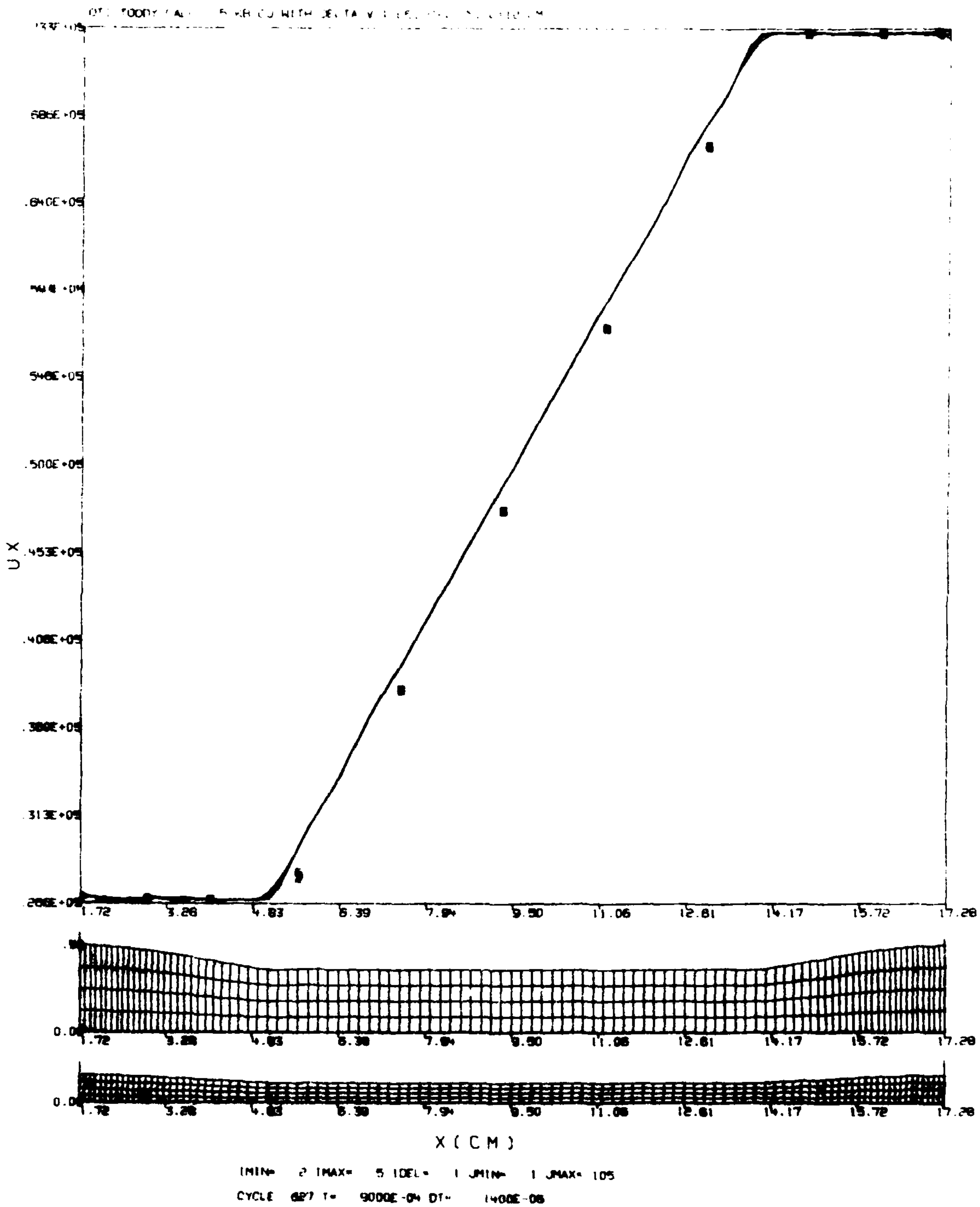

Figure 12. Grid and Velocity Plot at 90 Microseconds - 5-Kb Copper with 1×10^4 sec^{-1} Gradient

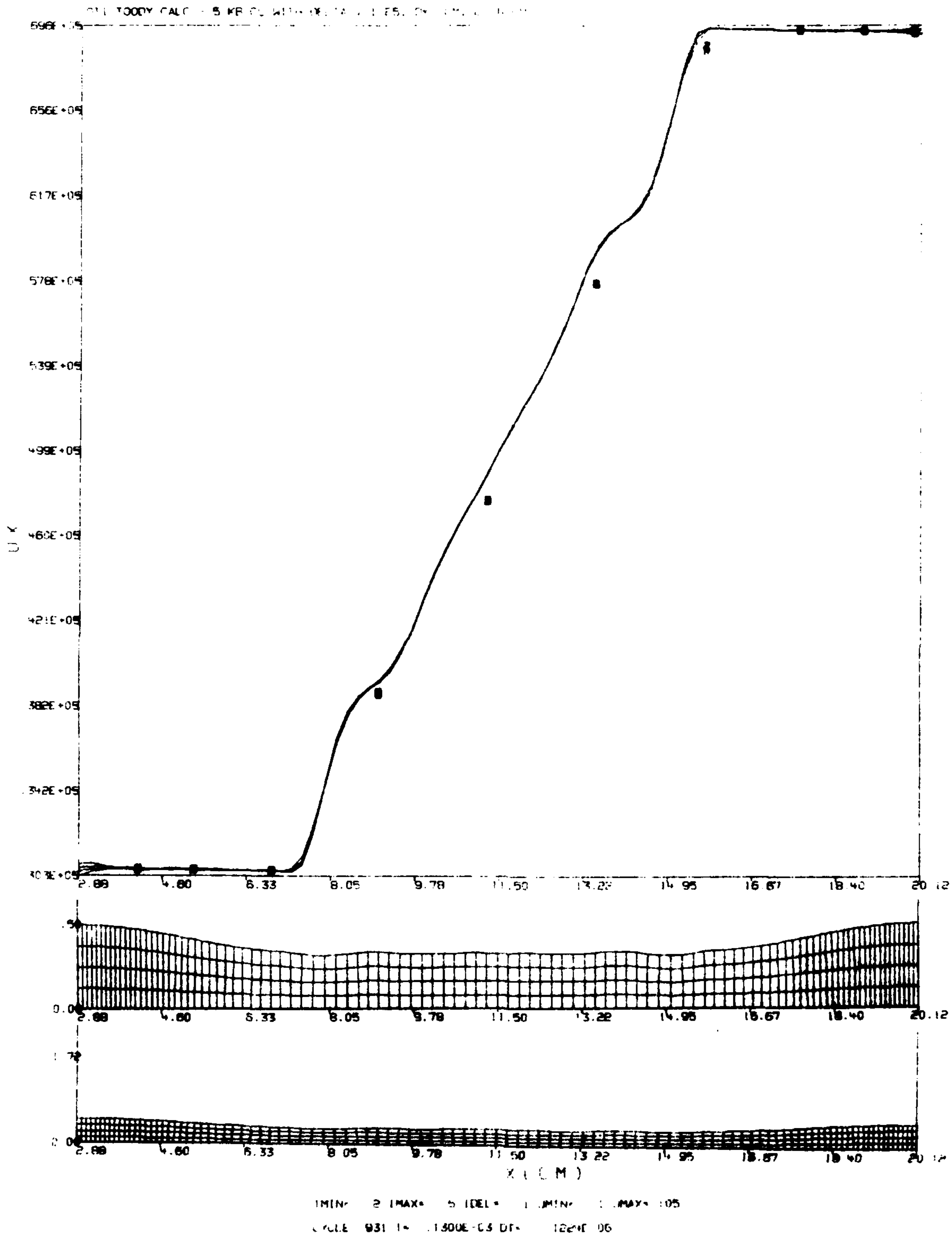

Figure 13. Grid and Velocity Plot at 130 Microseconds - 5-Kb Copper with 1×10^{4} sec^{-1} Gradient

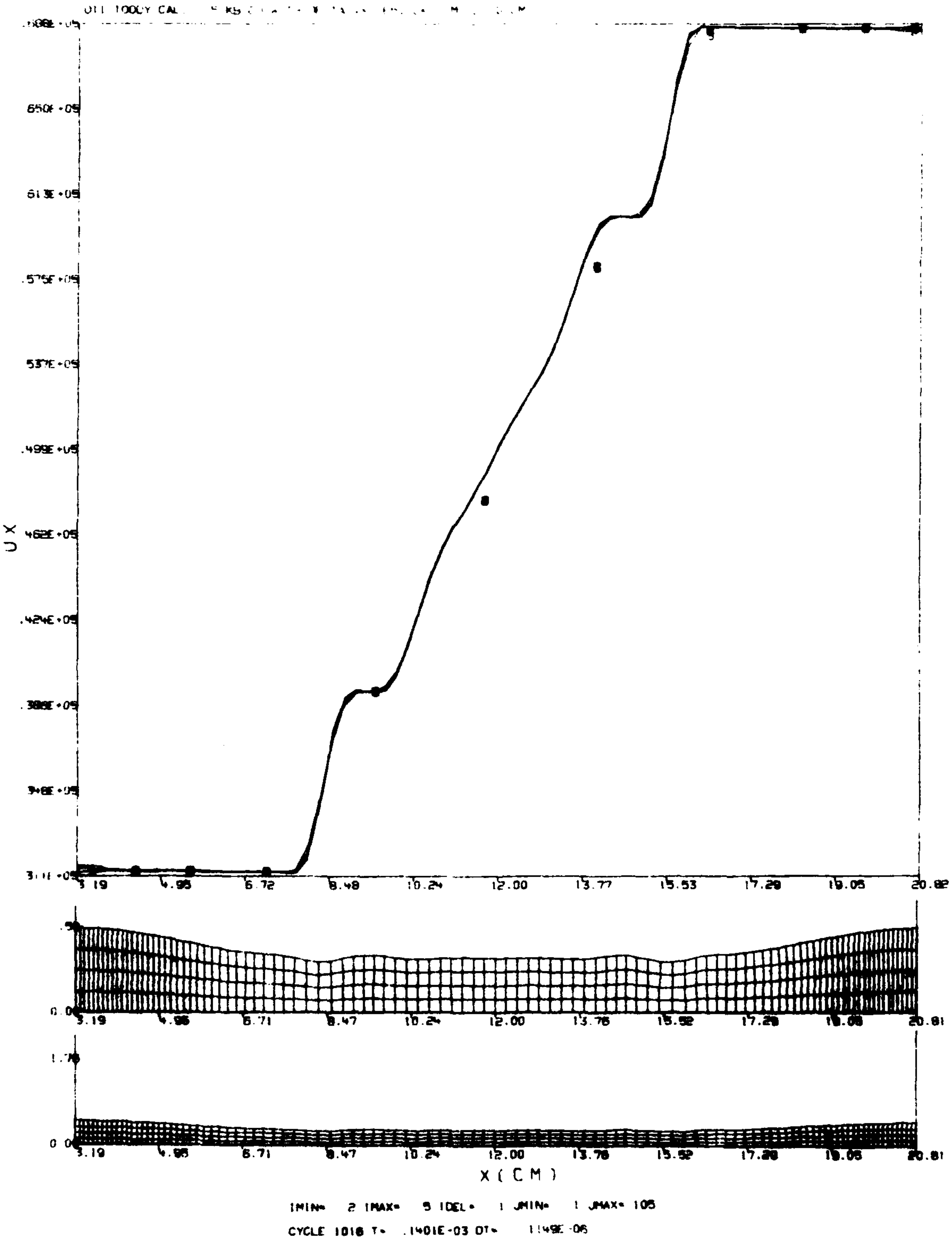

Figure 14. Grid and Velocity Plot at 140 Microseconds - 5-Kb Copper with $1x10^4$ sec^{-1} Gradient

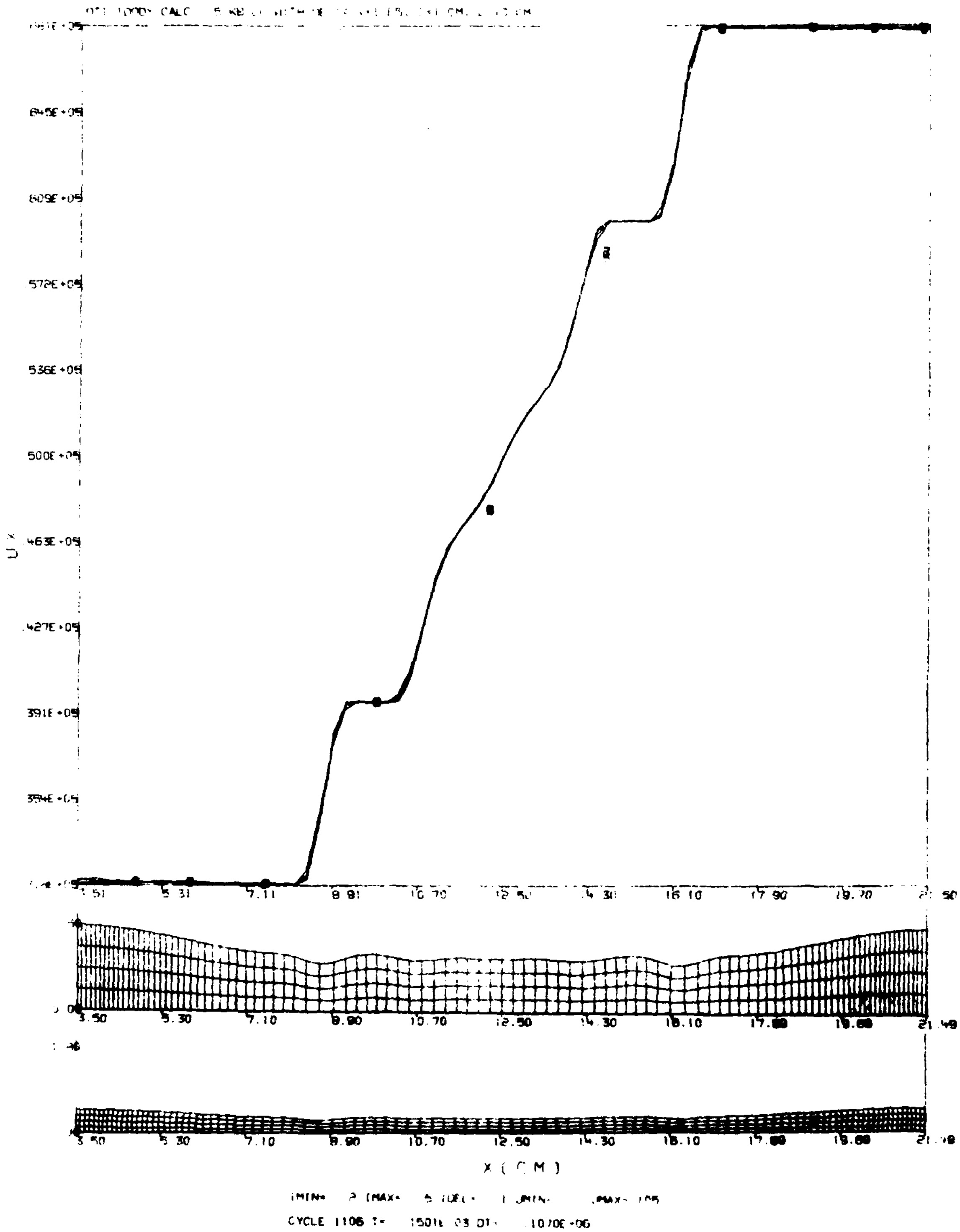

Figure 15. Grid and Velocity Plot at 150 Microseconds - 5-Kb Copper with 1x10^4 sec^{-1} Gradient

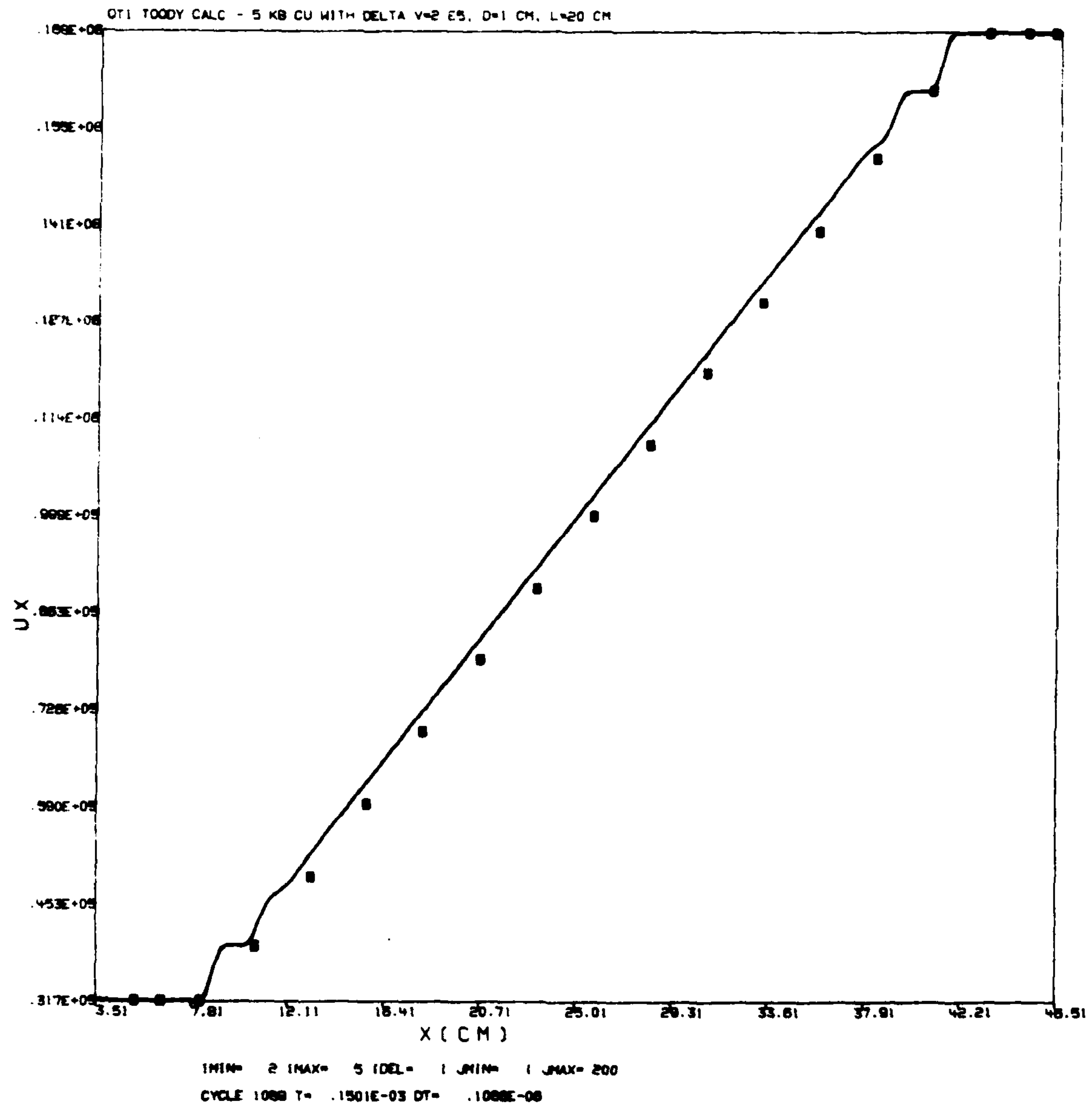

Figure 16. Velocity Plot at 150 Microseconds - 5-Kb Copper with 1×10^4 sec^{-1} Gradient - 20-cm-Long Rod

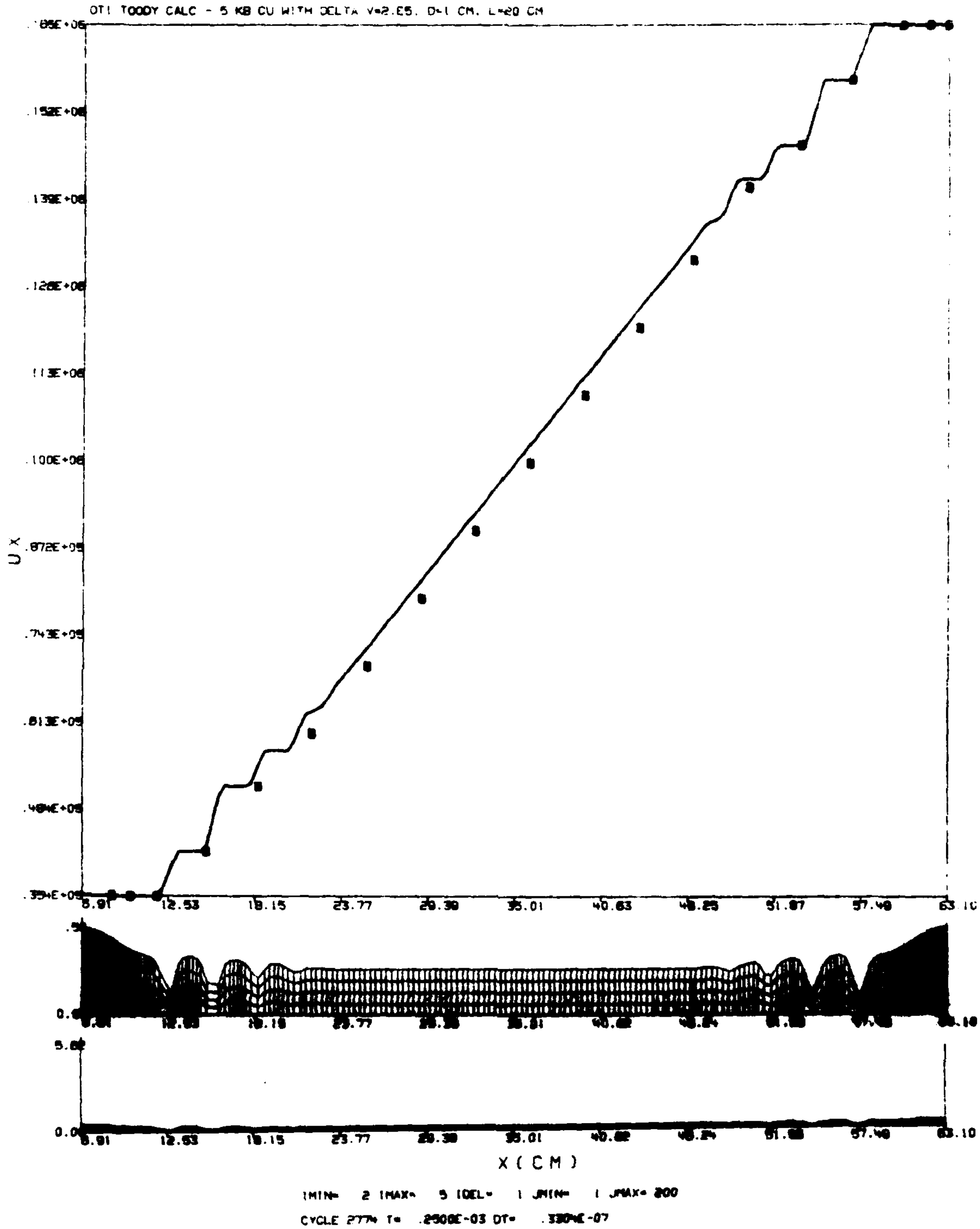

Figure 17. Grid and Velocity Plot at 250 Microseconds - 5-Kb Copper with 1×10^4 sec^{-1} Gradient - 20-cm-Long Rod

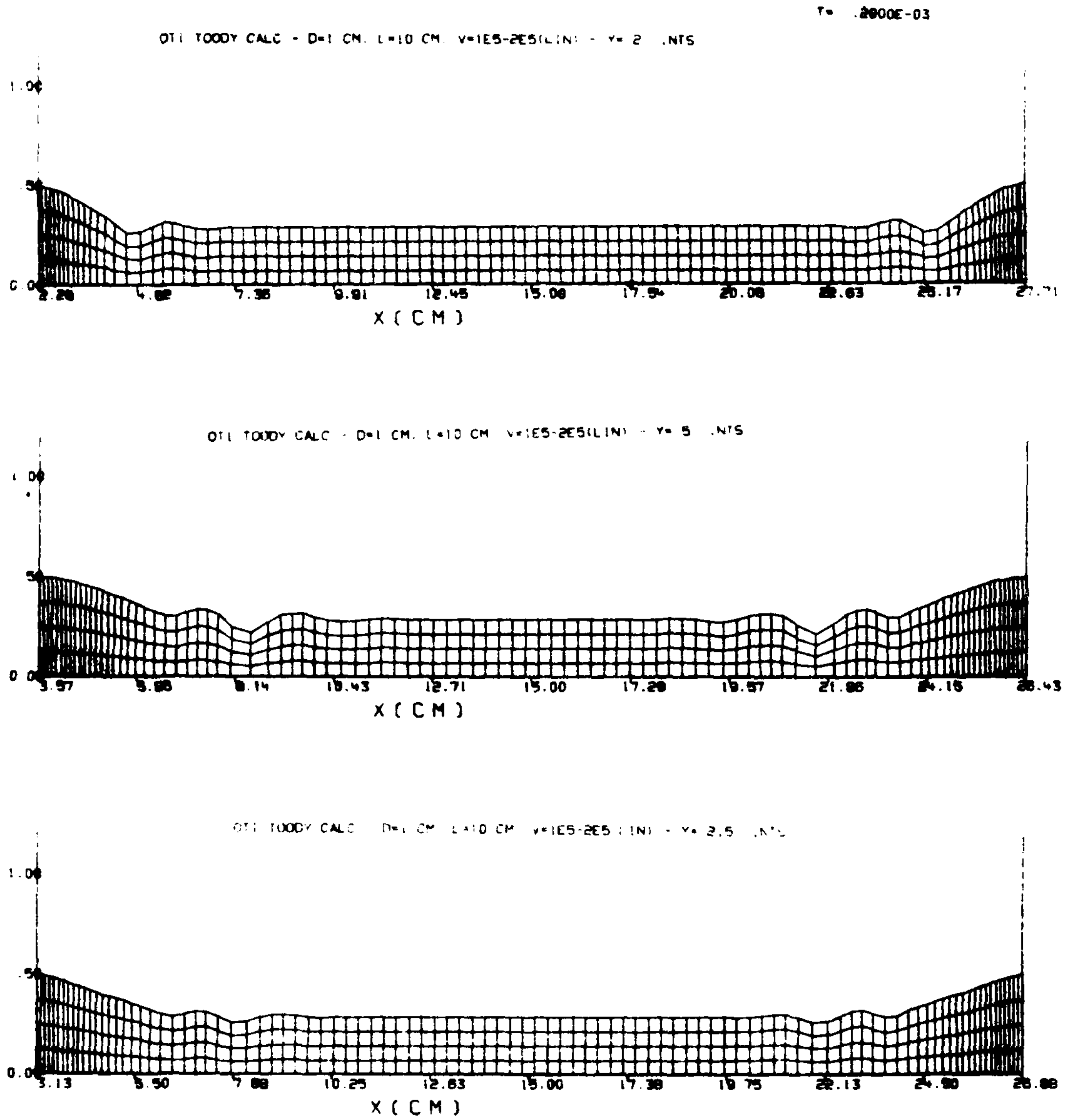

Figure 18. Grid Plots for 10-cm-Long Uranium Rods at 200 Microseconds

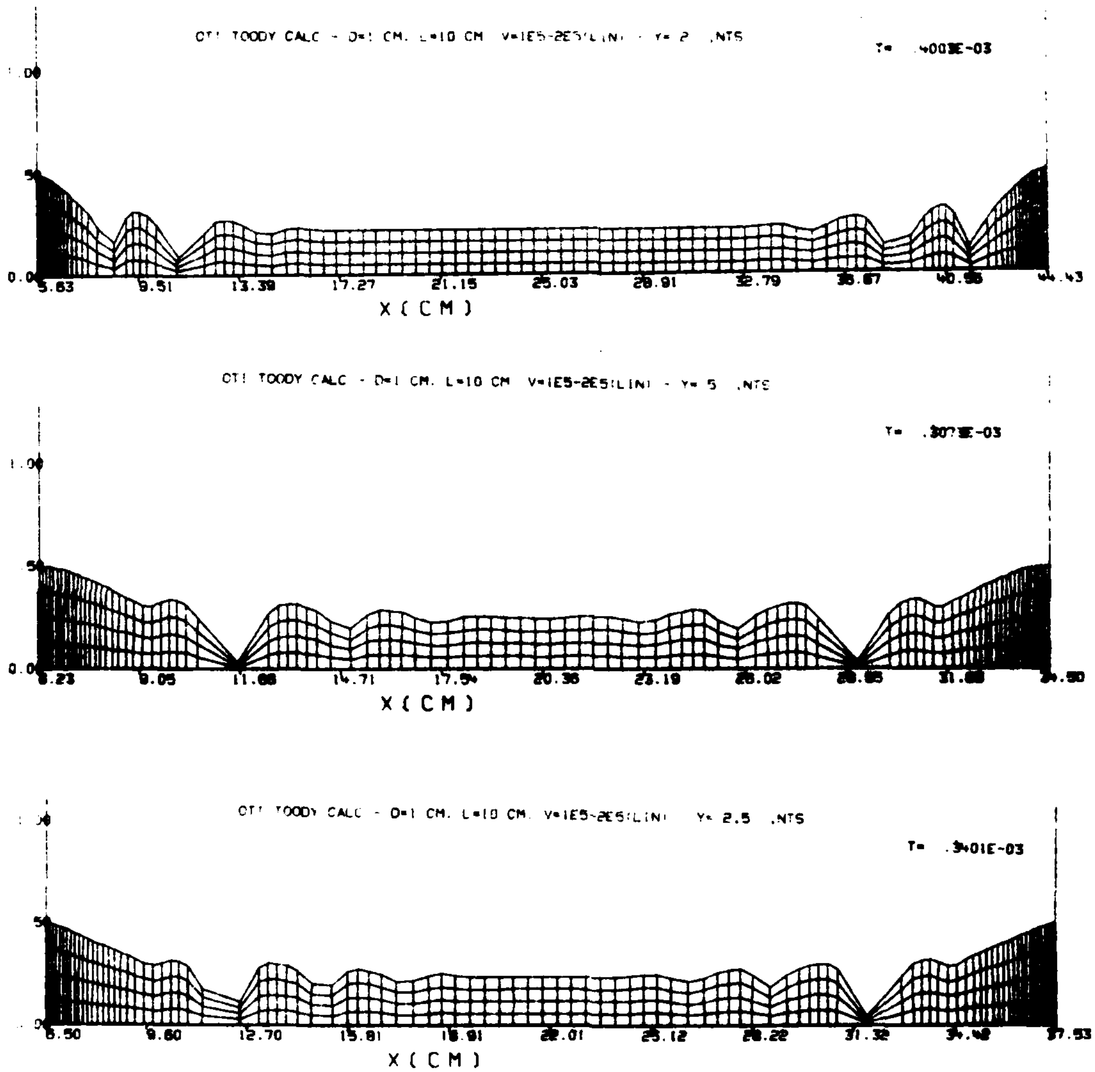

Figure 19. Grid Plots for 10-cm-Long Uranium Rods at 300 to 400 Microseconds

a density of 19.0 gm/cc, a bulk sound speed of 2.42×10^5 cm/sec, a shock velocity/particle velocity slope of 1.6, a Gruneisen ratio of 1.6, and a Poisson's ratio of 0.3.

Figure 18 presents the rods at 200 microseconds for three cases. The top plot is for an elastic/perfectly plastic yield strength of 2 Kb, the middle rod raises this to 5 Kb, and the bottom plot is for a linearly work hardening material. The work hardening material initial yield strength is 2 Kb, and it rises to a saturation level of 5 Kb at a strain of 50 percent. The work hardening rod and the 5-Kb rod appear very much alike at this time. This similarity is expected since the work hardening material is limited to 5 Kb in strength. The 2-Kb rod is significantly different. The elastic segments are not as large as those in the other rods, and the number of necks is reduced at this time. Figure 19 presents later time plots for these same cases. Again, the 5 Kb and the work hardening rods are very similar at times close to 300 microseconds. The time in seconds is indicated on each plot. The 2-Kb rod is pictured at 400 microseconds. It still has a long central section stretching plastically, whereas the other rods have virtually completed necking.

Figure 20 is the same staballoy rod at 400 microseconds but with no limit on the work hardening yield strength. A tangent modulus of 6 Kb is used, but there is assumed to be no saturation stress level in the material. Neck formation is considerably retarded over the 2 Kb case. Necks have begun to form at 400 microseconds but are of very limited radial extent.

A zero yield strength copper rod stretching under a $1\times10^4\ \mathrm{sec}^{-1}$ gradient is shown in Figures 21 and 22. There is only slight velocity retardation at the ends, and there is no necking whatsoever. The grid plots in Figure 21 show the rod at 0, 150 and 230 microseconds. The velocity versus axial position plot in Figure 22 is at 230 microseconds.

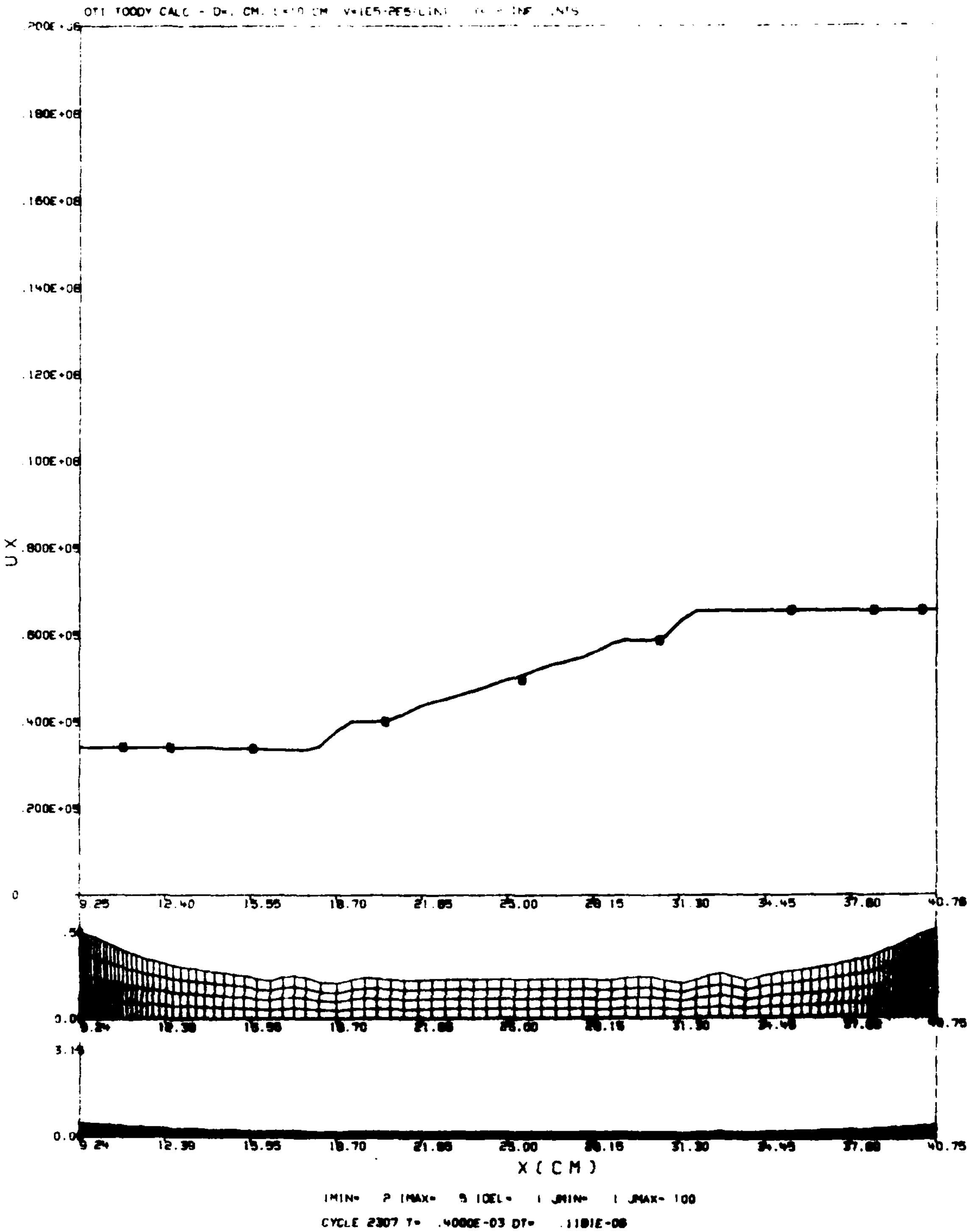

Figure 20. Grid and Velocity Plot for Staballoy Rod with Infinite Work Hardening at 400 Microseconds

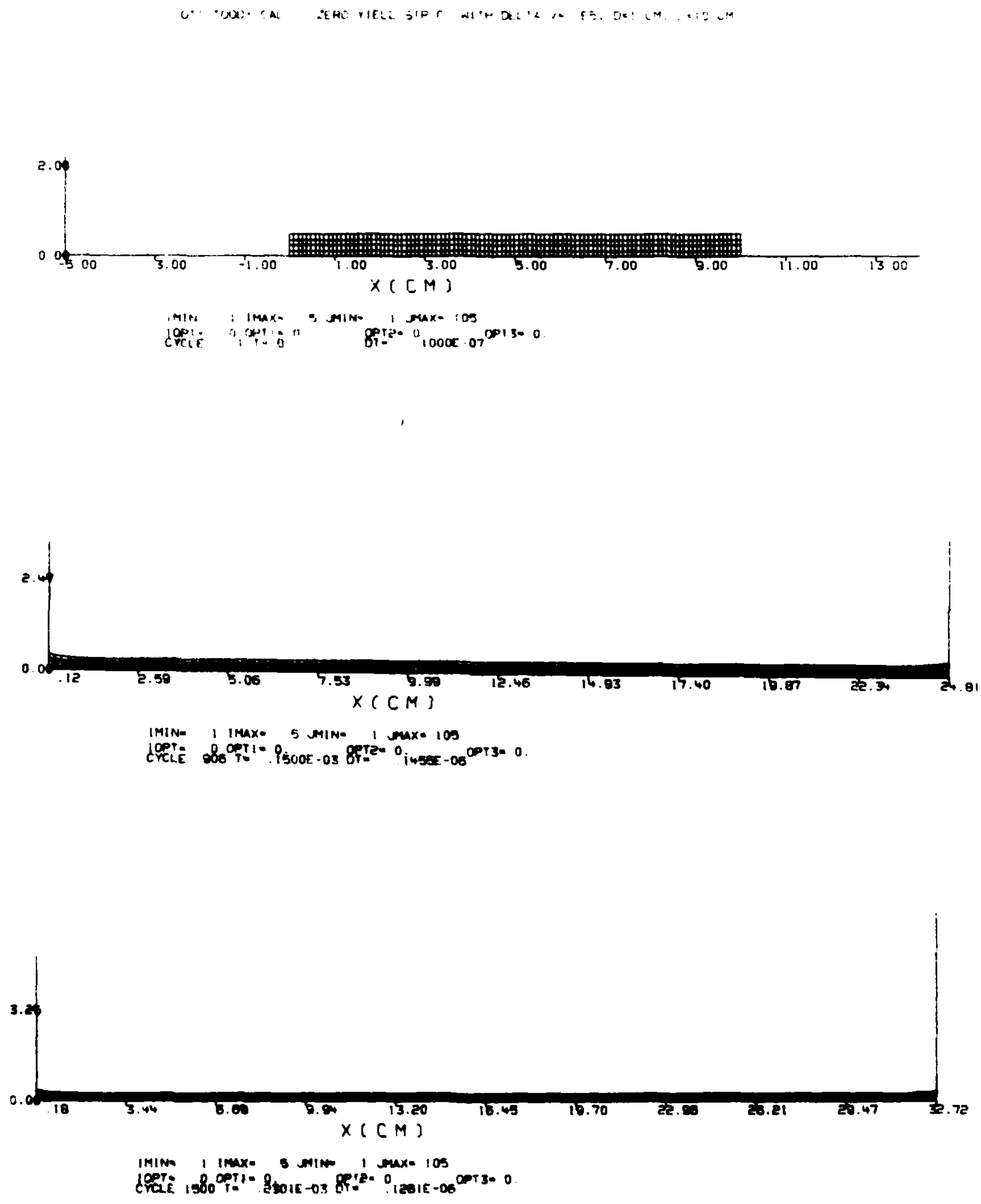

Figure 21. Grid Plots for Copper Rod with Zero Yield Strength

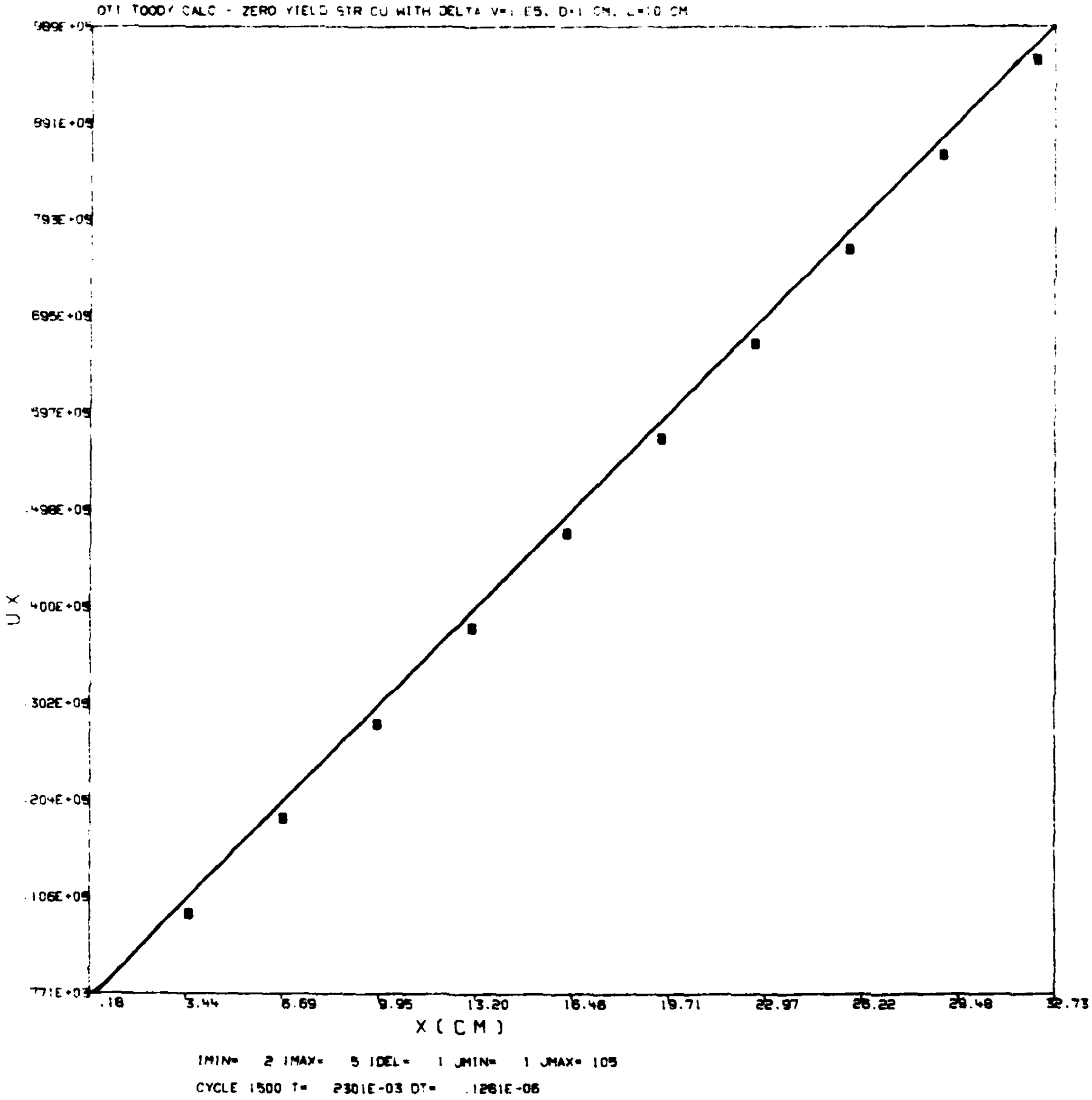

Figure 22. Velocity Plot at 230 Microseconds for Copper Rod with Zero Yield Strength

The calculations presented in Figures 23 and 24 illustrate the almost nonexistent effect of material sound speed on rod deformation. Figure 23 shows one-half of a copper rod with a yield strength of 5 Kb and the normal sound speed of 4×10^5 cm/sec at 200 microseconds. The velocity gradient is 1×10^4 cm/sec, and the rod was initially 10 cm in length. At 200 microseconds just one-half of the rod is almost 10 cm in length. Two necks exist, and the stabilized elastic segments are travelling at 3.4×10^4 cm/sec, 4.1×10^4 cm/sec, and 5.0×10^4 cm/sec. Elastic velocity for the three segments seen in the half-rod picture are 3.4×10^4 cm/sec, 4×10^4 cm/sec, and 4.85×10^4 cm/sec. These velocities are within 3 percent of those seen in Figure 21. Clearly then, sound speed has little effect on the rod's deformation.

Varying density does have an effect as one can see by comparing the staballoy rod in Figure 18 with the 5-Kb copper rod in either Figure 23 or 24. It is more dramatically illustrated in Figures 25 through 28. These figures are one-half rod grid and velocity plots for an aluminum rod stretching under a 1×10^4 sec^{-1} gradient. The plots show the lower velocity end of the rod at 40, 80, 140, and 200 microseconds. The aluminum has a density of 2.7 gm/cc, a bulk sound speed of 5.4×10^5 cm/sec, a shock velocity/particle velocity slope of 1.34, a Gruneisen ratio of 2.1, a Poisson's ratio of 0.33, and a yield strength of 3 Kb. At 200 microseconds a 5-Kb copper rod with identical initial conditions has formed 6 elastic segments with the first segment from each end being approximately 5 cm in length. The 3-Kb aluminum, at 200 microseconds, has formed only 2 elastic segments, and each segment is almost 8 cm in length. The grid and velocity plot at 140 microseconds (Figure 27) shows that a second set of elastic segments briefly formed but were not sustained.

In the next section a simplified model will be presented which explains all of the phenomena seen in these rod calculations with density and yield strength as the only material properties affecting deformation and necking. The calculations and the model both predict that necking advances from the

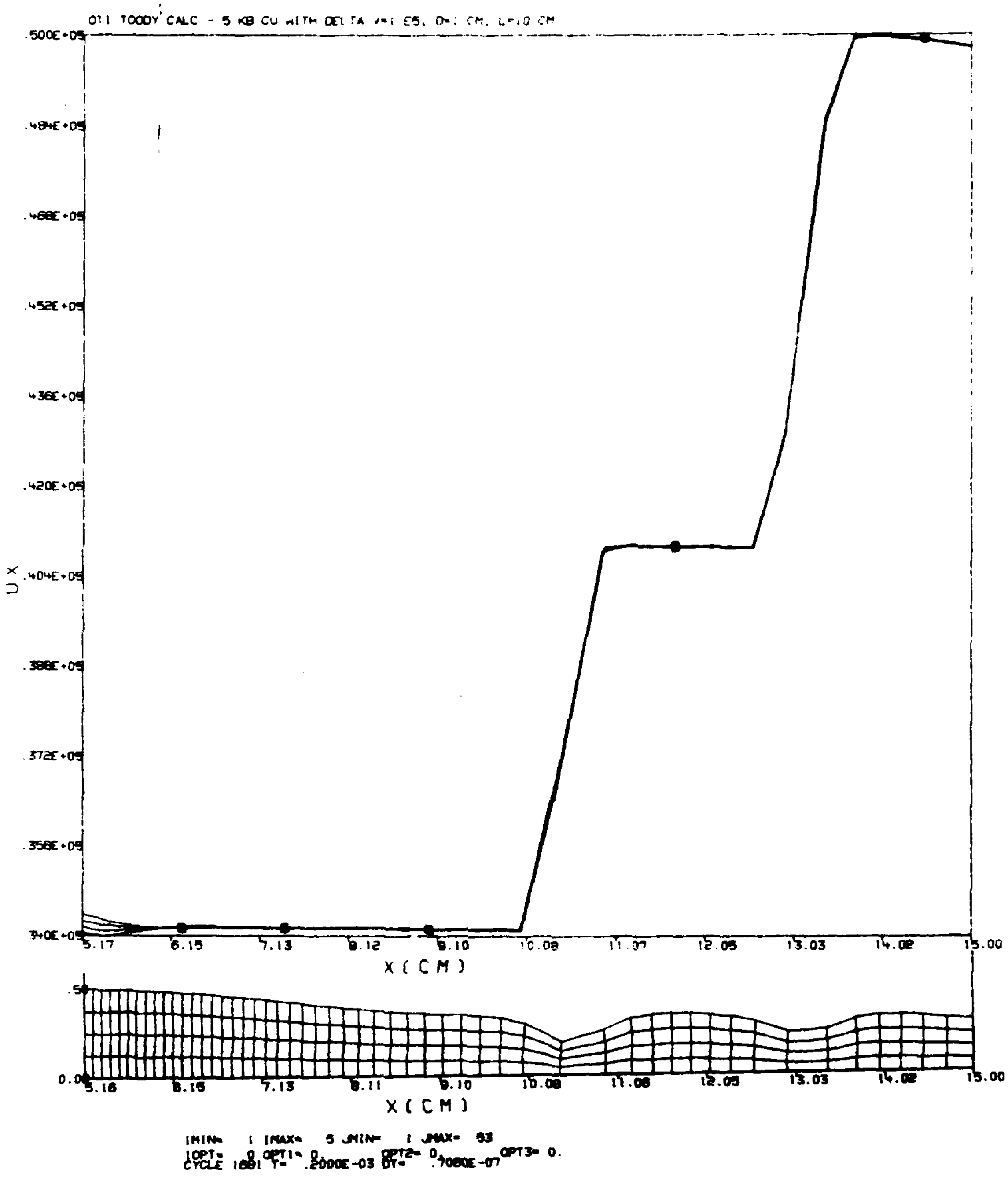

Figure 23. Grid and Velocity Plot at 200 Microseconds 5-Kb Copper with 1×10^4 sec^{-1} Gradient and 4×10^5 cm/sec Sound Speed

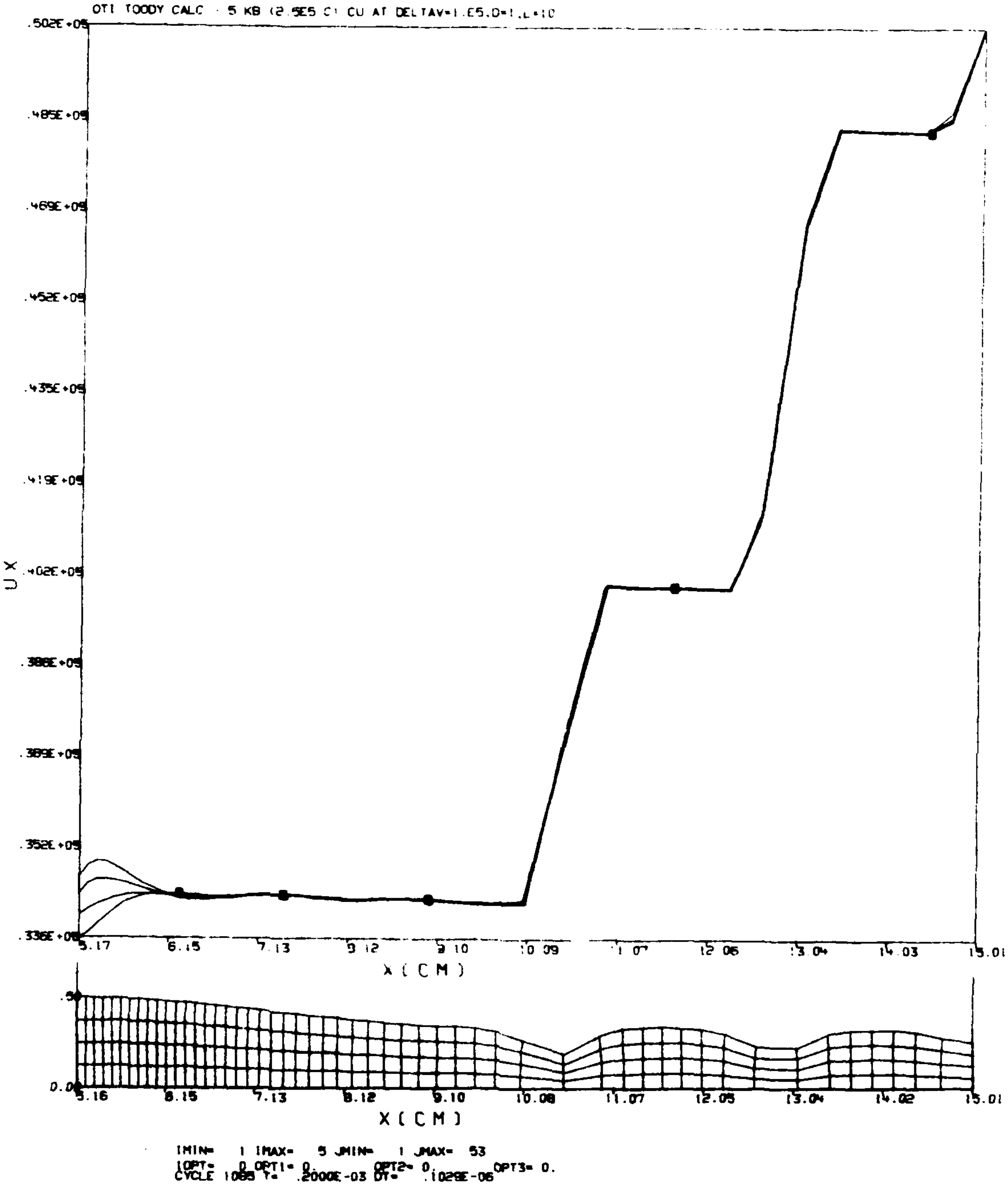

Figure 24. Grid and Velocity Plot at 200 Microseconds - 5-Kb Copper with 1x10^{4} sec^{-1} Gradient and 2.5x10^{5} cm/sec Sound Speed

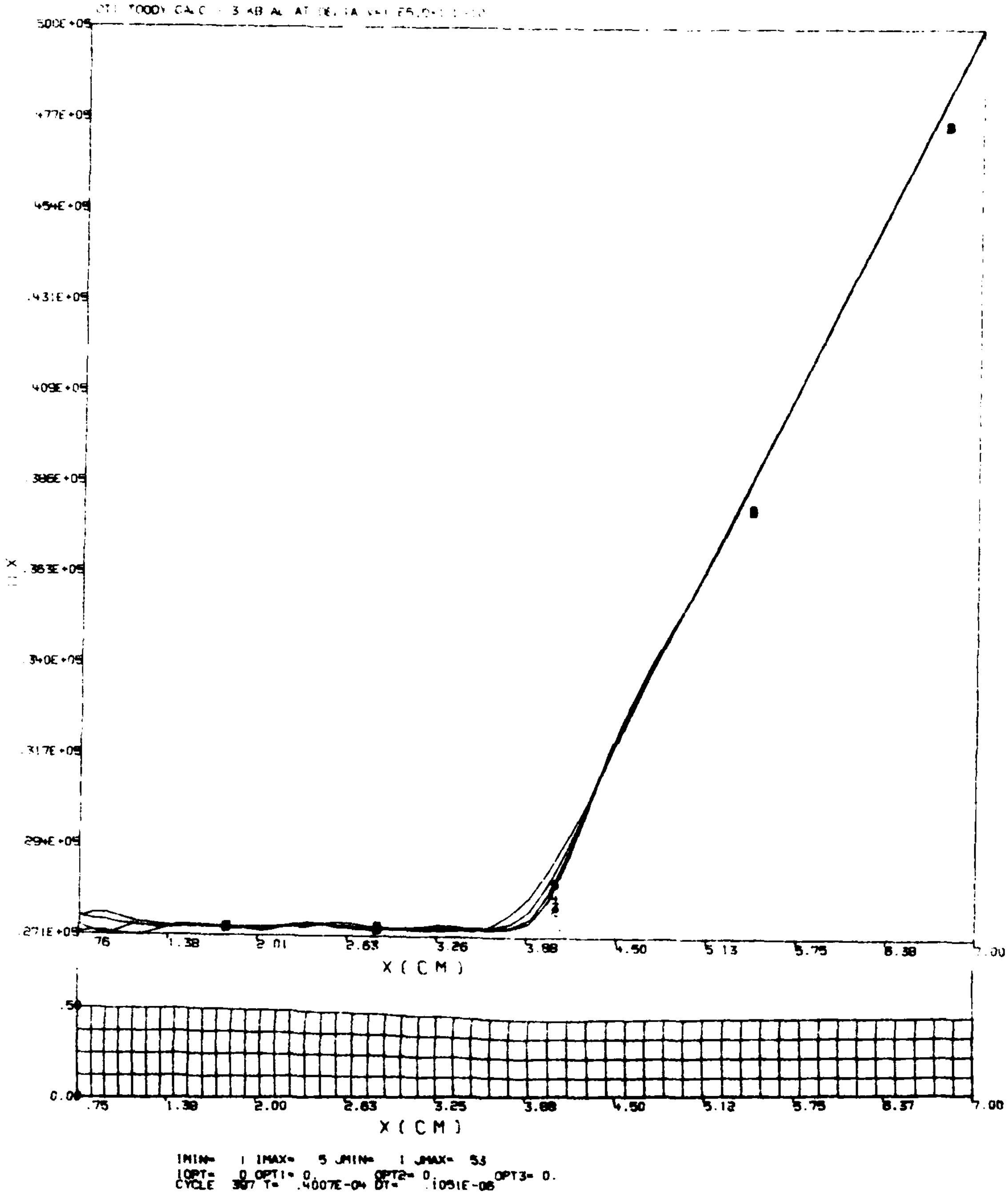

Figure 25. Grid and Velocity Plot for 3-Kb Aluminum at 40 Microseconds

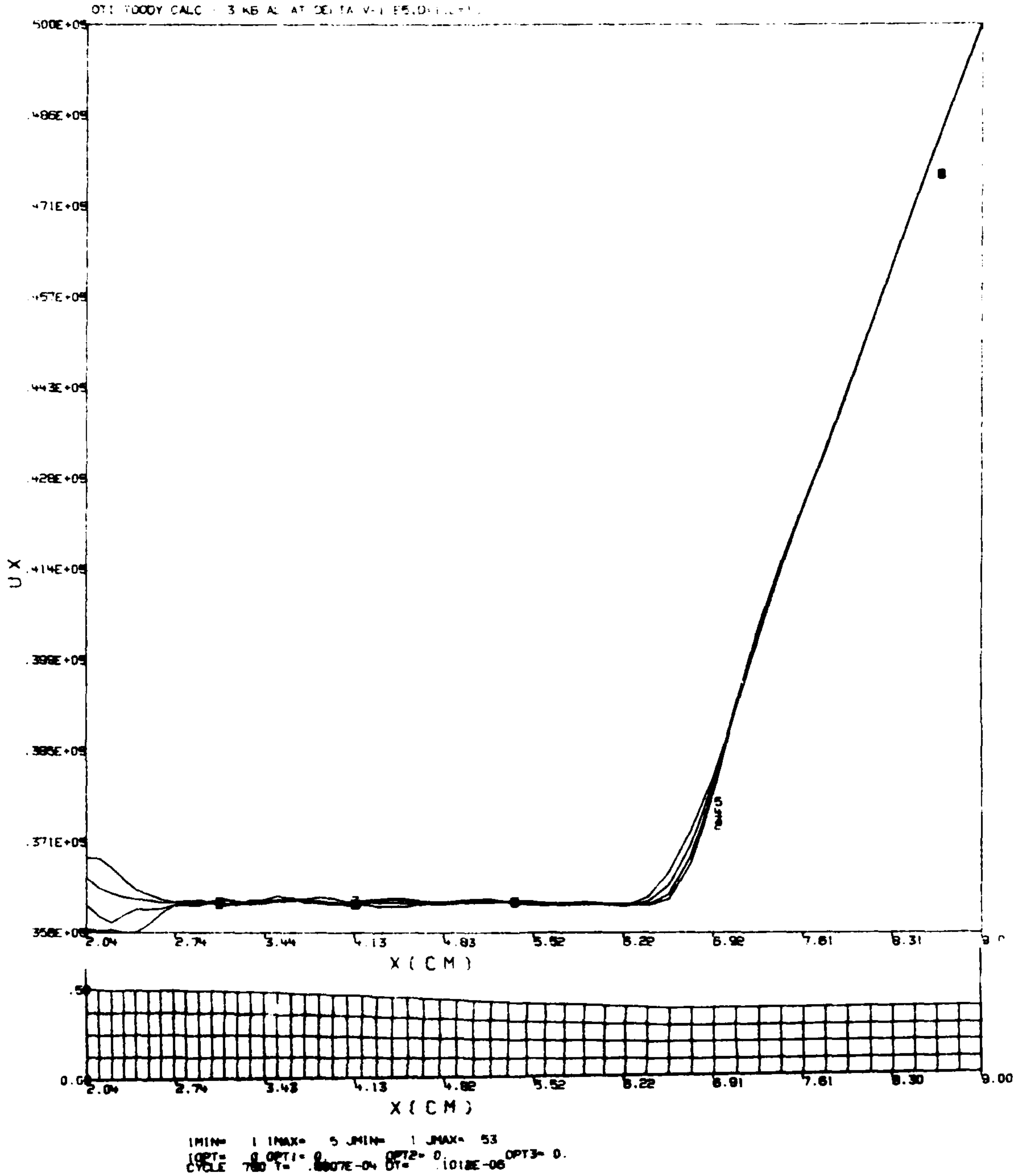

Figure 26. Grid and Velocity Plot for 3-Kb Aluminum at 80 Microseconds

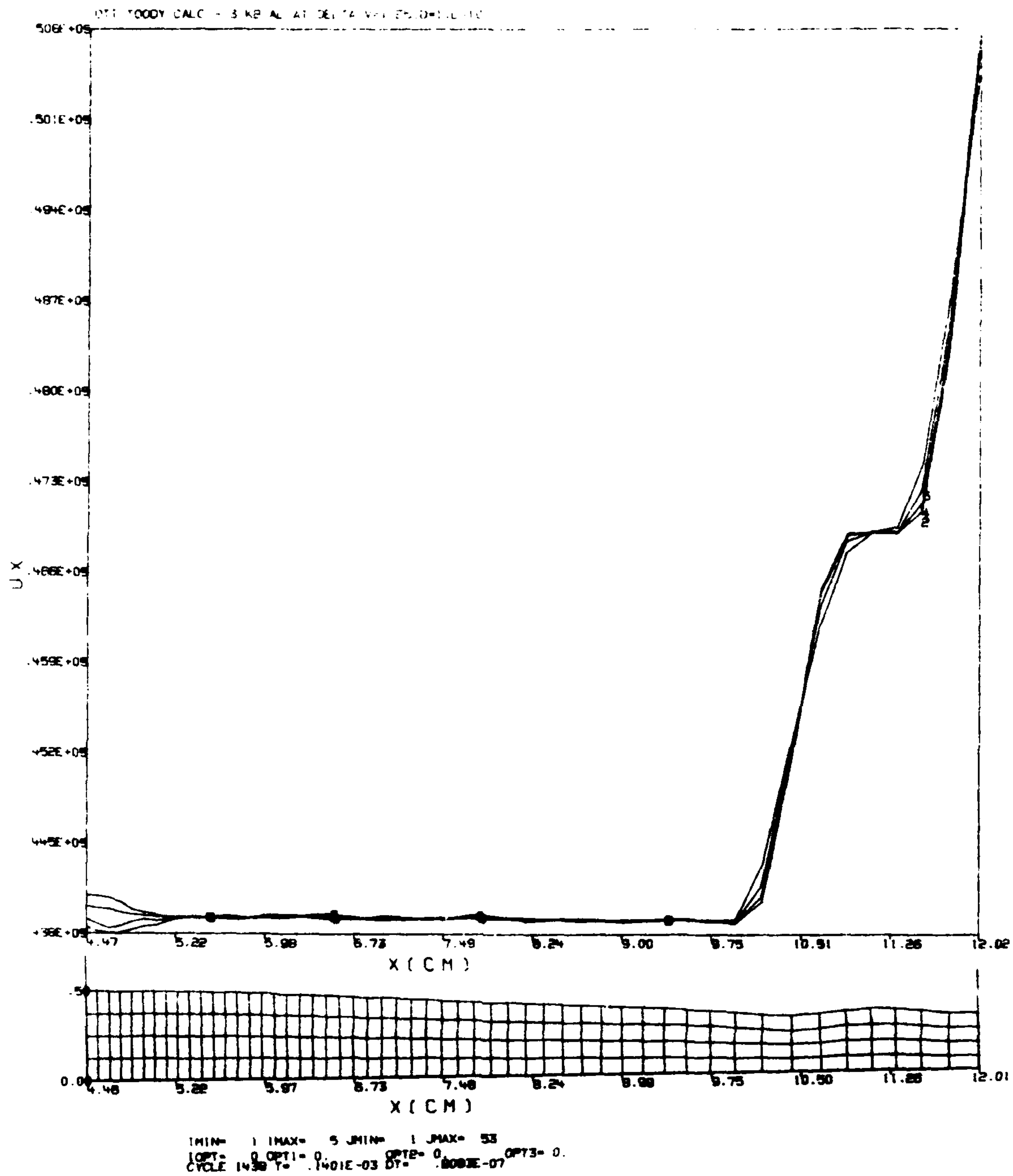

Figure 27. Grid and Velocity Plot for 3-Kb Aluminum at 140 Microseconds

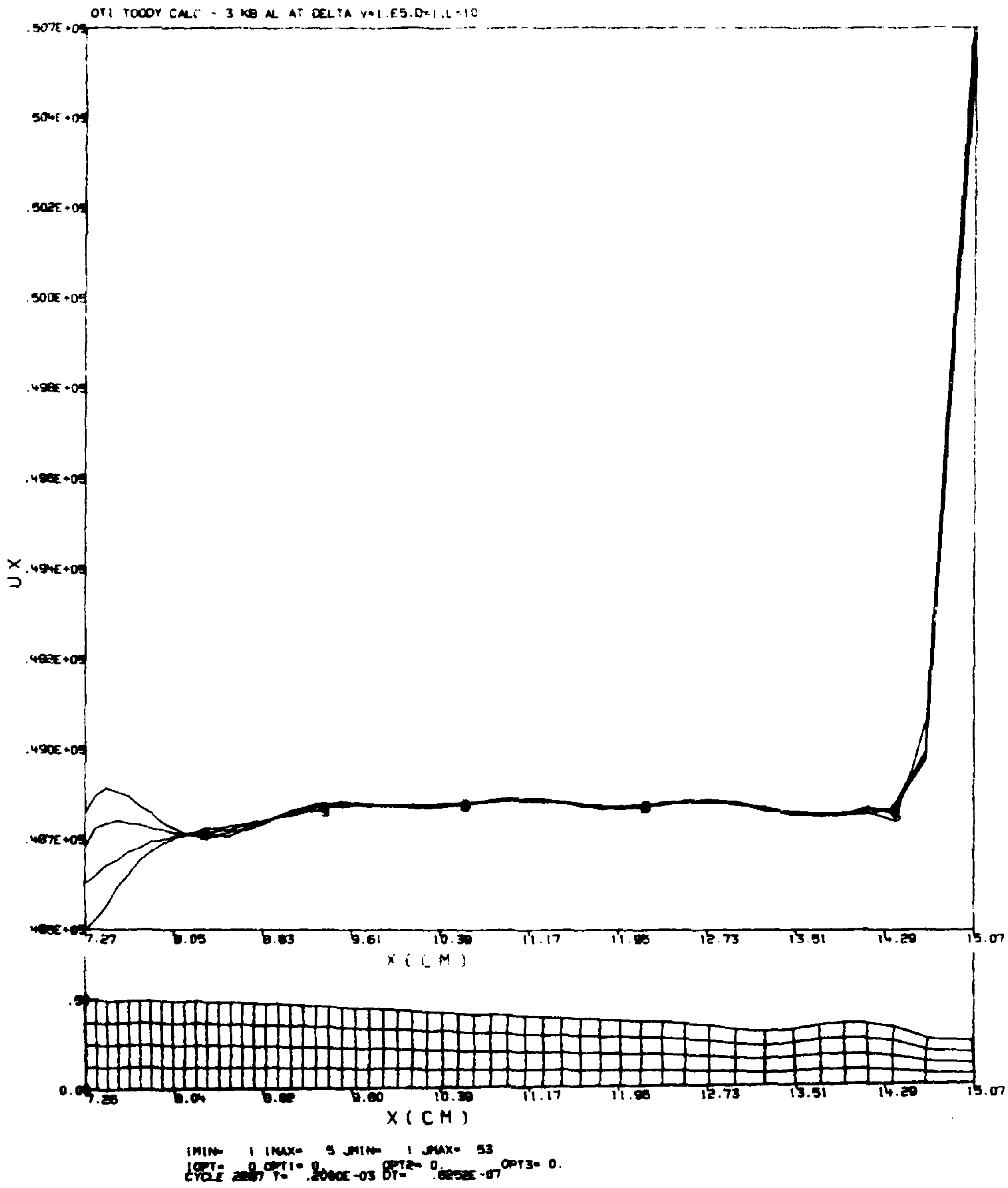

Figure 28. Grid and Velocity Plot for 3-KL Aluminum at 200 Microseconds

ends of the rod slowly toward the center. Observation of jets from hemispherical liners indicates that this model does duplicate phenomenon seen in initially constant diameter rods with linear velocity gradients. The calculations and model indicate that necking and fracture which initiates at any other locations first is caused by sharp changes in shape (mass) or in the velocity gradient itself.

SECTION III

A SIMPLIFIED MODEL

In this section, a model will be developed which explains the phenomena seen in the rod-stretching calculations. Comparisons with the calculations indicates that the model is extremely accurate in predicting many of the details of deformation and necking. It is currently limited to initially constant diameter rods with linear velocity gradients. The fundamental differential equations include all cases of interest, and it is a relatively simple task to expand the model beyond these limitations. The model explains necking and breakup phenomena observed in shaped-charge jets with recourse to none but the most basic physics equations.

Figure 29 defines nomenclature to be used in model development. The figure shows a velocity versus axial position plot at a time when many necks have been formed. Elastic segments exist between axial positions $X_{i,0}$ and $X_{i,1}$ where i is the number of the segment beginning with unity at the lower velocity end. These values are functions of time. Initial values will be indicated as $X_{i,j}(0)$. Velocity will always be assumed to be initially zero at the lower velocity end of the rod, and initial rod position will be assumed to be zero at this location. These assumptions cause no loss of generality but merely require that constants be added to velocities and positions computed using the model.

The velocity gradient, $\frac{\partial v}{\partial X}$, is designated as K. Initial velocity gradient is K(0). Y is the flow stress of the rod and can be a function of strain and/or internal energy. The density of the rod is ρ and is assumed to remain constant. The cross-sectional area is designated as A and is A(0) initially.

Consider the formation of the first elastic segments at each end. The velocity of the first segment on the low velocity end of the rod will be $V_1(t)$. The velocity of the first segment on the high velocity end of the rod will be $V_n(t)$. Conservation of momentum in an initially constant diameter rod

NOMENCLATURE/DEFINITIONS

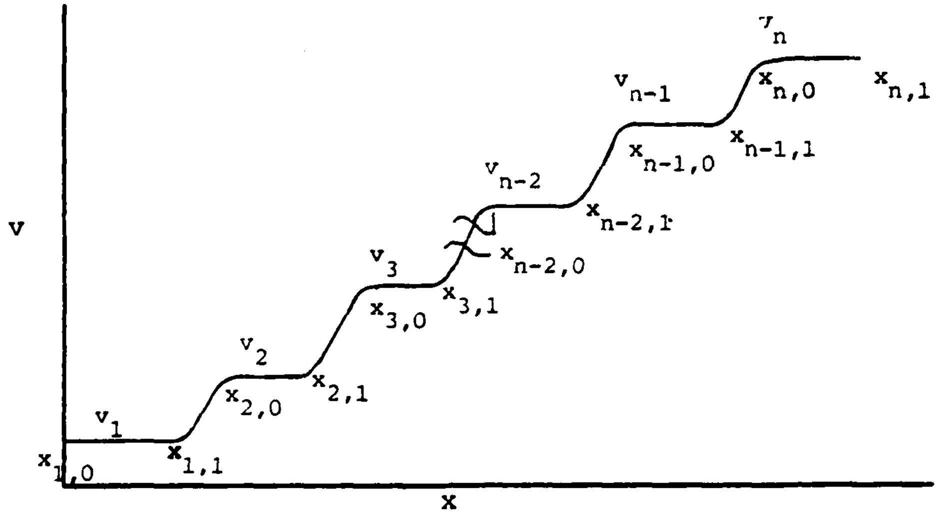

$X_{i,k}$ ARE FUNCTIONS OF TIME

INITIAL POSITIONS VARY FROM $X_{1,0}(0)$ TO $X_{n,1}(0)$

$K(0) \equiv \frac{\partial v}{\partial x}\ (t=0)$

Y = FLOW STRESS OF THE ROD

ρ = DENSITY OF THE ROD

A(t) = ROD CROSS SECTIONAL AREA AT TIME t

A(t=0) = INITIAL CROSS SECTIONAL AREA

Figure 29. Model Nomenclature and Definitions

stretching under a linear gradient requires that:

$$V_n(t) = K(0)X_{n,1}(0) - V_1(t) \tag{1}$$

In other words, the velocity gain at the lower velocity end of the rod must be equal to the velocity loss at the high velocity end.

There are two methods available for solving for $V_1(t)$ and, through Equation (1), for $V_n(t)$. The simplest is to consider a balance of forces across the interface between the elastic end segments and the plastic, still-stretching central section. Considering the lower velocity, V_1, and setting elastic segment deceleration equal to the force at the interface provides the equation:

$$M \frac{dV_1(t)}{dt} = YA(t) \tag{2}$$

where Y is the yield strength of the material at the interface and M is the mass of the constant-velocity, elastic segment.

The mass, M, can be most easily written in terms of the mass in initial, or Lagrangian, coordinates.

$$M = \rho A(0)X_{1,1}(0) \tag{3}$$

Equation (3) assumes that $X_{1,0}(0)$ is 0 and that the rod has a constant diameter at t=0. The constant-volume, plastic stretching in the central rod section requires that:

$$A(t) = A(0)/(1+K(0)t) \tag{4}$$

substituting Equations (3) and (4) into Equation (2) provides:

$$\rho A(0)X_{1,1}(0) \frac{dV_1(t)}{dt} = YA(0)/(1+K(0)t) \tag{5}$$

The quantity $X_{1,1}(0)$ can be written as:

$$X_{1,1}(0) = V_1(t)/K(0)$$

which reduces Equation (5) to:

$$V_1(t)\,\frac{dV_1(t)}{dt} = \left(\frac{Y}{\rho}\right) K(0)/(1+K(0)t) \tag{6}$$

Equation (6) can be integrated from t=0 to t and V_1=0 to V_1 and yields the following relationship for V_1 for the case in which Y is constant.

$$V_1(t) = \left[\left(\frac{2Y}{\rho}\right) \mathrm{Ln}(1+K(0)t)\right]^{1/2} \tag{7}$$

The velocity, $V_n(t)$, of the upper end segment will be the tip velocity of the rod minus $V_1(t)$. The strain in the center rod section will be exactly equal to the strain at the elastic interface until necking becomes predominant. The accumulated strain in the center section can be written as:

$$\varepsilon = -\mathrm{Ln}\ (A(t)/A(0)) \tag{8}$$

With substitution of Equation (4), the strain can be written as:

$$\varepsilon = -\mathrm{Ln}\ (1/(1+K(0)t)) = \mathrm{Ln}\ (1+K(0)t) \tag{9}.$$

For a work-hardening material, then, the value of Y at the interface can be written:

$$Y = Y_o + T_M\ \mathrm{Ln}\ (1+K(0)t) \tag{10}$$

where Y_o is the initial yield strength and T_M is the tangent modulus. Substitution of Equation (10) into Equation (6) and integration yields:

$$V_1(t) = \left\{2\mathrm{Ln}\ (1+K(0)t) \left[\frac{Y_o}{\rho} + \frac{T_M}{2\rho}\ \mathrm{Ln}\ (1+K(0)t)\right]\right\}^{1/2} \tag{11}$$

If Y is also a function of internal energy density, Equation (6) can be solved by including the appropriate functional relationship. The internal energy is simply the strain energy developed as the rod stretches. It can be written as:

$$\int_{\tau} Y(\varepsilon, I)\, \varepsilon\, d\tau / M \tag{12}$$

where τ is the volume under consideration, M is the mass of material in the volume, and I is the internal energy density. The difficulty of incorporating energy dependence into Equation (6) is determined by the complexity of the functional relationship between Y and I.

Consider the case of a very simple relationship:

$$Y = Y_o\ (1 - I/I_M) \tag{13}$$

where I_M is melt energy density. The internal energy density, I, is that existing at the interface which is equal to that existing over the uniformly-stretching center section of the rod. For this relatively simple case Equation (12) can be written as:

$$\begin{aligned} I &= Y\ \varepsilon/\rho \\ &= Y_o\ (1-I/I_M)\ \mathrm{Ln}\ (1+K(0)t)/\rho \end{aligned} \tag{14}$$

Equation (14) can be solved for I to provide:

$$I = \frac{Y_o \mathrm{Ln}(1+K(0)t)/\rho}{1+I_M Y_o \mathrm{Ln}(1+K(0)t)/\rho} \tag{15}$$

Equation (13) then becomes:

$$Y = Y_o\ \left(1 - \frac{Y_o \mathrm{Ln}(1+K(0)t)/\rho}{1+I_M Y_o \mathrm{Ln}(1+K(0)t)/\rho}\right) \tag{16}$$

Substituting Equation (16) into Equation (6) and integrating yields:

$$V_1(t) = \left\{ \frac{2Y_o}{\rho} Ln(1+K(0)t) \left[1 - \frac{\frac{Y_o}{\rho} Ln(1+K(0)t)}{I_M(1 + \frac{Y_o}{\rho I_M} Ln(1+K(0)t))}\right]\right\}^{1/2} \tag{17}$$

Equations (7), (11,) and (17) were compared with values of V_1 from rod calculations, several of which were discussed in the previous section. The comparisons are contained in Table 1. All comparisons are within 6 percent, and most are within 1 percent.

The position, $X_{1,1}(t)$, of the interface can be predicted from:

$$X_{1,1}(t) = X_{1,1}(0)(1+K(0)t) \tag{18}$$

where:

$$X_{1,1}(0) = V_1(t)/K(0)$$

The accuracy of this position prediction is again within a few percent until very late times when it diverges slightly from the calculations. The divergence is caused by the necking process. Equation (18) assumes that stretching continues at a constant rate. When a second elastic segment is formed, the comparison begins to diverge because the local gradient is no longer exactly equal to the gradient in the central, plastic region of the rod. Table 2 provides a comparison between some calculated $X_{1,1}(t)$ values and those predicted by Equation (18).

TABLE 1. MODEL/CALCULATION COMPARISONS FOR V_1

Rods With Diameter = 1 cm and Length = 10 cm

Material	Y(Kb)	K(0)(sec^{-1})	T(μsec)	Simple Model V_1(km/sec)	Calculation V_1(km/sec)
Aluminum	3	$1x10^4$	40	0.27	0.27
			80	0.36	0.36
			140	0.44	0.44
			200	0.49	0.49
Copper	2	$1x10^4$	160	0.20	0.21
			200	0.22	0.22
Copper	5 with linear thermal stretching and $I_M=1x10^9$ ergs/gm	$1x10^4$	50	0.19	0.20
			100	0.24	0.25
			200	0.28	0.28
Copper	5 with linear thermal stretching and $I_M=2x10^9$ ergs/gm	$1x10^4$	50	0.20	0.21
			100	0.26	0.27
			150	0.29	0.30
			200	0.31	0.31
Copper	5	$2x10^4$	100	0.35	0.35
Staballoy	5	$1x10^4$	200	0.24	0.24
			322	0.25	0.25
Staballoy	$Y_o=2$	$1x10^4$	150	0.21	0.21
	$T_M=6$		635	0.41	0.40

Rods with Diameter = 1 cm and Length = 20 cm

Material	Y(Kb)	K(0)(sec^{-1})	T(μsec)	Simple Model V_1(km/sec)	Calculation V_1(km/sec)
Copper	5	$1x10^4$	240	0.37	0.35

TABLE 2. MODEL/CALCULATION COMPARISONS FOR $X_{1,1}(T)$

Rods with Diameter = 1 cm and Length = 10 cm

Material	Y(Kb)	K(0)(sec^{-1})	T(μsec)	Simple Model $X_{1,1}(t)$	Calculation $X_{1,1}(t)$
Aluminum	3	$1x10^4$	40	3.8	3.8
			80	6.5	6.5
			140	10.6	10.1
			200	14.7	14.3
Copper	2	$1x10^4$	160	5.0	5.1
			200	6.7	7.8
Copper	5	$1x10^4$	20	1.7	1.7
			140	7.4	7.9
			200	10.5	10.1
Copper	5 with linear thermal softening and I_M=$1x10^9$ ergs/gm	$1x10^4$	50	2.9	3.2
			100	4.7	5.0
			200	8.3	8.9
	5 with linear thermal softening and I_M=$2x10^9$ ergs/gm		50	3.0	3.2
			100	5.1	5.2
			150	7.2	7.8
			200	9.2	9.6
Copper	5	$2x10^4$	100	5.3	5.0
Staballoy	5	$1x10^4$	200	7.2	8.1
			322	10.6	10.9
Staballoy	Y_o=2 T_M=6	$1x10^4$	150	5.3	5.3
			635	30.1	26.6

Rods with Diameter = 1 cm and Length = 20 cm

Copper	5	$1x10^4$	240	12.6	10.2

It is interesting to investigate the effect of material properties on the length of the first stabilized segment at each end of the rod. If L(t) is the length of this segment and $X_{1,0}(0)$ is 0, then:

$$L(t) = X_{1,1}(t) - X_{1,0}(t)$$
$$= X_{1,1}(0)(1+K(0)t) - \int_0^t V_1(t)dt$$
$$= \frac{V_1}{K(0)}(1+K(0)t) - \int_0^t V_1(t)dt$$

Substituting V_1 from Equation (7),

$$L(t) = \left(\frac{2Y}{\rho}\right)^{1/2} \left\{\frac{[Ln(1+K())t)]^{1/2}(1+K(0)t)}{K(0)} - \int_0^t \left[Ln(1+K(0)t)\right]^{1/2} dt\right\} \quad (19)$$

Inspection of Equation (19) indicates that L decreases as Y decreases and that it decreases as ρ increases. Longer initial segments can then be expected for high strength, low density materials. As a specific example, compare copper with staballoy. If each has a 5-Kb-yield strength, then Equation (19) provides an L of 4.5 cm for copper and 3.07 cm for staballoy at a strain of 90 percent, assuming an initial gradient of $1x10^4$ sec^{-1}. If both have a 1-Kb yield strength, then the L for copper is 2 cm and that for staballoy is 1.4 cm at a time when the strain in the plastic section of the rod is 90 percent. The time for a strain of 90 percent can be calculated from Equation (9), given the gradient. For $K(0)=1x10^4$ sec^{-1} this time is 146 microseconds. Comparing copper and aluminum shows that the aluminum length is always greatest. For example, at 200 microseconds, a 5-Kb copper has an L of 4.9 cm whereas a 3-Kb aluminum would have an L of 7.14 cm, given an initial gradient of $1x10^4$ sec^{-1}. If the aluminum also had a 5-Kb-yield strength, its stabilized segment length would be $(5/3)^{1/2}$ times the length at 3 Kb, or 9.2 cm.

This result is reasonable physically. It says simply that more rod will become elastic if the yield strength is greater or if the mass of the rod is lower. Whether this is advantageous from a jet penetration standpoint is another issue. In the real world it appears that tradeoffs occur between density and yield strength. For example, staballoy is more dense than copper, but it also has a higher yield strength. Copper is more dense than aluminum, but copper has a higher yield strength. Effects within a target favor the higher density material even though necking and fracture may be more inhibited in a lighter density material.

These equations can also be used to investigate the effects of velocity gradient on the length of the first elastic segments. The length decreases as velocity gradient increases. This again is physically reasonable since the relief wave velocity is opposed by the stretching velocity of the rod. For example, the length of the first elastic segment is 4.5 cm for copper at a yield strength of 5 Kb and a strain of 90 percent and a velocity gradient of $1x10^4$ sec^{-1}. The length becomes 2.3 cm if the gradient increases to $2x10^4$ sec^{-1}, and it drops to 1.1 cm if the gradient is $4x10^4$ sec^{-1}. For staballoy under the same conditions, the lengths are 3.1, 1.6 and 0.8 cm.

It was mentioned earlier in this section that there are two methods for deriving Equation (7). The first method was balancing force across the elastic/plastic interface. The second method involves balancing energy for the entire rod. The method will be presented here for the insight it provides into energy transfer mechanisms.

The initial energy in the rod is given by:

$$E(o) = \frac{1}{2}\int V^2 dm = \frac{1}{2}\int V^2 \rho A(0) dx(0)$$

Substitution of:

$$V = K(0)x(0)$$

provides the equation:

$$E(0) = \frac{1}{2} \int_0^{X_{n,1}(0)} \rho A(0)\ K(0)^2\ X(0)^2\ dX(0) \tag{20}$$

Integration yields:

$$E(0) = \frac{1}{6}\ \rho A(0)\ K^2(0)\ X^3_{n,1}(0) \tag{21}$$

where it has been assumed that $X_{1,0}(0) = 0$, i.e., that the initial Lagrangian coordinate of the rod is 0.

The energy in Equation (21) must be balanced, at any time, by the kinetic and internal energy in the rod. The kinetic energy in the still-stretching plastic center of the rod can be written as:

$$KE_2 = \rho A(0)\ K(0)^2\ (X^3_{n,o}(0) - X^3_{1,1}(0))/6. \tag{22}$$

The internal energy of the section is:

$$I_2 = \int_{X_{1,1}(0)}^{X_{n,o}(0)} Y\ Ln\ (1+K(0)t)\ A(0)\ dX(0)$$

$$I_2 = YA(0)\ (X_{n,o}(0) - X_{1,1}(0)\ Ln\ (1+K(0)t) \tag{23}$$

The kinetic energy of the stabilized elastic segment at the lower velocity end of the rod is:

$$KE_1 = \frac{1}{2}\ \rho A(0)\ X_{1,1}(0)\ V_1^2 \tag{24}$$

assuming $X_{1,0}(0) = 0$. The internal energy of this segment can be approximated by assuming that the axial stress and strain vary linearly from zero values at $X(0)=0$ to the plastic values at $X(0)=X_1(0)=V_1/K(0)$. The stress at the elastic/plastic interface is the yield strength, Y. The strain is $Ln(1+K(0)t)$. Therefore:

$$I_1 = \int_o^{X_{1,1}(0)} \sigma(X)\ \varepsilon(X)\ A(0)\ dX(0) \tag{25}$$

$$= \int_o^{X_{1,1}(0)} \frac{YX(0)}{X_{1,1}(0)} \cdot \frac{Ln(1+K(0)t)X(0)}{X_{1,1}(0)}\ A(0)dX(0)$$

$$= YA(0)\ Ln(1+K(0)t)\ X_{1,1}(0)/3.$$

For the elastic segment at the upper velocity end of the rod, the kinetic energy is:

$$KE_3 = \frac{1}{2}\rho A(0)\ (X_{n,1}(0) - X_{n,o}(0))\ V_n^2 \tag{26}$$

and the internal energy, I_3 is:

$$I_3 = YA(0)\ \text{Ln}\ (1+K(0)t)\ (X_{n,1}(0) - X_{n,o}(0))/3. \tag{27}$$

setting:

$$KE_1 + I_1 + KE_2 + I_2 + KE_3 + I_3 = E(0)$$

and making the substitutions:

$$V_n = X_{n,1}(0)\ K(0) - V_1$$

and

$$X_{n,o}(0) = X_{n,1}(0) - X_{1,1}(0)$$

The equation can be solved for V_1 as given by Equation (7). Energy is balanced completely in Equation (28) by the appearance of the two end elastic segments. It is transferred from the upper velocity end of the rod to the lower velocity end. Table 3 provides internal and kinetic energies for the three sections of the rod at different times for a 5-Kb copper rod, 10 cm in length, 1 cm in diameter with a velocity gradient of $1x10^4$ sec^{-1}. The table shows that energy is transferred from the central plastically-stretching section to both ends of the rod, providing the additional kinetic and internal energies required to stabilize these end sections. The rate of total energy transfer is changing with time. The rate of energy transfer virtually stabilizes quickly in terms of energy density (energy per unit mass). Initially, the transfer rate is $5.56x10^{13}$ ergs/gm/sec. By 50 microseconds it has been reduced, somewhat, to $4.8x10^{13}$, by 100 microseconds it is reduced to $4.66x10^{13}$, and it changes very little thereafter.

TABLE 3. ENERGY TRANSFER

Copper Rod with $Y = 5$ Kb, $L = 10$ cm, $D = 1$ cm, $K(0) = 1\times10^{4}$ $\sec^{-1}$

Total initial energy is 1.165×10^{11} ergs

Time (μsec)	I_1 (ergs)	KE_1 (ergs)	I_2 (ergs)	KE_2 (ergs)	I_3 (ergs)	KE_3 (ergs)
0	0	0	0	11.65×10^{10}	0	0
50	0.113×10^{10}	0.340×10^{10}	0.913×10^{10}	5.56×10^{10}	0.113×10^{10}	4.62×10^{10}
100	0.253×10^{10}	0.760×10^{10}	1.20×10^{10}	4.11×10^{10}	0.253×10^{10}	5.07×10^{10}
150	0.385×10^{10}	$1.16.10^{10}$	1.29×10^{10}	3.26×10^{10}	$0.385.10^{10}$	5.17×10^{10}
200	0.505×10^{10}	1.52×10^{10}	1.28×10^{10}	2.67×10^{10}	0.505×10^{10}	5.17×10^{10}
250	0.615×10^{10}	1.85×10^{10}	1.23×10^{10}	2.23×10^{10}	0.615×10^{10}	5.12×10^{10}

Time (μsec)	I_1+KE_1 (ergs)	I_2+KE_2 (ergs)	I_3+KE_3 (ergs)
0	0	11.65×10^{10}	0
50	0.453×10^{10}	6.473×10^{10}	4.733×10^{10}
100	1.013×10^{10}	5.310×10^{10}	5.323×10^{10}
150	1.545×10^{10}	4.550×10^{10}	5.555×10^{10}
200	2.025×10^{10}	3.950×10^{10}	5.675×10^{10}
250	2.465×10^{10}	3.460×10^{10}	5.735×10^{10}

It is a fairly simple matter to demonstrate that energy remains balanced whether elastic segments exist beyond the end segments. The first elastic segments on each end totally satisfy all momentum and energy requirements. Were it not for the effects of neck curvature on the axial stress in the rod, no more necks or elastic segments would be formed. However, neck curvature just beyond the elastic/plastic interface gives rise to a tensile hydrostatic pressure which increases the tensile axial stress in the neck. Since a stress gradient such as this precipitates material acceleration or deceleration, a new wave is formed at the neck. At the low velocity end of the rod this stress gradient is positive toward the center of the rod, giving rise to an acceleration in that direction. Conversely, a small deceleration wave travels into the first elastic segment. This deceleration has little effect on the relatively large first elastic segment. As it advances from the neck toward the center of the rod, mass is accelerated until all of the momentum in the wave is converted. At this point another elastic/plastic interface is formed and the process is repeated. Wave activity at the upper velocity end of the rod is identical except that accelerations become decelerations and vice versa.

The necks at the first elastic/plastic interface begin to become important and influence flow when the acceleration of the interface drops below that induced by the stretching process. The rate of change of velocity due to stretching is approximated by:

$$\frac{dV}{dt} = \frac{\partial V}{\partial X} \cdot \frac{\partial X}{\partial t} = V \frac{\partial V}{\partial X} = \frac{VK(0)}{1+K(0)t} \tag{29}$$

The neck region should begin to develop curvature when:

$$\frac{dV_1}{dt} = \frac{V_1K(0)}{1+K(0)t} \tag{30}$$

Differentiating Equation (7), substituting the derivative into Equation (30) and simplifying yields the equation:

$$\left[Ln(1+K(0)t) \right]^{-1} = 2 \tag{31}$$

which indicates that, for elastic, perfectly plastic materials, the time at which significant curvature occurs is a function of gradient only. The solution to Equation (31) is:

$$t = (e^{0.5} - 1)/K(0) = 0.648/K(0) \tag{32}$$

For $K(0) = 1x10^4 \ sec^{-1}$, Equation (32) predicts that neck curvature will begin at t=64.8 microseconds. Examination of rod calculations indicates that this equation provides a reasonably accurate estimate of the time at which necking becomes important, i.e., the time at which the axial stress begins to exceed the flow stress of the material. The equation is not valid for work hardening or thermally softening materials. Equations for these types of materials can be derived by combining equation Equation (30) with the appropriate equation for V_1.

As curvature in the first neck becomes important, the second neck in from each end begins to form. The neck forms on the central rod section side of a second elastic/plastic front. The velocity of this second elastic/plastic front can be found from equating the acceleration in the first neck region to the difference in forces between the first and second elastic/plastic interfaces.

The equation to solve is:

$$\frac{1}{2} M \left(\frac{dV_1}{dt} + \frac{dV_2}{dt}\right) = YA(t) - M \frac{dV_1}{dt} \tag{33}$$

Substituting:

$$M = \rho\ A(0)\ (X_{2,0}(0) - X_{1,1}(0))$$

$$= \rho\ A(0)\ \left(\frac{V_2}{K(0)} - \frac{V_1}{K(0)}\right)$$

into Equation (33) and regrouping terms yields:

$$(V_2 - V_1)\ \left(3\ \frac{dV_1}{dt} + \frac{dV_2}{dt}\right) = \frac{2YA(t)K(0)}{\rho A(0)} = \frac{2Y}{\rho}\ \frac{K(0)}{1+K(0)t} \tag{34}$$

Equation (29) can be used to approximate the time derivatives in Equation (34), reducing the equation to an arithmetic relationship.

$$(V_2 - V_1)\ (3V_1 + V_2) = 2Y/\rho \tag{35}$$

The solution of Equation (35) is:

$$V_2 = -V_1 + (4V_1^2 + 2Y/\rho)^{1/2} \tag{36}$$

To maintain momentum balance, the corresponding velocity at the upper end (high velocity end) of the rod must be:

$$V_{n-1} = K(0)X_{n,1}(0) - V_2 \tag{37}$$

After the second neck begins to form, a third elastic/plastic interface will begin formation. The equation for the velocity for this third interface will be:

$$V_3 = -V_2 + (4V_2^2 + 2Y/\rho)^{1/2} \tag{38}$$

In general, then, interface velocities will be given by the relationship:

$$V_i = -V_{i-1} + (4V_{i-1}^2 + 2Y/\rho)^{1/2} \tag{39}$$

for interfaces propagated from the rod's lower velocity end. These values can be subtracted from the initial peak velocity, $K(0)X_{n,1}(0)$, to obtain the velocity for the corresponding upper-end interface.

Table 4 provides some comparisons between calculations and the simple model for these velocities at the lower end of the rod. The maximum difference is 7 percent, and most comparisons are much closer. As indicated in the table, in some cases segments have blended into other segments as time increases.

Given a rod velocity gradient and velocities for all elastic/plastic interfaces, one can determine the position of these interfaces at a given time and the mass between interfaces. The hydrocode calculations indicate that these interface positions for second and subsequent rod segments remain in the center of the segment as each elastic region grows.

Given a set of velocity—position elastic/plastic interfaces, one can estimate a yield strength and subsequent segment growth as well as details of the necking between segments.

TABLE 4. SECOND AND GREATER SEGMENT VELOCITY COMPARISONS

Material	Y(Kb)	K(0)(sec^{-1})	T(μsec)	Simple Model Velocities (km/sec) V_1	V_2	V_3	V_4	Calculated Velocities (km/sec) V_1	V_2	V_3	V_4
Rods with Diameter = 1 cm and Length = 20 cm											
Copper	5	$1x10^4$	170	0.33	0.41	0.48	*–	0.33	0.40	0.49	–
			220	0.36	0.43	0.49	0.55	0.35	0.41	0.50	0.57
			240	0.37	0.44	0.51	0.56	0.35	0.42	0.52	0.58
Rods with Diameter = 1 cm and Length = 10 cm											
Staballoy	5	$1x10^4$	200	0.24	0.29	0.34	–	0.25	blended	0.35	–
Staballoy	Y_o=2Kb T_M=6Kb	$1x10^4$	400	0.34	0.38	–	–	0.35	0.40	–	–
Copper	5	$1x10^4$	140	0.31	0.39	–	–	0.31	0.40	–	–
			180	0.34	0.42	0.48	–	0.34	0.41	0.48	–
			200	0.35	0.43	0.49	–	0.35	0.41	0.50	–
Copper	2	$1x10^4$	180	0.22	0.26	0.30	–	0.22	0.28	0.31	–
			200 1st/2nd Segments blended together			0.31	–	–	–	0.31	–
Copper	5	$2x10^4$	80	0.33	0.41	–	–	0.33	0.41	–	–
			120	0.37	0.44	0.50	–	0.37	0.41	0.55	–
			140	0.39	blended	0.52	–	0.39	–	0.56	–

* – means not applicable

SECTION IV
CONICAL RODS

The equations developed in the previous section apply to the situation of an initially constant diameter rod stretching under a linear velocity gradient. In this section, the solution for rods with a variable diameter will be explored. The specific case to be addressed is that of a rod which initially is the frustum of a cone.

Figure 30 shows the TOODY hydrocode initial shape and zoning for a 10-cm long rod with an aft diameter of 2 cm and a forward diameter of 1 cm. The gradient is a linear 1×10^4 sec^{-1}, i.e., the forward tip of the rod is travelling at 1×10^5 cm/sec and the rear of the rod is initially at rest. Because of the shape of the rod, a velocity versus mass curve would not be a linear curve. Instead, more mass would travel at the lower velocities. The rod is copper with a 2-Kb yield strength.

Figures 31 through 38 present grid plots and axial velocity versus length plots for the rod at 40, 80, 120, 160, 200, 240, 280, and 300 microseconds. As in all previous cases, necking begins at the ends of the rods and proceeds toward the center. In this particular case there is not a great deal of difference between the segment velocities in the calculation and those computed from the simple equations of the last section. For example, constant diameter equations would predict that $V_1 = 0.25 \times 10^5$ cm/sec at 300 microseconds. The hydrocode calculation predicts 0.224×10^5 cm/sec. The simple equations predict $V_2 = 0.29 \times 10^5$ cm/sec given the erroneous V_1 of 0.25×10^5, and they predict $V_2 = 0.27x105$ cm/sec given the correct V_1. The hydrocode calculation predicts that V_2 should be 0.26×10^5 cm/sec.

It is apparent in the calculations that the rod assumes a more constant diameter shape as time proceeds so that it would be expected that elastic segment velocities would be more nearly predictable from the constant diameter equations as one proceeds away from the ends of the rod.

Figure 39 is the initial grid plot for a more conically shaped rod. In this case the base, or aft, diameter is 4 cm and the tip diameter is 1 cm. Other rod features are identical to the previous case. Figures 40 through 47 show grid and axial velocity plots at 40, 80, 120, 160, 200, 240, 280, and 300 microseconds. There is far more difference in this case between the hydrocode calculation and the simplified constant diameter equations. For example, it is seen that the first neck has barely formed on the low velocity end of the rod where two necks have been formed on the upper velocity end. The prediction of V_1 from the constant diameter equations at 300 microseconds is the same as in the previous case, i.e., $V_1 = 0.25\text{x}10^5$ cm/sec. The calculation predicts $0.219\text{x}10^5$ cm/sec on the low velocity end and $0.646\text{x}10^5$ cm/sec on the upper velocity end (instead of $1\text{x}10^5 - 0.25\text{x}10^5 = 0.75\text{x}10^5$ cm/sec). Clearly, a 4-to-1 diameter difference over the rod's length is sufficient to cause large errors in the predictions for the constant diameter equations.

The simplified equations of the last section can be written for variable diameter rods, but they do not remain so simple. In fact, there is no obvious analytic solution to the equations, and they must be solved numerically. In this era of programmable hand calculators, this does not present a serious problem.

The volume of a frustum is given by:

$$\tau = \frac{\pi h}{3} (A_1 + A_2 + \sqrt{A_1 A_2})$$

where A_1 and A_2 are the base and top areas and h is the length of the frustum along its axis. The constant volume plastic relation then is:

$$h(0)\ (A_1(0) + A_2(0) + \sqrt{A_1(0)A_2(0)}) \tag{40}$$

$$= h(t)\ (A_1(T) + A_2(T) + \sqrt{A_1(T)A_2(T)})$$

Now,

$$h(0) = X_{1,1}(0) \quad \text{assuming } X_{1,0}(0) = 0$$

and $h(T) = X_{1,1}(T) - X_{1,0}(T)$

Also, the areas are functions of the initial and final values of $X_{1,1}$ and $X_{1,0}$

$$A_1(0) = \pi r_1(0)^2$$

where $r_1(0)$ is the initial base radius.

$$A_2(0) = \pi r_2(0)^2 = \pi \left[r_1(0) + \frac{(r_E(0) - r_1(0))}{L_o} X_{1,1}(0) \right]^2 \qquad (41)$$

where $r_E(0)$ is the initial radius of the upper velocity end of the rod and L_o is the initial rod length.

Since the ends of the rod are relieved almost instantaneously,

$$r(T) = r_1(0)$$

and $A_1(T) = A_1(0) = \pi r_1(0)^2$

However, $r_2(T)$ must be calculated from Equations (40) and (41) given $A_1(0)$, $A_2(0)$, and $A_1(T)$. The equation is a quadratic with the only positive value of $r_2(T)$ given by:

$$r_2(T) = \frac{-r_1(0)}{2} + 1/2 \left[r_1(0)^2 + 4 \left(\frac{B}{\pi h(T)} - r_1^2(0)\right) \right]^{1/2}$$

where the term B is given by:

$$B = X_{1,1}(0) \left(A_1(0) + A_2(0) + \sqrt{A_1(0) A_2(0)}\right)$$

Thus, the area at the first elastic/plastic interface is a complex function of initial geometry and the position of the interface in laboratory and Lagrangian frames. This is the primary complication in solving for an analytic function providing the position $X_{1,1}$. The equations analogous to Equations (7), (11), and (17) then become very complex. There may be substitutions available to provide analytic solutions, but they were not found during this study. It remains then to solve the equations numerically. Numerically solving the equations is a straightforward exercise but one which will not be pursued in this report.

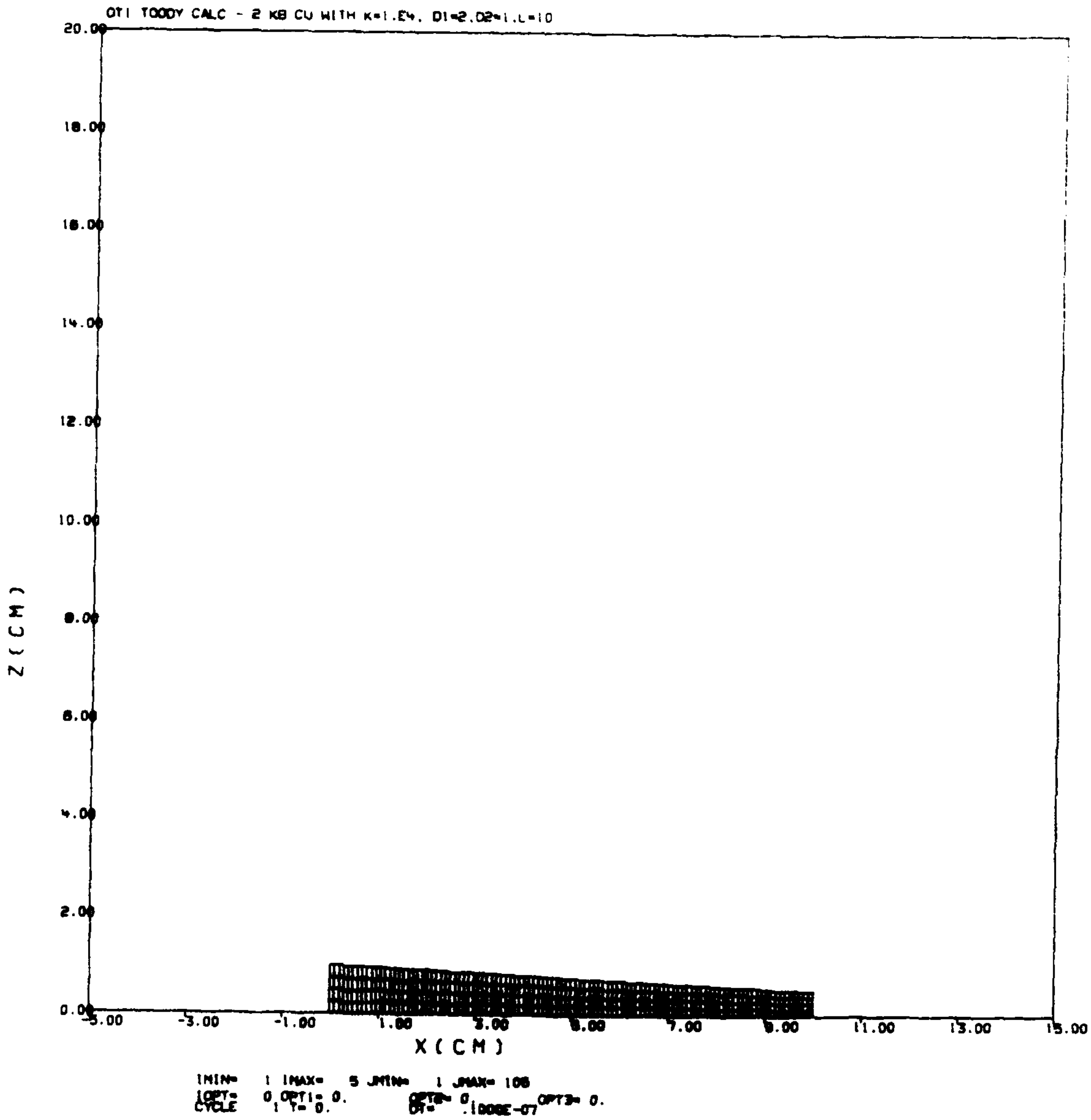

Figure 30. Grid Plot for 2-Kb Copper Conical Rod, D1/D2=2

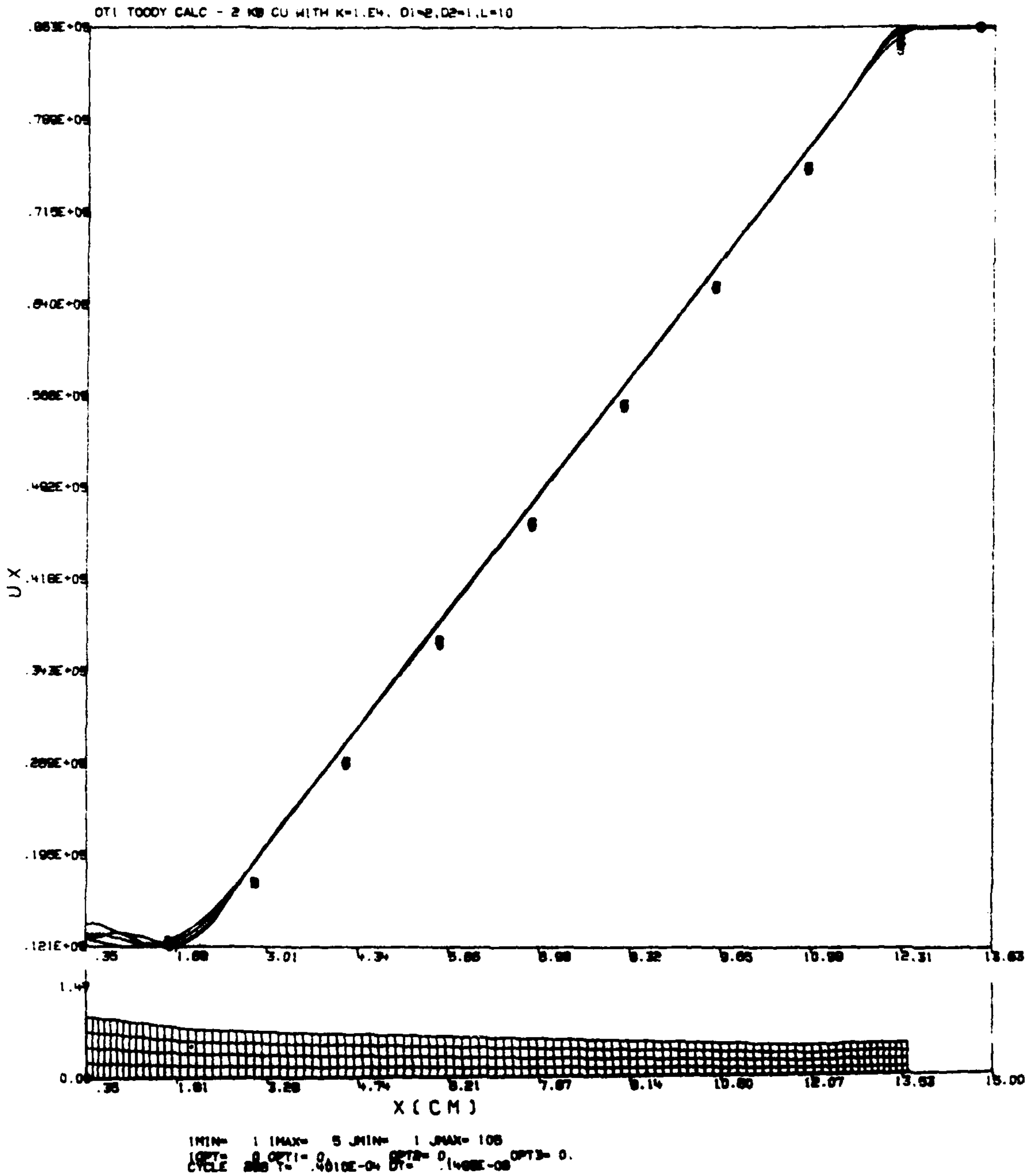

Figure 31. Grid and Velocity Plot for 2-Kb Copper Conical Rod, D1/D2=2 at 40 Microseconds

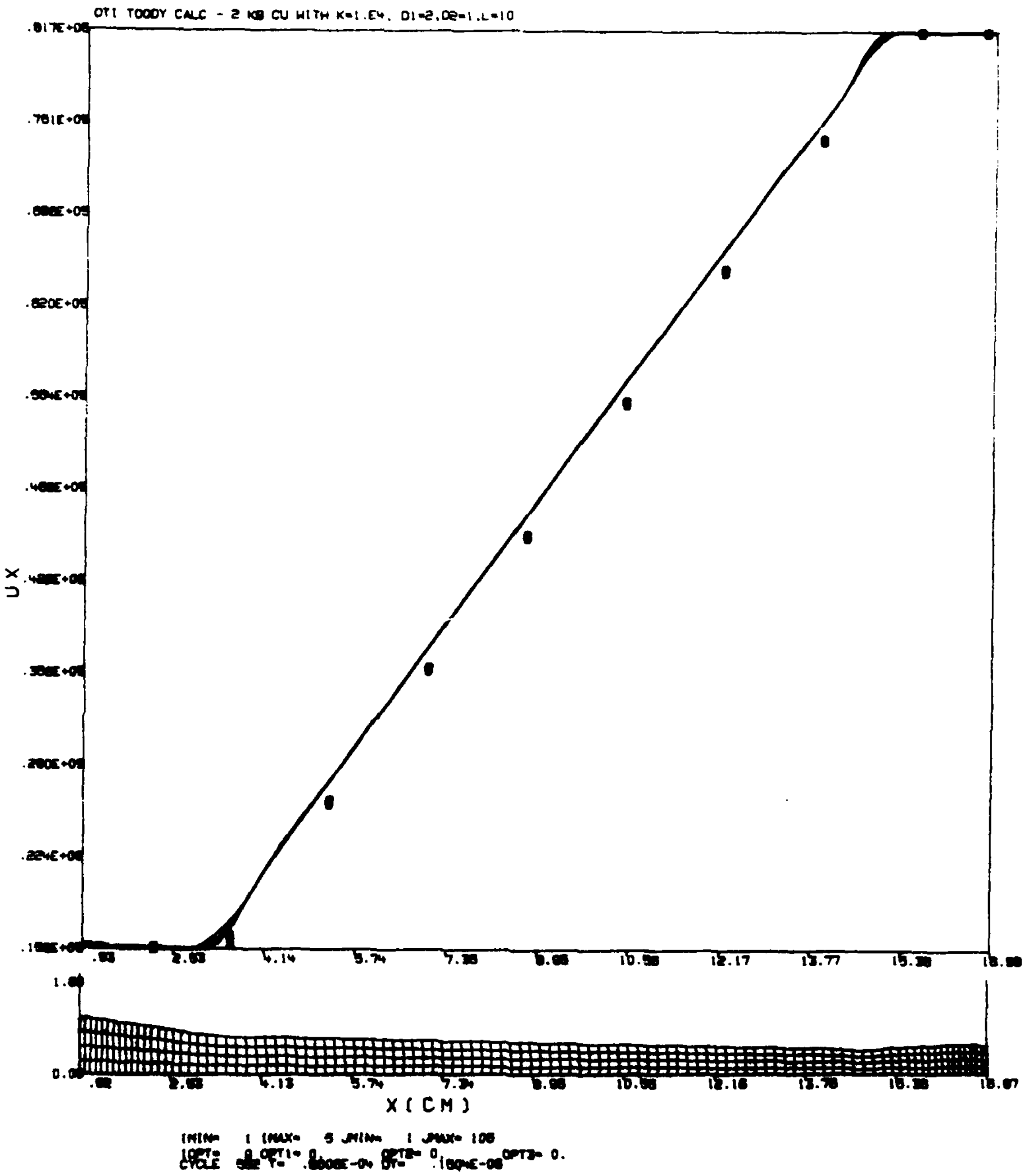

Figure 32. Grid and Velocity Plot for 2-Kb Copper Conical Rod, D1/D2=2 at 80 Microseconds

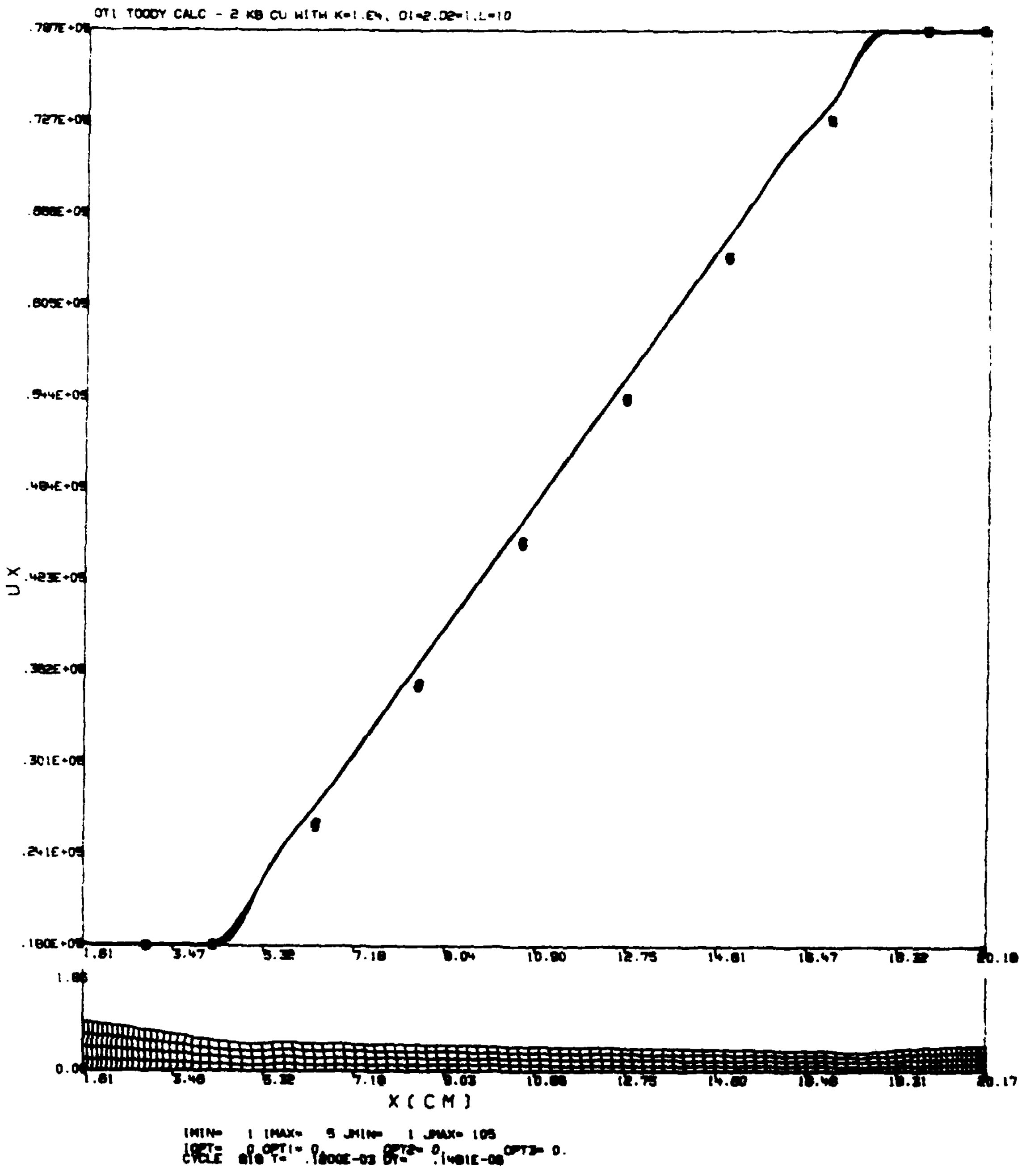

Figure 33. Grid and Velocity Plot for 2-Kb Copper Conical Rod, D1/D2=2 at 120 Microseconds

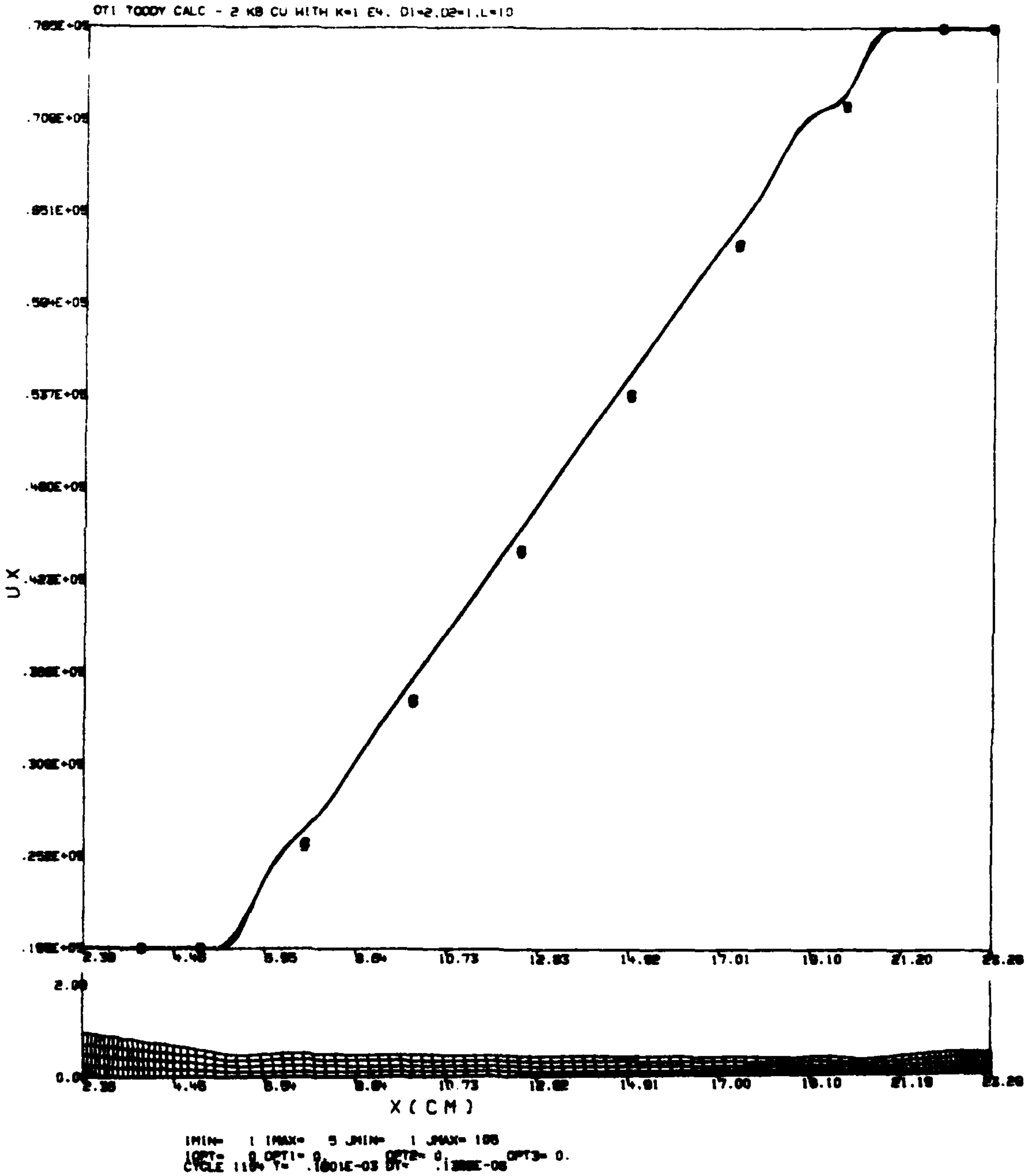

Figure 34. Grid and Velocity Plot for 2-Kb Copper Conical Rod, D1/D2 at 160 Microseconds

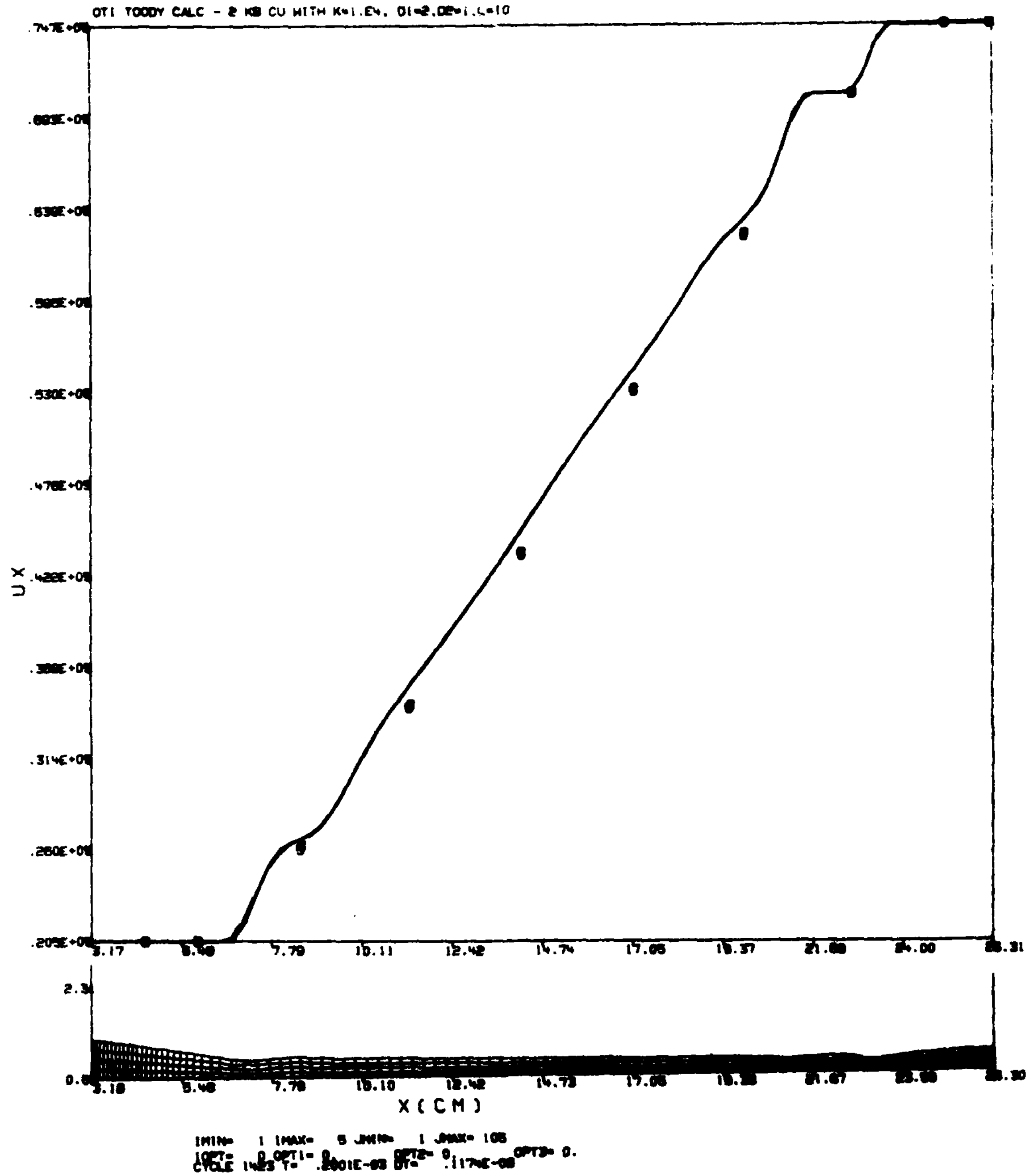

Figure 35. Grid and Velocity Plot for 2-Kb Copper Conical Rod, D1/D2=2 at 200 Microseconds

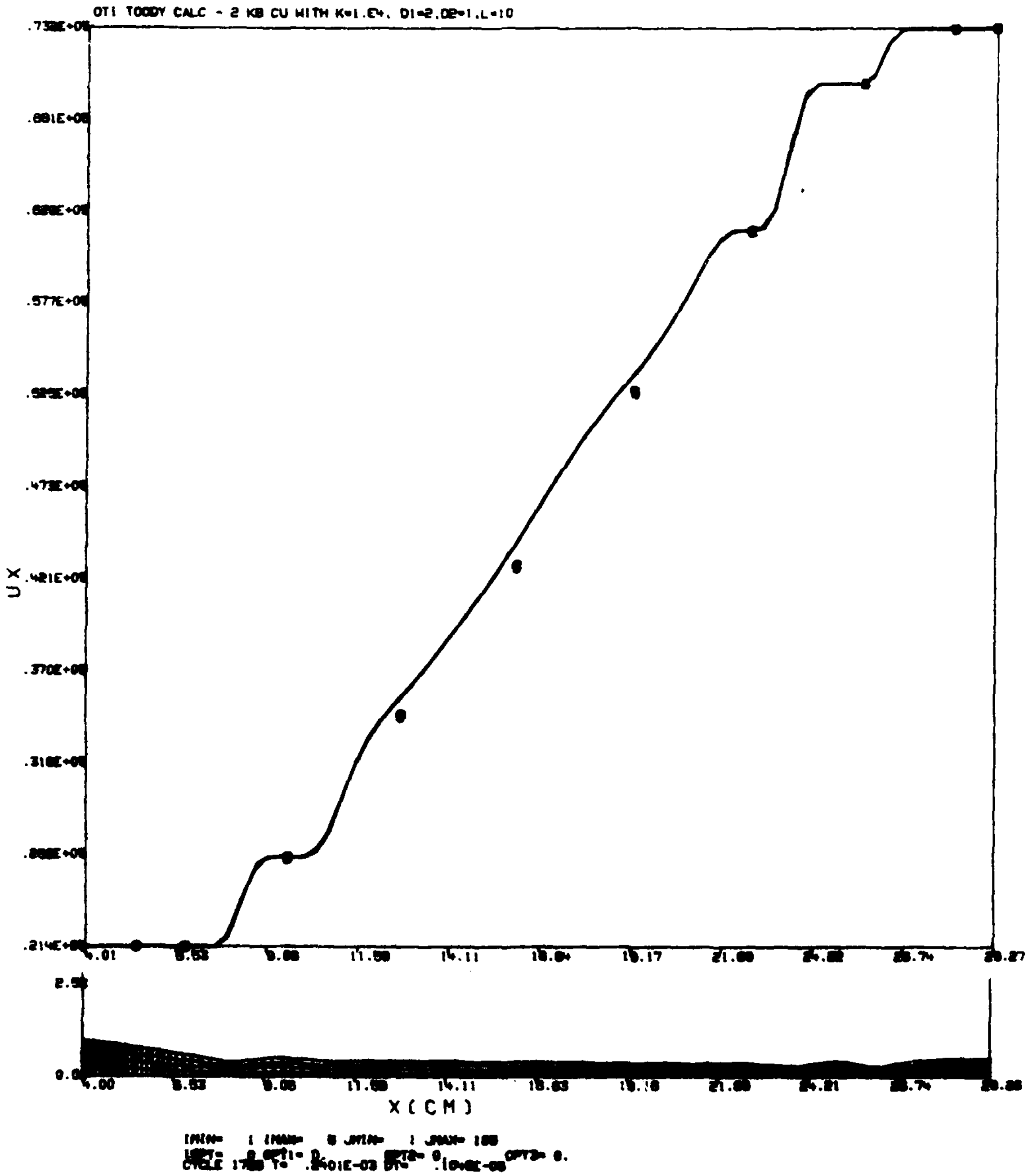

Figure 36. Grid and Velocity Plot for 2-Kb Copper Conical Rod, D1/D2=2 at 240 Microseconds

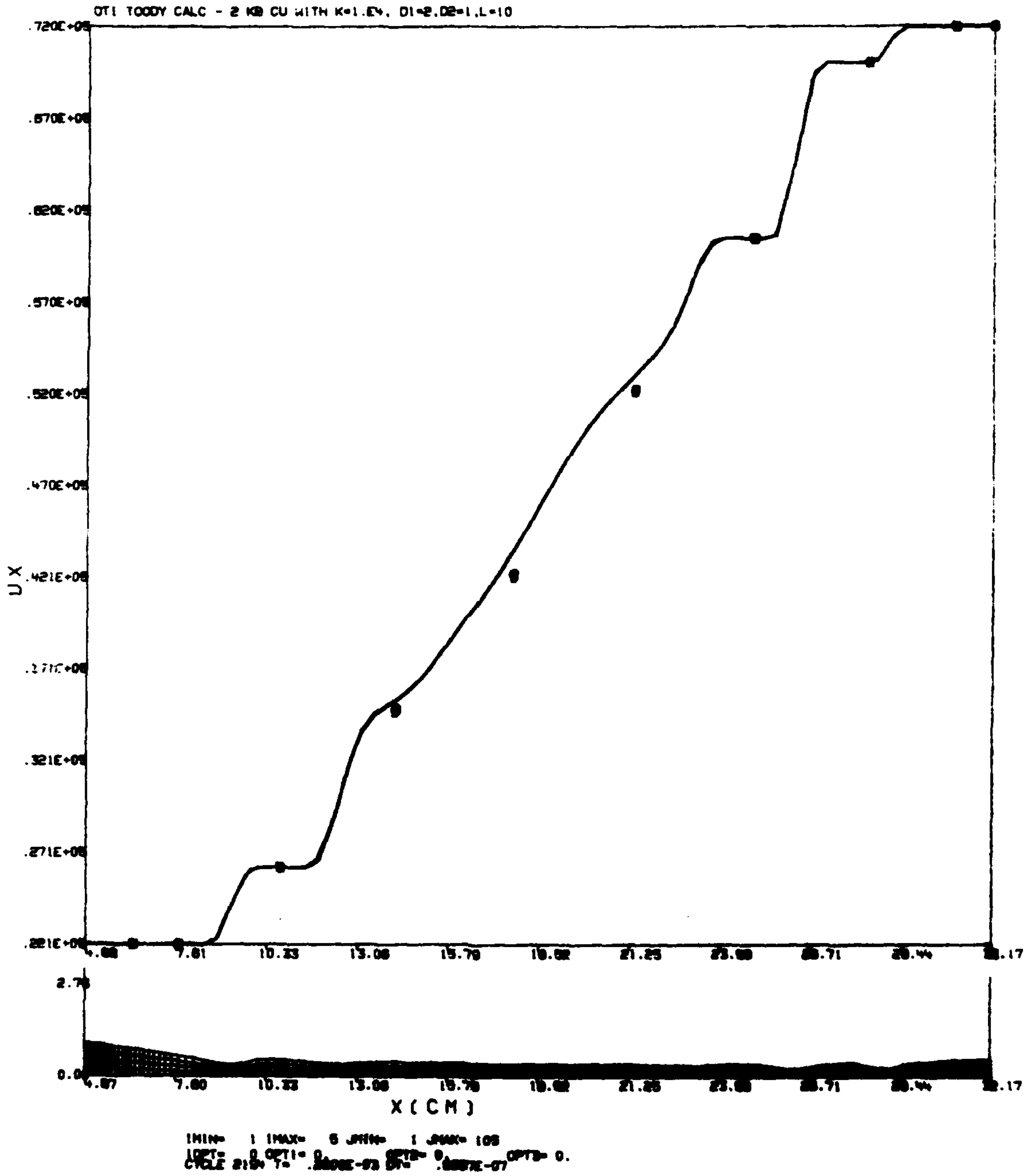

Figure 37. Grid and Velocity Plot for 2-Kb Copper Conical Rod, D1/D2=2 at 280 Microseconds

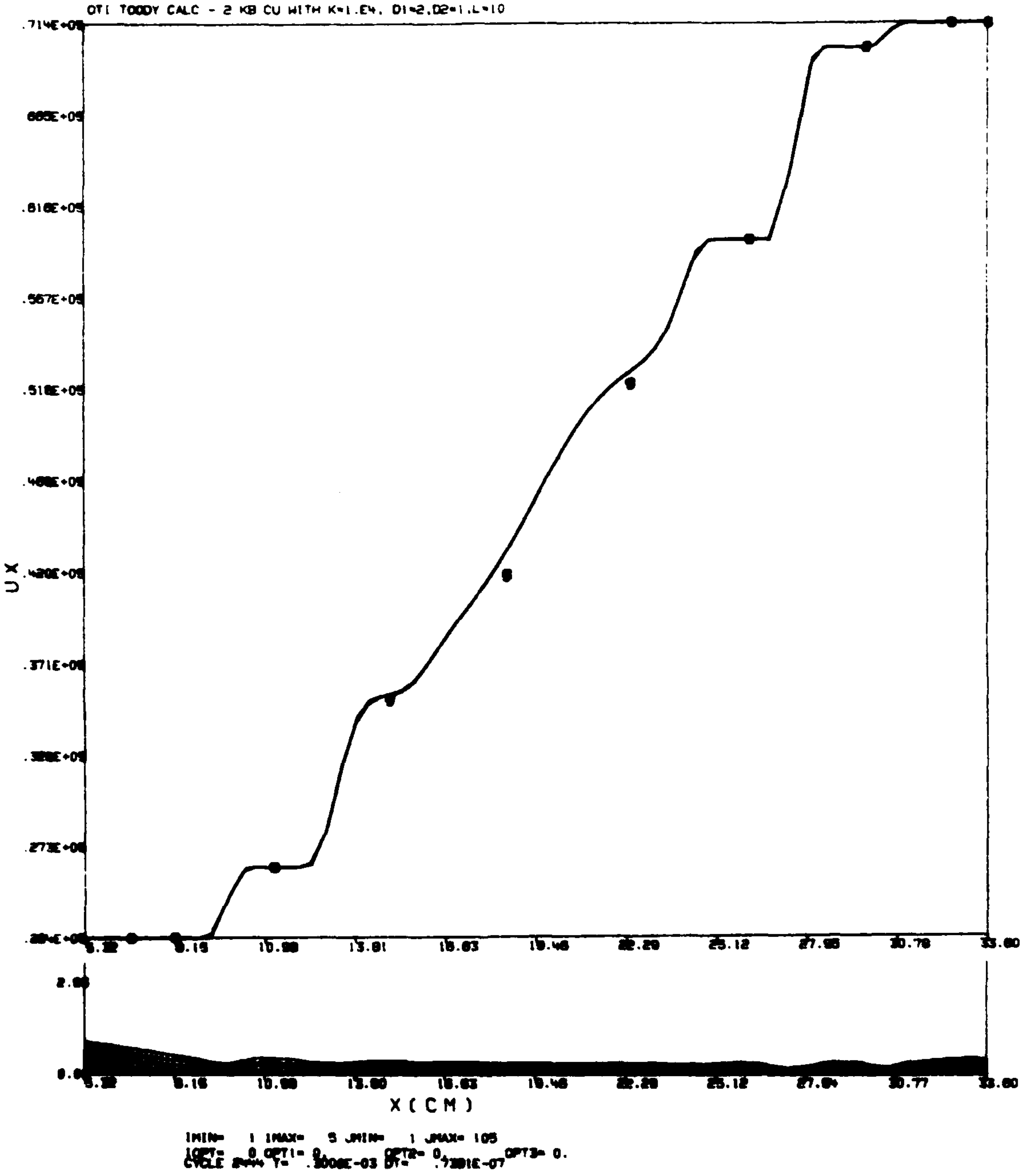

Figure 38. Grid and Velocity Plot for 2-Kb Copper Conical Rod, D1/D2=2 at 300 Microseconds

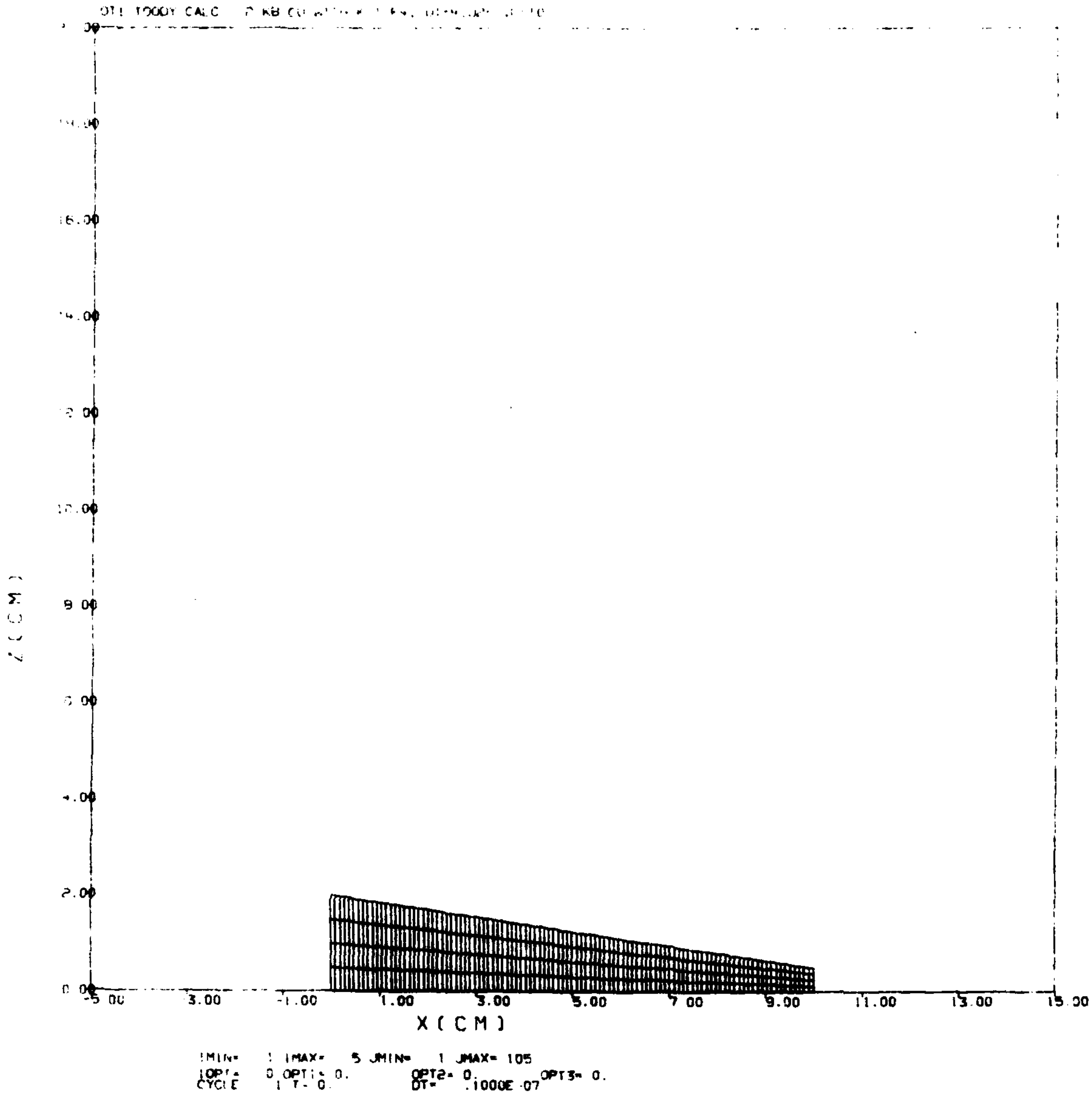

Figure 39. Grid Plot for 2-Kb Copper Conical Rod, D1/D2=4

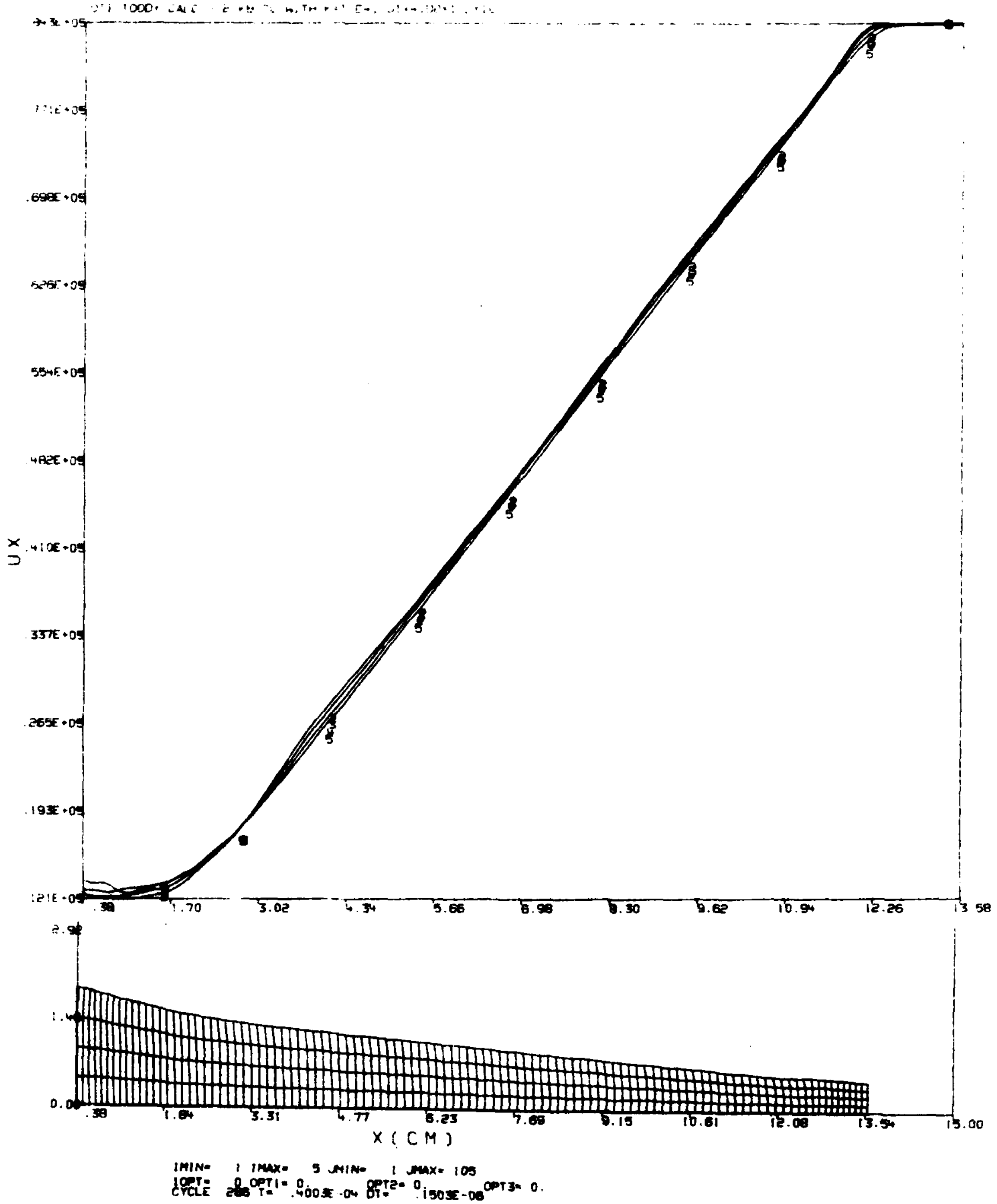

Figure 40. Grid and Velocity Plot for 2-Kb Copper Conical Rod, D1/D2=4 at 40 Microseconds

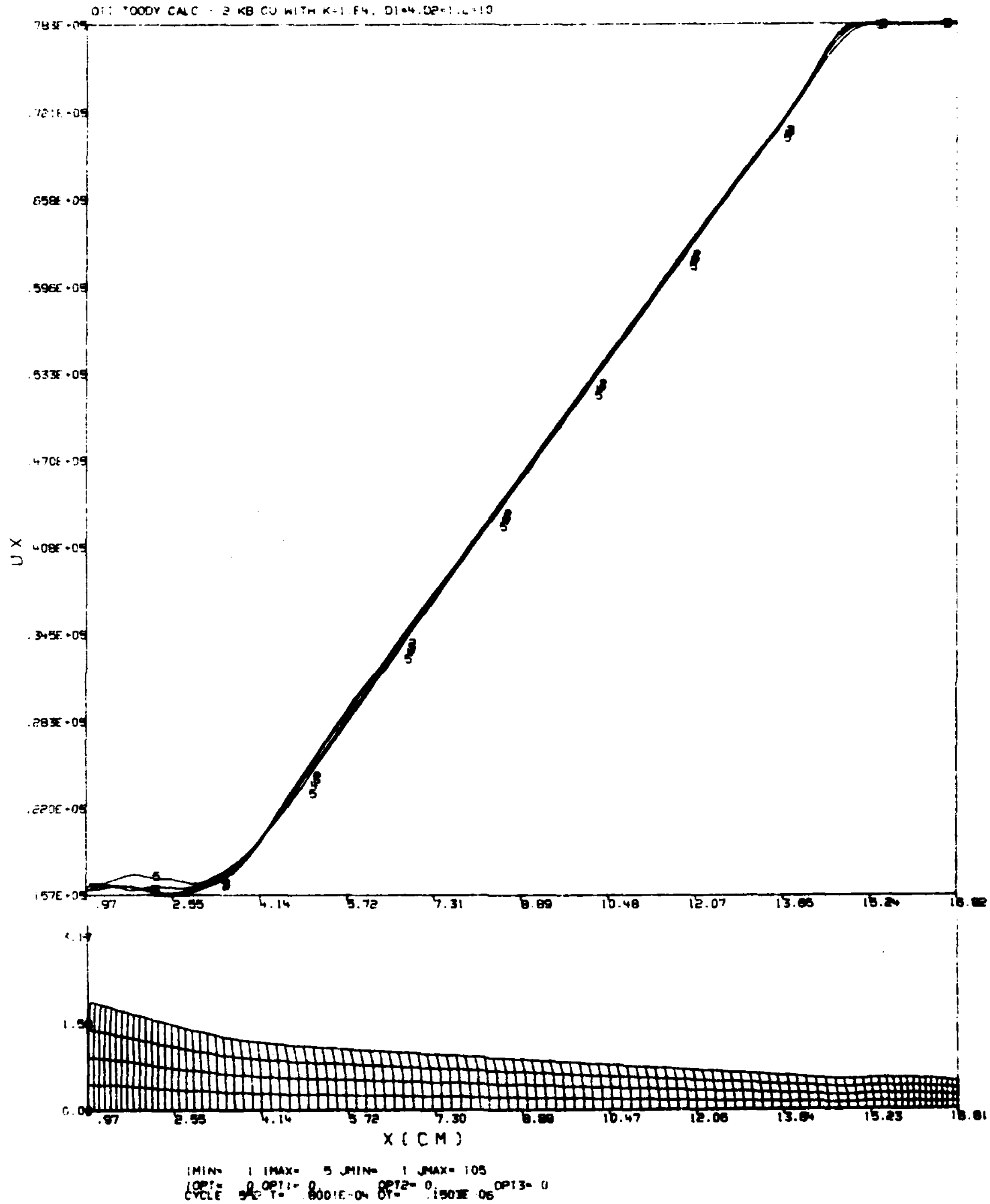

Figure 41. Grid and Velocity Plot for 2-Kb Copper Conical Rod, D1/D2=4 at 80 Microseconds

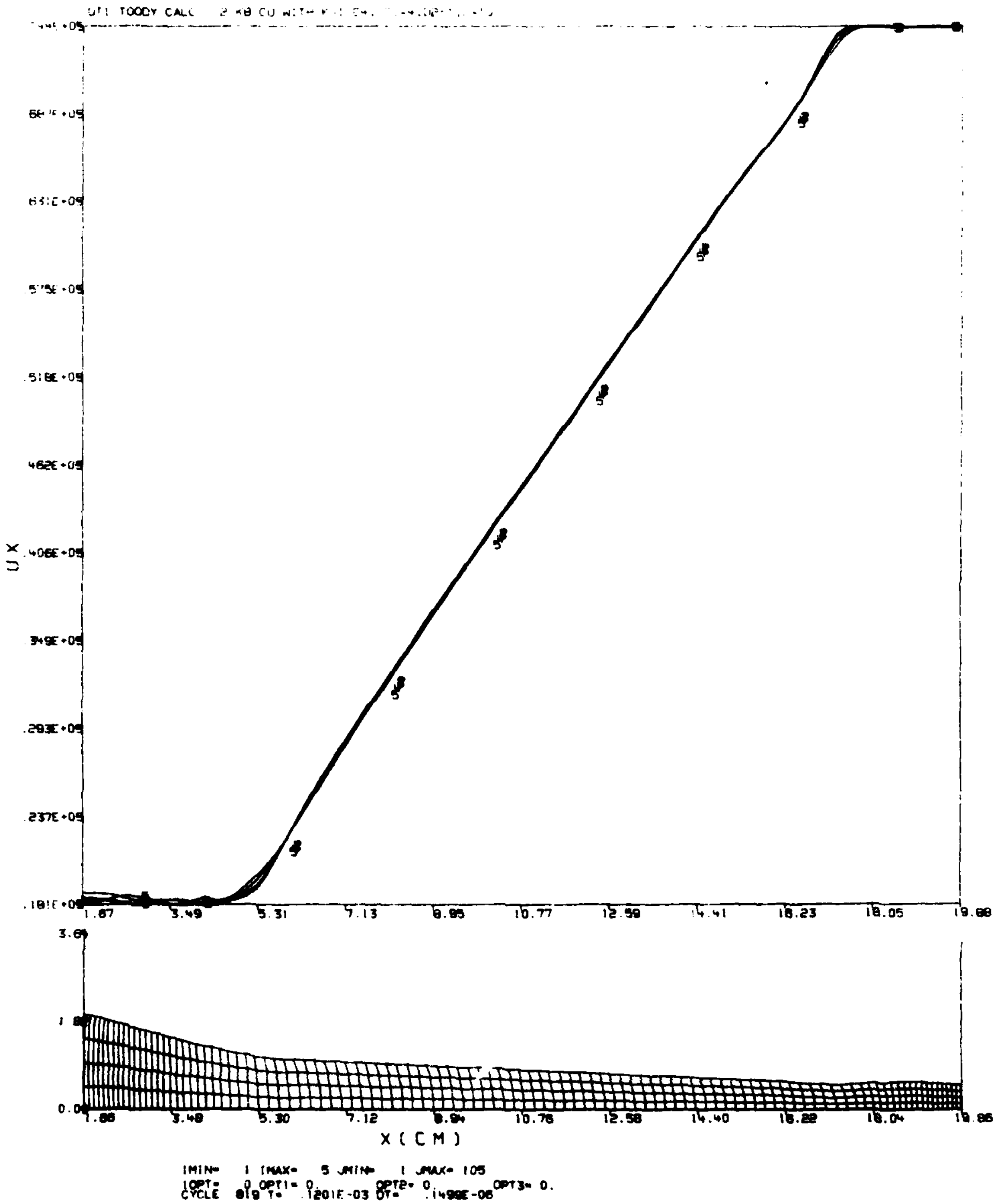

Figure 42. Grid and Velocity Plot for 2-Kb Copper Conical Rod, D1/D2=4 at 120 Microseconds

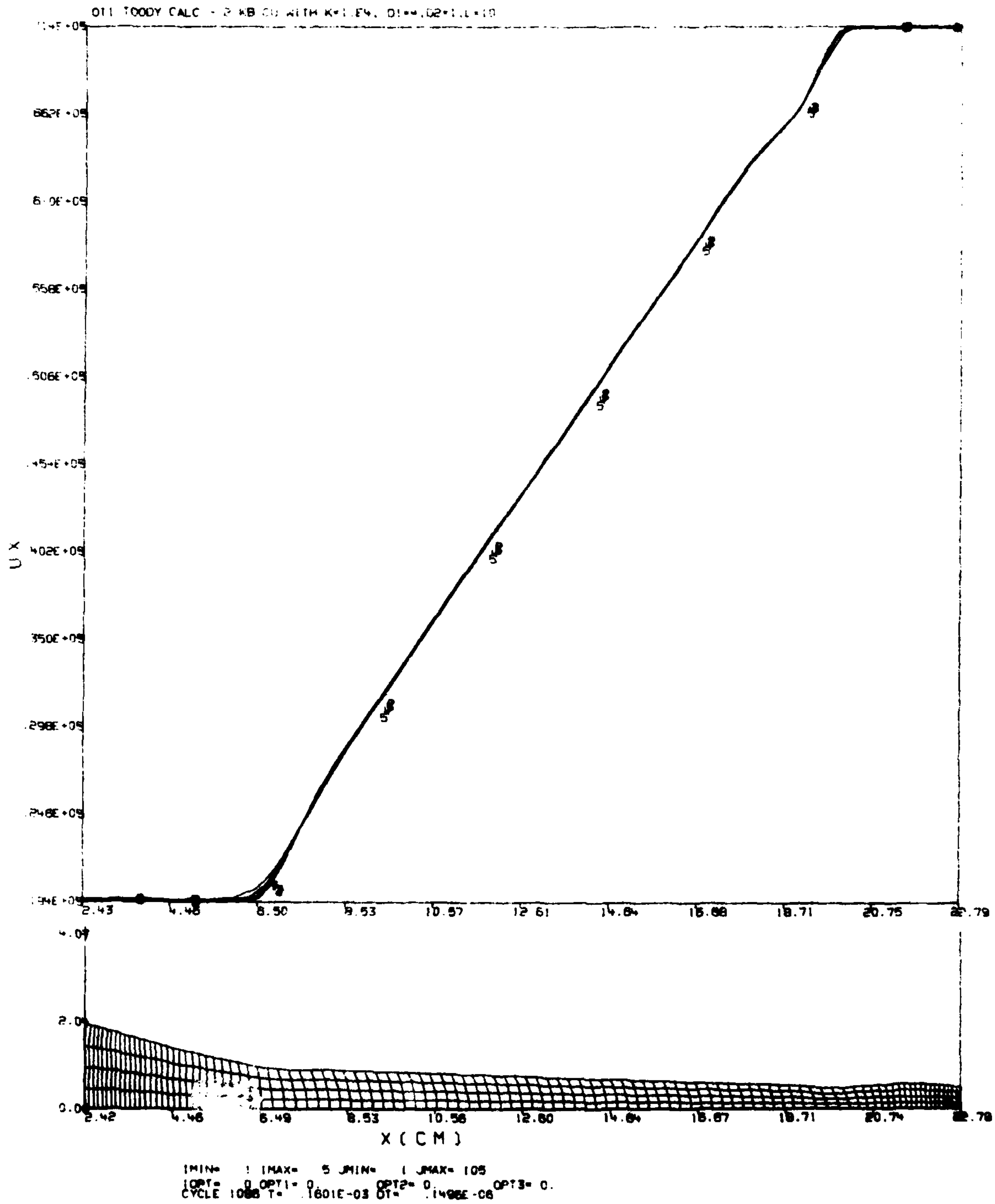

Figure 43. Grid and Velocity Plot for 2-Kb Copper Conical Rod, D1/D2=4 at 160 Microseconds

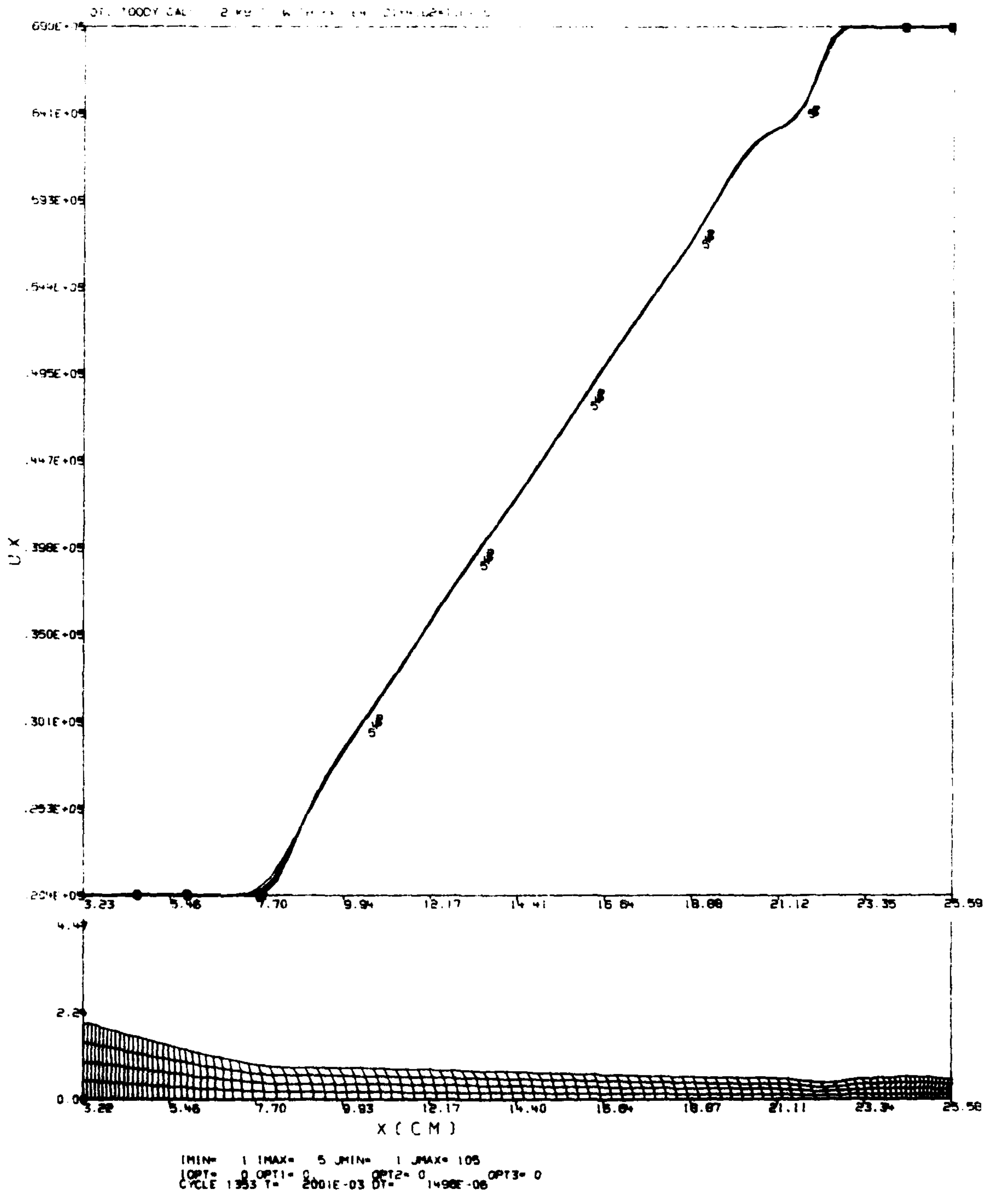

Figure 44. Grid and Velocity Plot for 2-Kb Copper Conical Rod, D1/D2=4 at 200 Microseconds

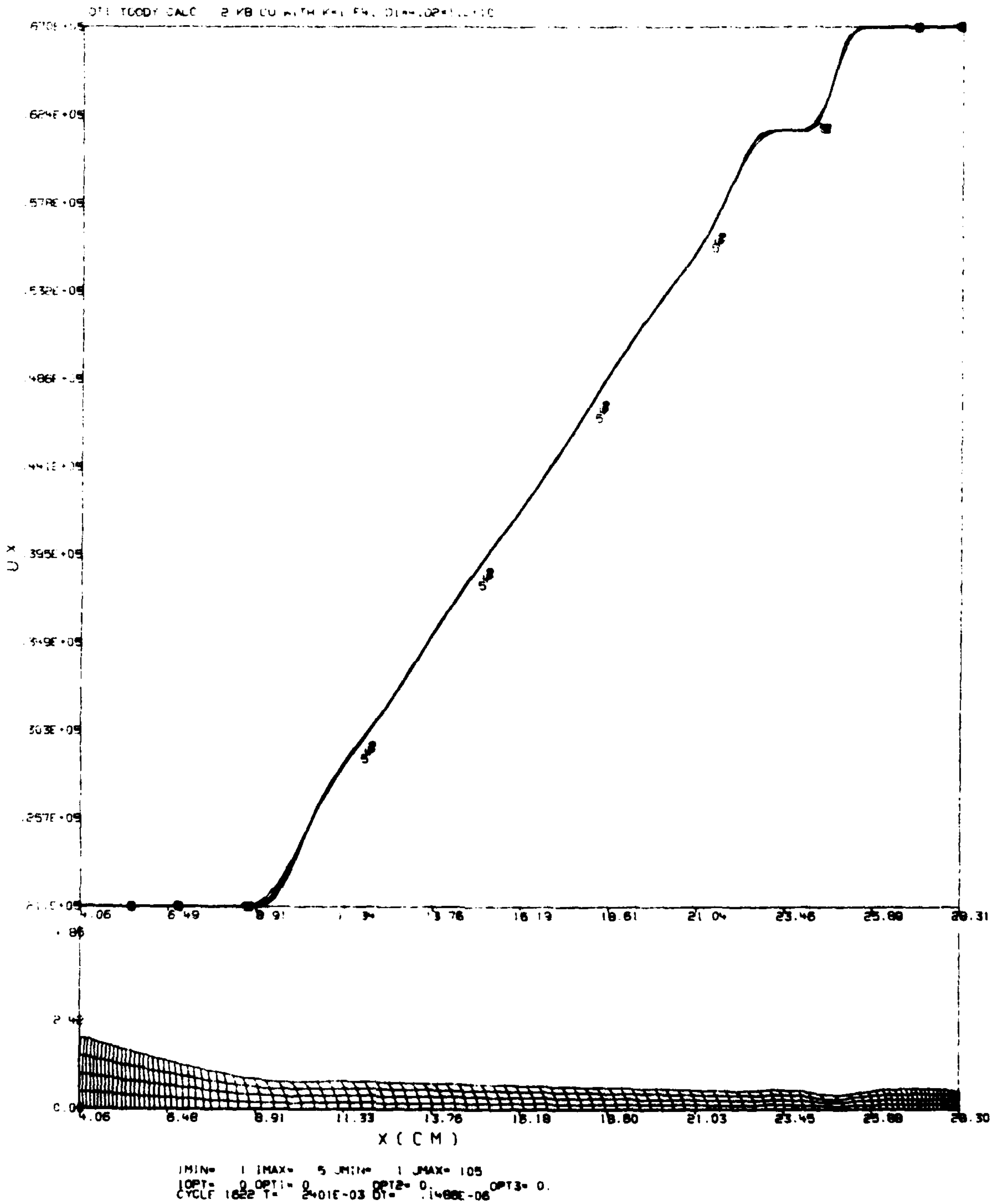

Figure 45. Grid and Velocity Plot for 2-Kb Copper Conical Rod, D1/D2=4 at 240 Microseconds

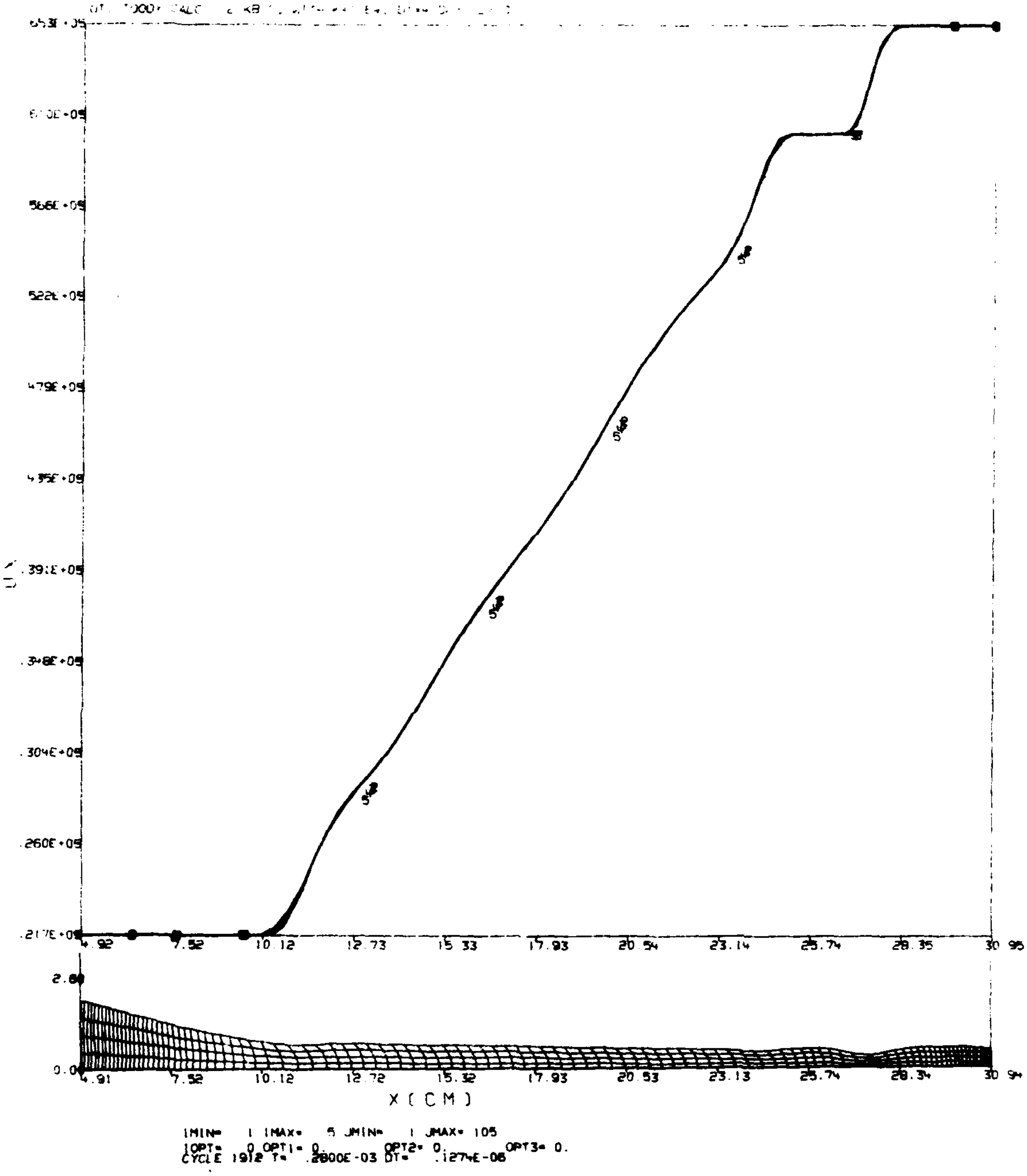

Figure 46. Grid and Velocity Plot for 2-Kb Copper Conical Rod, D1/D2=4 at 280 Microseconds

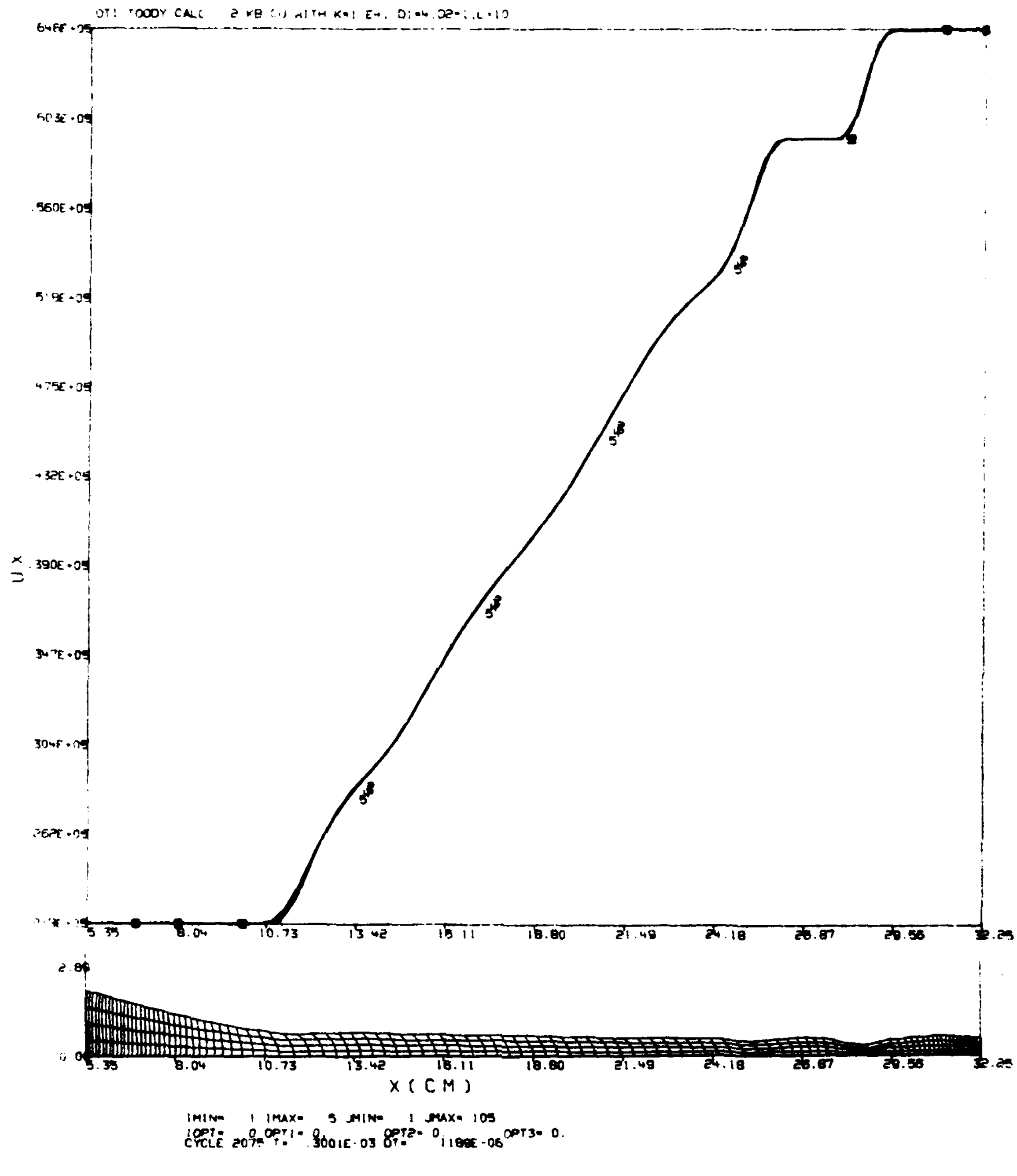

igure 47. Grid and Velocity Plot for 2-Kb Copper Conical Rod, D1/D2=4 at 300 Microseconds

SECTION V

CONCLUSIONS AND RECOMMENDATIONS

It is concluded from this study that all phenomena seen in the stretching and deformation of jets under large velocity gradients can be explained by assuming that the jet has some strength, i.e., it is not completely melted. It is further concluded that careful examination of the positions and velocities of jets will allow predictions of strength to be made for very high strain, high temperature states of metals.

Further work is indicated in the application of the equations developed in this report to actual jets of various metals. Some predictions have been made for a classified munition and are included in a separate letter report. Further theoretical work on the equations themselves should provide an understanding of the growth of the elastic portion of jet segments beyond the end segments. It is believed that a great deal of material property information is contained within the equations which predict this growth. There was insufficient time under this project to solve for those relationships. It would also be of interest to apply these equations to stretching self-forging fragments with gradients far below those seen in jets.

This report basically initiates a technology area which appears quite fruitful for pursuit in terms of understanding jet behavior and the behavior of materials in very high strain and temperature environments.

REFERENCES

1. Swegle, J. W., "TOODY-IV, A Computer Program for Two-Dimensional Wave Propagation," SAND-78-055, Sandia National Laboratory, September 1978.

2. Bridgman, P. W., "Studies in Large Plastic Flow and Fracture," McGraw-Hill Book Company, Inc., 1952.

DATE
FILMED